NOTE TO USERS

This reproduction is the best copy available.

UNIVERSITY OF CINCINNATI

May 27 , 2003

I, Kimberly Kay Stonesifer ,

hereby submit this as part of the requirements for the degree of:

Master of Science

in Geology

It is entitled Lead Mineralization

in Natural and Drinking Water Distribution Systems

Approved by:

LEAD MINERALIZATION IN NATURAL AND DRINKING WATER DISTRIBUTION SYSTEMS

A thesis submitted to the

Division of Research and Advanced Studies of the University of Cincinnati

in partial fulfillment of the requirements for the degree of

MASTER OF SCIENCE

in the Geology Department of the College of Arts and Sciences

May 2003

by

Kimberly Kay Stonesifer

B.S., University of Arkansas at Little Rock, 1999

Approved by: _____

Chairperson of Supervisory Committee

UNIVERSITY OF CINCINNATI

ABSTRACT

LEAD MINERALIZATION IN NATURAL AND DRINKING WATER DISTRIBUTION SYSTEMS

Kimberly Kay Stonesifer

Chairpersons of the Supervisory Committee: Dr. J. Barry Maynard and
Dr. Craig Dietsch
Department of Geology

The processes of lead mineralization under highly oxidizing conditions are not well understood. A case study from the Cincinnati Water Works Distribution System (CWW DS) plus the aid of a natural analog of extreme oxidation of native lead in southern Greenland coupled with the experimental data provides a means of testing current models. The results of this study are not consistent with the prevailing stagnation-diffusion model proposed by Kuch and Wagner (1983).

This research implemented an experimental loop apparatus system designed to replicate the oxidation/corrosion process that occurs in the drinking water distribution system through the use of metal coupons in a controlled reaction cell. By integrating Eh, pH, oxidant, aqueous water chemistry, and solids analysis, this

study has identified the phase forming reactions and their relative rates of phase formation and alteration. These experimental results are comparable to solids data collected from the CWW DS.

The important reactions are:

i) $Pb_{(s)} \leftrightarrow Pb^{2+} + 2e^-$,

ii) $Pb^{2+} + HCO_3^- \leftrightarrow PbCO_{3\,(s)} + H^+$,

iii) $Pb_3(CO_3)_2(OH)_{2\,(s)} \leftrightarrow 2PbCO_{3\,(s)} + H_2O + PbO_{(s)}$, and

iv) $PbO + HCO_3^- \leftrightarrow PbCO_{3\,(s)} + OH^-$.

During loop apparatus system operation, reaction *ii* initially dominates from day 1 until day 6. For reasons not well understood, the product is a combination of cerussite and hydrocerussite. Reaction *iii* prevails from day 6 to approximately day 40. During the period of this reaction, a nanocrystaline/ nanoparticulate mixed phase solid product coats the entire coupon and also settles in the bottom of the reaction cell. The large amount of nano product and its reactive surface area generated by this reaction shifts the control of the reactions from a more thermodynamic to a more kinetic mechanism. Beyond Day 40, the significant reaction is ii, once again. Although this reaction is the slowest, it is the most persistent. It is important to note that while one reaction appears to dominate the system at any given time, multiple reactions are actually at play. The re-reaction of previously formed phases as represented by iii) and iv) results in stepped reaction progress, contrary to true monotonic curves required by simple diffusion models.

TABLE OF CONTENTS

LIST OF FIGURES

LIST OF TABLES

ACKNOWLEDGMENTS

The author wishes to thank:

Dr. J. Barry Maynard (UC), for bringing me onto the project and providing endless support with out which, I would not have completed this project. Thank you in your efforts to "build a bridge" between academia and government environments. This experience has taught me more than just redox. Sir, your awesome!

Dr. Craig Dietsch (UC), for being a great co-advisor and keeping me on schedule. I would not have applied to UC if it were not for you. Thank you for your continued encouragement and understanding.

Dr. Warren Huff (UC), for being a great committee member and teacher. Your clay mineralogy class provided me with a solid background for interpreting x-ray diffraction patterns for this study. Thank you for leading the trek in Hawaii in which we found a green sand beach - a day I hope to never forget.

Mr. Schock (US EPA), for being a mentor. Mr. Schock has provided endless support for the project, advice, professional development, and personal growth. Mr. Schock contributed his time and efforts for the XRD analysis and operational instruction for

various softwares. He has provided me with text material on current views pertaining to the study, pipe samples from the Cincinnati Water Works Distribution System, and the materials/ supplies to carry out the experimental portion of the project. This project would have never been completed without his wise insight and management skills.

Mr. Steve Harmon (US EPA), for his generous time and use of the SEM. Mr. Harmon performed a significant amount of the logged SEM time and discussions pertaining to the project.

Mr. Keith Kelty (US EPA), who manages a team of analysts for all ICP data. This study has generated hundreds of samples, and without his support, this project would not have been possible.

Mr. Lytle (US EPA), for providing a "real-world" experience while at the US EPA.

Ian LaSeke, Sun Cao, Cheryl James, Jeff Causey, Christy Fritsch, Mr. Leo, Mr. Herb Braxton, Mrs. Barbara Francis for their intermittent assistance, back-up labor support, and/or moral support throughout the experimental portion of the project. These people each contributed to the success of the project. Rome was not built in a day and certainly not by one person alone.

Dr. Buchbuger, University Cincinnati Engineering Department, for providing one academic year financial support as a fellowship for the Free Chlorine Run experimental portion of the project.

The Environmental Careers Organization (ECO) for their financial support for the Non-Chlorinated Run experimental portion of the project and travel expenses to present data at the WQTC AWWA conference in November 2002.

The entire University of Cincinnati Geology Department for such a wonderful place to be. Mr. Matt Fenwick for emergency data back-up. Mrs. Sandi for being such a great woman who always has time to listen.

Last but certainly not least, I'd like to thank my great-grandparents, Rev. R. T. and Garnet Ludden. They took me in, raised me, and taught me how to live life. They taught me the skills (i.e. a strong work ethic and the strength of fellowship and faith) I'd need to face my future. Everything I have and will accomplish in this life is a direct result of their firm and loving kindness.

1.0 INTRODUCTION

1.1 Statement of Problem

The Cincinnati Water Works (CWW) California Treatment facility, also known as the Miller Plant, has been ranked as one of the best in the country for water quality (CWW, 1999). However, high lead levels (>15 ppb) have occasionally been reported at the consumers' tap (CDM, 2003). The source of the lead is likely from within the extensive distribution system itself, including lead pipes and/or brass fittings. Knowledge of the nature and reactions of secondary lead minerals is key to understanding how to control lead release from such distribution systems.

In recent years, an unusual lead phase, plattnerite (PbO_2) has been reported in the Cincinnati Water Works Distribution System (CWW DS) and from other municipalities nation-wide (Schock et al., 2001). Plattnerite is a rare mineral that typically forms under extremely oxidizing conditions as an oxidation product of native lead. Identification of plattnerite via X-ray Powder Diffraction (XRD) can be difficult in the presence of other lead phases. The identifying peaks of plattnerite overlap those of the common lead carbonates (cerussite and hydrocerussite) and native lead from sample preparation, so that plattnerite would easily be overlooked.

A unique and rare natural occurrence of native lead and associated phases is the Ilimaussaq Alkaline Complex of southern Greenland. This locality provides a natural analog for the formation and alteration of scales found in lead drinking water pipe materials including plattnerite. The natural analog shows that extreme oxidizing conditions are needed to form plattnerite from native lead.

From the Greenland example, it is clear that redox state, and not just pH, is key to controlling the lead minerals formed. However, most earlier work has focused on pH as the controlling variable. In the study I have continually monitored both Eh and pH and daily measured metal levels in a bench-scale system designed to replicate as closely as possible normal distribution pipes.

1.2 Historical Lead Studies

An excellent and detailed summary of historic lead studies is thoroughly given in Schock et al. (1996). A study in Berlin, East Germany by Feller et al. (1984, 1988) noted the existing corrosion surface prior to their study as a porous surface film consisting of cerussite, hydrocerussite and litharge. Howard (1923) studied lead pipe sections from the New Hampshire area from 1909 to 1922. He observed hydrocerussite plus a very thick loosely adherent brown coating that appeared "vegetable in nature". A study in the Netherlands, in the 1980's investigated lead pipes that were 30 to 80 years old. XRD analysis indicated the presence of hydrocerussite ($2PbCO_3Pb(OH)_2$), cerussite ($PbCO_3$), and litharge (PbO).

Although early studies did not always record pH (or change in pH), Baylis (1926) did record a significant rise in pH (several pH units) for a three-day stagnation time for his bench-scale study.

Fine-grained/colloidal/microcrystalline lead phases have also been described in the literature. Donaldson (1924) noted a colloidal lead hydrate formed with dissolved oxygen present. A "vegetable" –like coating material was described by Howard (1923). His description of its physical characteristics is consistent with that of other worker's interpretations of particulate/colloidal lead phase and not that of any type of biological growth.

2.0 BACKGROUND

2.1 Theory: Eh and pH Chemistry

Redox potential is a very useful parameter in describing and predicting the behavior of many important elements, such as lead, copper, and iron, that occur in more than one oxidation state in the natural environment. Redox reactions occur when electrons are transferred during a chemical reaction, resulting in a change of oxidation states of both reactants and products. The redox potential of a reaction is the electromotive force, (emf) measured or calculated in volts, and is reported as Eh (with respect to the standard hydrogen electrode), or may be expressed as pe (Morel

and Hering, 1993). Eh is related to the activity of electrons (e^-) similar to the way pH is related to the activity of protons (H^+).

To understand Eh, consider the reaction...

$$aA + bB \leftrightarrow gG + hH$$

For this reaction, Eh is defined as

$$Eh = E^\circ - \frac{RT}{nF} \ln \frac{(a_g^G a_h^H)}{(a_a^A a_b^B)}$$ (Garrels and Christ, 1965)

a's = activities of products and reactants
E° = the standard electromotive force (in volts), measured against the standard hydrogen electrode (SHE), which is an accepted reference value where $E^\circ=0$ at 25°C and 1 atm of pressure, in the half cell reaction $H_2 \leftrightarrow 2H^+ + 2e^-$.

Note that the basis of the above reaction is the Nernst Equation, given by

$$E_N = \frac{2.3\,RT}{nF}$$

where

E_N = Nernst Potential (in volts)
R = gas constant, 8.314 joules/deg mol
T= absolute Temp in °K
F= Faraday's constant, 96,500 coulombs/equiv
n= number of electrons

Accordingly, E° is given by

$$E^\circ = \frac{RT}{nF} \ln K \quad \text{or} \quad E^\circ = \frac{0.059}{n} \log K \quad @\ 25^\circ C$$

To experimentally determine Eh, the redox potential against the SHE Eh is given by:

$$E_h = E_{meas} + E_{ref}$$

where

E_{meas} = redox potential against the reference electrode
E_{ref} = standard potential of the reference electrode

Another common way of expressing Eh is pe. In this thesis, Eh is the preferred scheme because it follows the SI standard. However, the conversion from pe to Eh is given by:

$$Eh = \frac{2.3RT}{F}(pe) \qquad \text{or} \qquad Eh = 0.059(pe)$$

$$pe^0 = 16.9\, Eh^0 \text{ (Volts)}$$
$$pe^0 = 1/n \log K$$

$$pe^0 = -0.175\, \Delta G^0 \quad (\text{in kJ mol}^{-1}) \quad \text{(Morel and Hering, 1993)}$$

The centerpiece of this research is to use Eh and pH to identify the phase forming reactions that occur in the oxidation of lead. Therefore, understanding the measurement of Eh plays a key role in interpretation of systems that are not in thermodynamic equilibrium. Systems in a state of stress or rapid change need a kinetic or mechanistic model to describe their behavior (Breck, 1974). Strict interpretation of this need may have caused many workers to discount the meaningful use of the Eh measurement. Namely, it was assumed that Eh measurements could only be meaningful if performed under equilibrium conditions. Eh can be a useful

measurement, as long as the system is in equilibrium, near equilibrium, or at least in a "constant metastable state" to allow the concept of partial equilibrium to be applicable (Stumm and Morgan, 1996). For the current study, the constant metastable state occurs upon stagnation of water in a drinking water distribution system. However, kinetics may be needed to describe the system when it changes from stagnation (metastable state) to flow as water is turned on and off at the tap.

The Measurement of Eh and pH

Eh

The actual act of electrochemically measuring Eh has also been discredited in the past. The commonly used platinum electrode does not respond or responds incorrectly ("sluggishly") to some of the most important redox couples in natural waters SO_4^-—HS^-, O_2—H_2O, CO_2—CH_4, NO_3^-—N_2, and N_2—NH_4 (Bethke, 1996, Hostettler, 1984, and Bricker, 1982).

For instance, when the inert silver-silver chloride electrode is placed in water saturated with dissolved oxygen, it does not achieve the theoretical potential predicted for the oxygen-water redox couple. The measurement drifts due to a near zero exchange current. The stable redox potential measurement for the dissolved oxygen system has been reported to be lower than that predicted for the O_2-H_2O couple. There have been at least two reported hypothesis for this behavior. Sato (1960) noted that the system may be responding to the O_2-H_2O_2 couple instead of the

O_2-H_2O couple. Other workers, Watanabe and Devanathan (1964) for example, stated that the stable potential observed in this system may be the result of a PtOH film formed on the surface of the electrode (Bricker, 1982). (I am partial to the former O_2-H_2O_2 interpretation given that the electrodes were cleaned regularly during this research.)

From Brookins (1988):

$Eh = 1.23 + 0.059 \log P_{O_2} - 0.059 \log pH$

At $P_{O_2} = 1.00$ atm and $pH = 7$

The aqueous oxygen water calculated value for Eh is

$Eh = 1.23 - 0.41 = 0.82$ V

The gaseous oxygen water calculated value for Eh is

$Eh = 1.23 + 0.059 \log (0.20) - 0.059\ pH = 0.780$ V

This difficulty, like most of those for the Eh measurement, can be resolved. Consider that in reviewing the reaction steps that occur in pure water, one can see that although O_2 is at saturation, it may not be the rate determining reactant that controls the redox potential.

$O_2 + e^- \rightarrow O_2^- + H^+ \rightarrow HO_2 + e^- \rightarrow HO_2^- + H^+ \rightarrow H_2O_2 + e^- \rightarrow OH + OH^- + e^- \rightarrow 2OH^- + 2H^+ \rightarrow 2H_2O$

A complicating factor is that the above reaction mechanism has rarely been found to be reversible, meaning that it does not obey the Nernst equation. Therefore,

the Eh equation is not strictly satisfied. Fortunately, the controlling reaction in the dissolved oxygen system has been studied in some detail and is reported as:

$O_2 + 2H^+ + 2e^- \rightarrow H_2O_2 \quad E^o = 0.68$ V
"designated as O_2/ H_2O_2 control" (Breck, 1974).

Another significant difficulty in using Eh can be a "mixed potiential", which is a complex condition when the anodic and cathodic pairs involved are not directly related to a particular half-cell reaction. This is the most commonly observed in natural waters as a result of the mixture of products and reactants. When a mixed potential is present, the measured potential will continue to drift indefinitely or it will achieve a stable value that does not correspond to any thermodynamically reversible half-cell potential in the system (Bricker, 1982). However, the mixed potential can be used as a qualitative indicator of the dominant redox couple (i.e. brass resembles the copper system).

All in all, Eh can be used to aid in determining the reactions in a system as long as its limitations are understood and the system is not a mixture or totally chaotic.

pH

pH is the negative log of the hydrogen ion activity, and in dilute solutions, can be fairly accurately calculated as the negative log of the hydrogen ion concentration:

$(H^+) = 10\text{^}\text{-pH} \qquad pH = -\log (H^+)$

However, when measuring pH, at least two standard buffers must be used in which the measured pH value is relative to. This is done because the liquid junction potential and ion activities are difficult to quantify without non-thermodynamic assumptions (Stumm and Morgan, 1996).

$$pH = \frac{E_h - 0.2802}{0.0591} \qquad pH = -\log a_{H+}$$

$$pH = \frac{E - E^\circ - E_J}{\frac{2.303\,RT}{F}} - \tfrac{1}{2} \log P_{H2}$$

where

P_{H2} = partial pressure of H above the solution (in units of atm)
E_J = potential caused by the liquid junction which is assumed to be independent of the concentration of the acid solution

2.2 Eh-pH Realms of the Drinking Water Distribution System

Because Eh is so critical for determination the species lead mineral formation, we continually monitored both Eh and pH. Daily measurements of Cincinnati tap water for Eh and pH yielded a region of Eh-pH space in which chlorinated drinking waters are likely to occupy (Figure 2.1). These data indicate that 1.00 ppm of free chlorine will raise the Eh above the stability of water for the given pH range. The two diagonal lines on figure 2.1 indicate the uppermost stability of water (in which

water is oxidized) and the lowermost stability of water (in which water is reduced). Very high Eh values of this kind would favor the formation of Pb^{4+} and therefore minerals such as plattnerite.

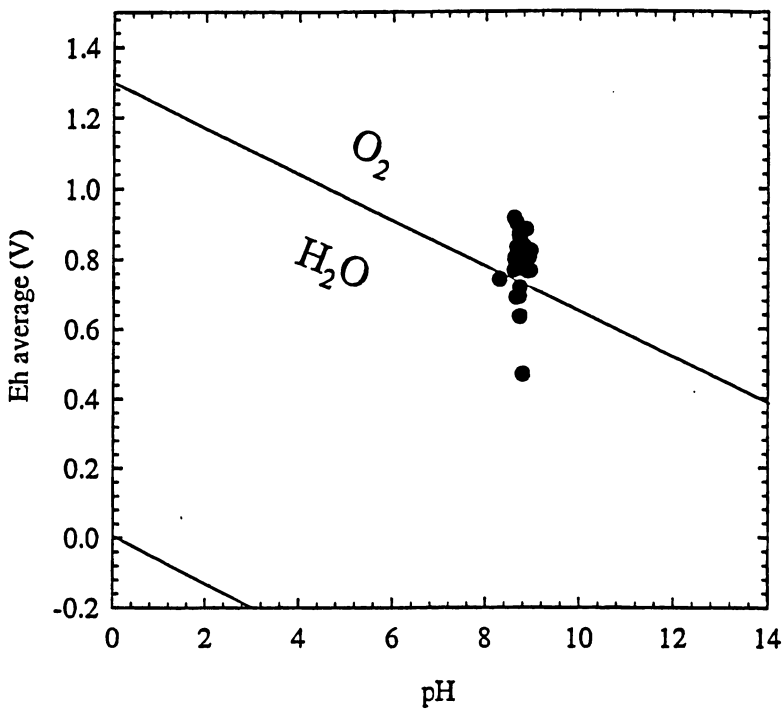

Figure 2.1 Measured Eh-pH from the CWW DS.

2.3 Natural Analog for Lead Mineralization (South Greenland)

The formation of lead phases under oxidizing conditions is not well understood, especially for plattnerite (PbO_2). Numerous workers have noted the presence of lead carbonates and the lead oxide polymorphs, litharge and massicot as oxidation products of native lead. However, plattnerite is rarely found in natural environments owing to the extreme conditions under which it forms.

A unique and rare occurrence of native lead and associated phases is located in the Ilimaussaq Alkaline Complex (IAC) of southern Greenland. This locality may provide a natural analog for the formation and alteration of scales found in lead drinking water pipe materials including the rare phase plattnerite. Although the rates, time, and temperature of hydrothermal fluids may not correspond exactly to those in drinking water pipes, the oxidation states ranging from native lead to highly oxidized fluid, do correspond the phases formed and processes.

A series of alkaline igneous complexes was intruded into the granites of the Ketilidian mobile belt of southern Greenland during the Middle Proterozoic Gardar period (Esher and Watt, 1976). The Ilimaussaq Alkaline Complex (IAC) is located in the eastern area of the Gardar rocks and is approximately 1,168 million years old. The IAC was formed by a pulsing of cylindrical igneous stock emplacements that produced a distinctive "igneous-ring-dike-like" structure, strikingly similar to the well studied Magnet Cove, Arkansas intrusion. A geological map of the intrusion is

included in Figure 2.2. Major rock types in the vicinity of the area of study include (from the inside towards the outside of the complex) kakortokite, a marginal pegmatite, and an augite-syenite along the border. Phases that make up these rock types are included in Table 2.1.

Rock Type	Phases Present	
Kakortokite	alkali feldspar +	$(K,Na)(Al,Si)_4O_8$
	nepheline +	$(Na,K)AlSiO_4$
	eduialyte +	$Na_{15}Ca_6Fe_3Zr_3Si(Si_{25}O_{73})(O,OH,H_2O)_3(OH,Cl)_2$
	aegirine +	$NaFe^{+3}Si_2O_6$
	arfvedsonite	$Na_3(Fe^{+2},Mg)_4Fe^{+3}Si_8O_{22}(OH)_2$
	Accessories:	
	sodalite +	$Na_4Al_3Si_3O_{12}Cl$
	aenigmatite +	$Na_2Fe_5TiSi_6O_{20}$
	rinkite +	$(Ca,Ce)_4(Na,Ca)_3(Ti,Nb)(Si_2O_7)_2(O,F)_4$
	fluorite +	CaF_2
	loellingite	$FeAs_2$
Marginal Pegmatite	arfvedsonite 50% +	$Na_3(Fe^{+2},Mg)_4Fe^{+3}Si_8O_{22}(OH)_2$
	microcline 50%	$KAlSi_3O_8$
	Accessories:	
	albite +	$mNaAlSi_3O_8$ with $nCaAl_2Si_2O_8$
	natrolite +	$Na_2Al_2Si_3O_{10}\bullet 2H_2O$
	aegirine +	$NaFe^{+3}Si_2O_6$
	stillwellite +	$(Ca,La,Ca)BSiO_5$
	Li-mica +	$K(Li,Al)_3(Si,Al)_4O_{10}(F,OH)_2$
	native lead +	Pb
	galena +	PbS
	sphalerite +	ZnS
Augite-Syenite	alkali feldspar +	$(K,Na)(Al,Si)_4O_8$
	olivine +	$(Fe,Mg,Mn,Ni)^{+2}{}_2SiO_4$
	ferroselite +	$FeSe_2$
	ferropargasite	$NaCa_2(Fe^{+2},Mg)_4Al(Si_6Al_2)O_{22}(OH)_2$
	Accessories:	
	titano-magnetite +	$Ti\ Fe^{+2}Fe^{+3}{}_2O_4$
	apatite	$(Ba,Ca,Ce,K,Na,Pb,Sr,Y)_5((As,P,Si,V)O_4)_3(F,Cl,OH)$

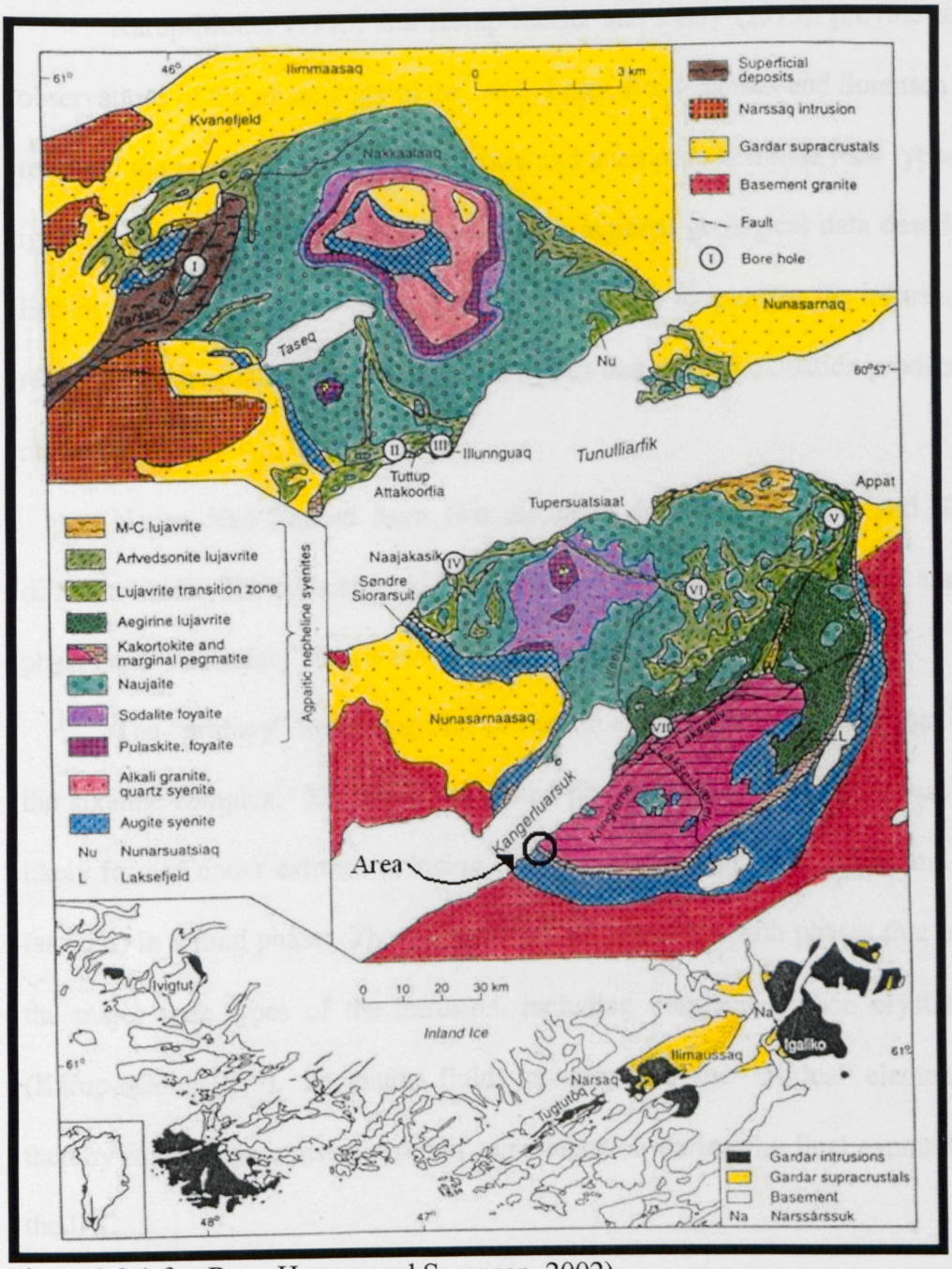

Figure 2.2 (after Rose-Hansen and Sorensen, 2002)

Karup-Moller (1975) and Karup-Moller and Pauly (1979), provide detailed, observations of the mineralogy of the IAC. Later, Rose-Hansen and Sorensen (2002) revisited the area to geophysically explore and attempt to correlate rock types of the igneous intrusion. Their data, coupled with regional geological data described by Escher and Watt (1976), provide a means with which to interpret the influences and relative timing of late structural and fluid events that yielded oxidation products from native lead.

Native lead formed from two distinctly different processes and likely at different times. The difference will be noted by "primary" native lead and associated phases and "secondary" native lead and associated phases.

The "primary" lead phases are present in the marginal pegmatite that borders the alkaline complex. These and associated phases are listed below. These phases likely formed under extreme reducing conditions with significant sulfur and carbon (as CH_4) in a fluid phase. These conditions are consistent with phases that make up the major rock types of the intrusion, including inorganic carbon crystallization (Karup-Moller,1975). Pegmatite fluids concentrated the residual elements, and thereby forming an unusual array of mineralization during the final events forming the IAC.

Reaction Path on Figure 2.3	Primary Lead and Associated Phases	Chemical Formula
(#1)	Native lead + galena	Pb +PbS
(#1)	Native lead + sphalerite	Pb + ZnS
(#1)	Native lead + galena + loellingite	Pb + PbS + $FeAs_2$

Table 2.2

The "secondary" lead phases are located on the surface of a fault plane that cuts through the kakortokite, marginal pegmatite, augite-syenite rock types at the area indicated in Figure 2.2. The lead phases and their associations are listed below in Table 2.3.

Reaction Path on Figure 2.3	Secondary Lead Phases	Chemical Formula	Host Rock
(#2)	Native lead → litharge → hydrocerussite	Pb→ PbO → $2PbCO_3Pb(OH)_2$	Marginal Pegmatite
(#3)	Native lead → plattnerite	Pb → PbO_2	Kakortokite

Table 2.3

The formation of the "primary" lead phases exhibit a very different genetic pathway than that of the "secondary" lead phases. The "primary" phases formed under extremely reducing conditions and high sulfur concentrations (Figure 2.3: reaction path #1). The "secondary" phases represent a lead remobilization event under highly oxidizing conditions, likely supergene (Karup-Moller, 1975) (Figure 2.3: reaction paths #2 and #3). This difference may likely be the result of a separate fluid event associated with late-stage faulting. The reaction path #3 branches off from reaction path #2 and reaches a higher redox potential. Reaction #3 is only observed where the fault plane cuts the kakorkite, a rock type rich in chlorine and fluorine, in contrast to the reduced sulfur-bearing pegmatite. Thus the plattnerite is associated to a more oxidized host rock. Because only a relatively small area of plattnerite mineralization occurred, it is likely that the concentration of chlorine and fluorine species present (as indicated in the mineralogy of phases in rock types) was not great enough to dominate Eh. Drinking water distribution systems are also likely reach this stability field of plattnerite because the water is treated with an oxidant (e. g. free chlorine as a disinfectant).

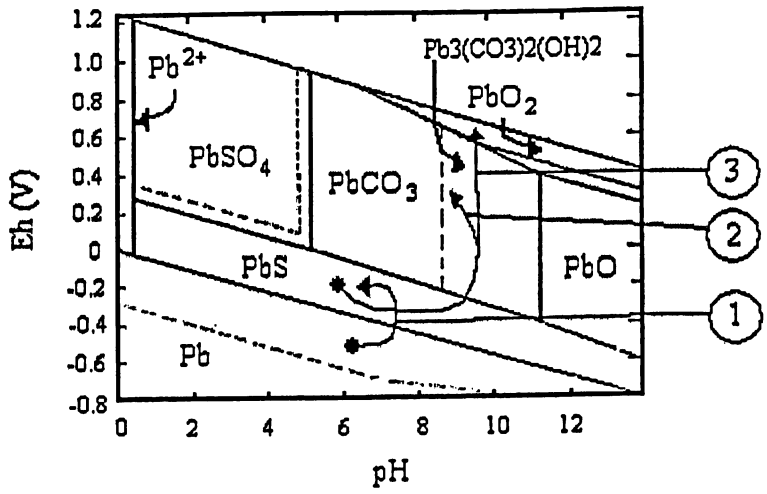

Figure 2.3 Relative reaction paths of lead mineralization from the Ilimaussaq Alkaline Complex (plotted on Brookins, 1988) The assumed activities of dissolved species include Pb= $10^{-6,-8}$, C= 10^{-3}, S=10^{-3}

3.0 METHODS

3.1 The Loop Apparatus System

A test loop apparatus was constructed by IT Corporation (now operating as Shaw Company) based on a previous design developed by Stan Tackett. The construction of the loop apparatus system was funded through the US EPA.

The test loop apparatus consisted of a 100-liter water reservoir connected to eight parallel test loops by polyvinylchloride (PVC) pipe. The reservoir for the test water had a recirculation pump system and a separate pump system to bring test water to the loops. All pump components in contact with the test water were constructed of metal-free materials (Figures 3.1, 3.2, and 3.3).

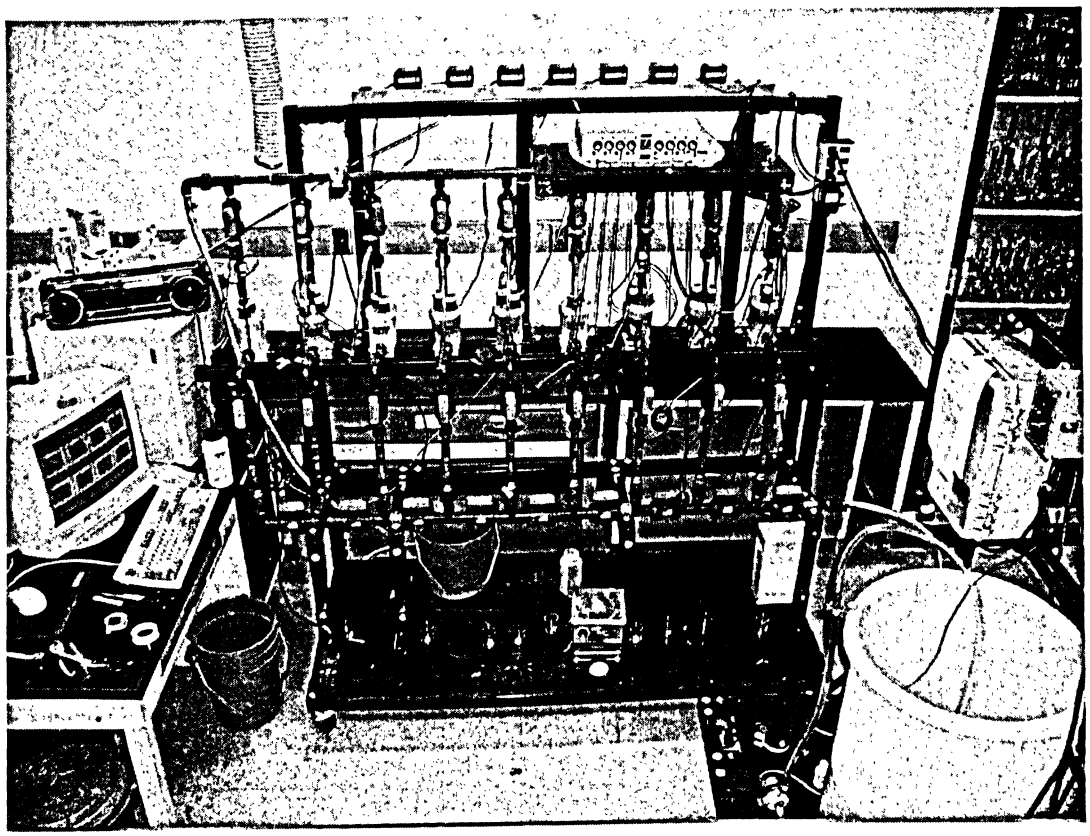

Figure 3.1. Loop Apparatus System (Stonesifer et al., 2002)

Figure 3.2 One Loop

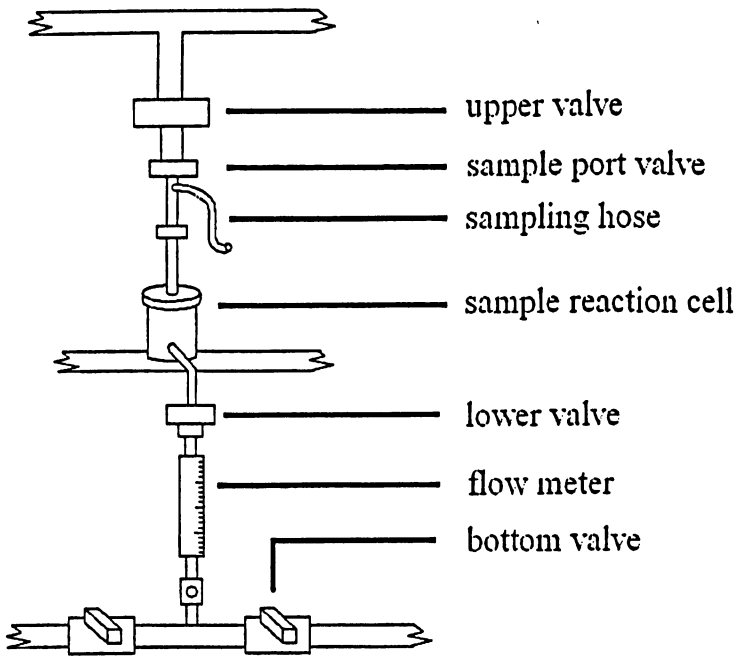

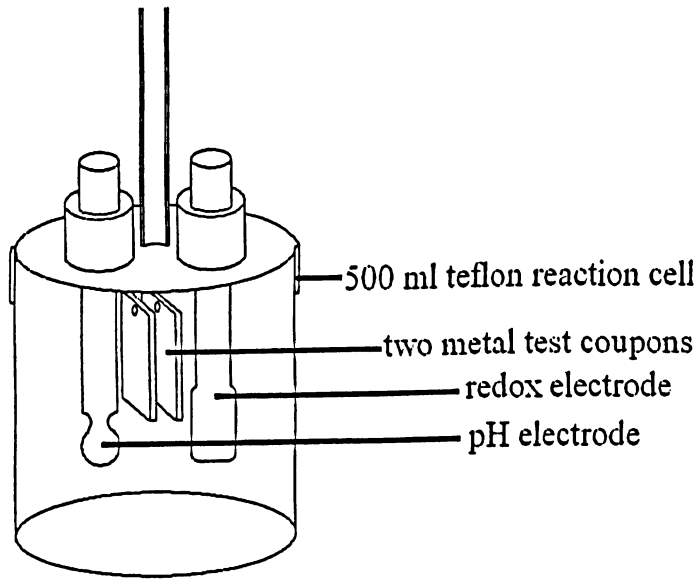

Figure 3.3 Reaction Cell

Each test loop (figure 3.2) contained one approximately 500-ml sample reaction cell (figure 3.3). The sample holding cells were equipped with ports for pH and redox potential electrodes. Two 1''x 2''x 1/8'' (2.4 cm x 4.8 cm x 0.3 cm) metal coupons with a total surface area of 9.5 in^2 (61.29 cm^2) yielded a surface area to volume ratio of 0.02 in^2/ml (0.13 cm^2/ml). The system simultaneously ran two reaction cells (duplicates) of each metal as an internal check of reproducibility. The metal coupons used in this study included pure lead, red brass, pure copper, and pure iron. However, only lead and red brass data will be reported in this thesis.

The experiments were initiated by the preparation/adjustment of the test water, which included adding free chlorine to a concentration of 3 mg/L, dissolved inorganic carbon (DIC) to a concentration of 10 mg/L, and adjusting the pH to 7 with

HCl and NaOH. The sample cells were then flushed at a flow rate of 80 ml/minute, followed by filling the sample holding cell from the reservoir. The basic test water chemistry is given in table 3.1. A 24-hour (or 72-hour for the weekends) stagnation time was maintained before sampling. Samples were drawn out of the cell through a sample valve port at a flow rate of approximately 80 ml per minute. Water samples were analyzed for the concentration of metal(s) via inductively coupled plasma atomic emission spectrometer (ICP-AES).

Analyte	Average Concentration (ppm)
Chloride	15
Sodium	24
Total Inorganic Carbon	10
Total Alkalinity	30
Free Chlorine	3 or 0
Dissolved Oxygen	saturated

Table 3.1 Average test water chemistry (Stonesifer et al., 2002)

3.2 Jensen on-line data collection system

An eight–port-on-line computer hardware/software (Jenson Systems) data collection system recorded the redox potential and pH of the sample cells every ten minutes for the 24- and 72-hour stagnation times.

3.3 Electrodes and Calibration

3.3.1 pH Electrodes

The pH of the test water was measured with a Hach Company EC40 bench top pH/ISE meter (model 50125) and a Hach Company combination pH electrode (model 48600) with temperature corrections. The electrodes were standardized daily using a two point calibration with pH 7 and 10 standard solutions.

The reaction cells contained Schott Brand combination pH electrodes and were standardized biweekly using a two point calibration with pH 7 and 10 standard solutions.

3.3.2 Redox Electrodes

The reaction cells contained Schott Pt, Ag/AgCl combination electrodes (model Pt 8281 HD). The electrodes were standardized biweekly using three standard solutions: ZoBell's, Light's, and a commercial Metrohm Redox Solution.

3.3.3 Dissolved Oxygen Electrodes

Dissolved oxygen (DO) was measured with a Hach Company Model DO175 dissolved oxygen meter and a Model 50180 dissolved oxygen probe. The DO electrodes were autocalibrated before daily use and received weekly calibration via the Winkler's Method.

3.4 Metal Coupons

Metal test coupons were purchased from the Metal Samples Company through the IT Corporation (now operating as the Shaw Company). The Material Test Report for the coupons is included in Appendix 2.

A coupon cleaning procedure was adapted from Lytle and Schock (1996) and included the following steps:

Lead
1) cleaned with 0.5% Titrox
2) ultra sonic bath for 10 seconds
3) rinse with DI water
4) rinse with acetone

Red Brass
1) soak in 1:4 HCl for 30 minuets
2) rinse with DI water
3) cleaned with 0.5% Titrox
2) ultra sonic bath for 5 minuets
3) rinse with DI water
4) rinse with acetone

3.5 Chemicals and Reagents

House deionized (DI) water was used to prepare the test water.

Unless otherwise specified, all chemicals used in this study were Analytical Reagent (AR) grade. Ultra pure nitric acid, HNO_3, was used to preserve samples for metals analysis using 1.5 ml/L sample. Dilute 0.6 M HCl and 0.5 N NaOH were used to adjust the pH. Sodium hypochlorite was used as the source of free chlorine.

Sodium bicarbonate (Fisher Scientific) was used as the source of dissolved inorganic carbon.

3.6 Palintest

Aqueous lead and copper metal concentrations were measured, during the profiling periods of the study, with a Palintest Instruments Scanning Analyzer SA-1000. The samples were conditioned with Soluprep SP-A tablets and single-use SE-1 pre-calibrated solid state electrodes were used.

3.7 ICP-AES

Metals were analyzed with a Thermo Jarrel Ash 61E® purged inductively coupled plasma atomic emission spectrometer (ICP-AES).

3.8 Total Inorganic Carbon (TIC)

Total inorganic carbon (TIC) was analyzed by a coulometric procedure on a UIC Model 5011 CO_2 coulometer with Model 50 acidification module, operated under computer control.

3.9 X-Ray Powder Diffraction (XRD)

X-Ray diffraction (XRD) was used to identify crystalline phases formed on the test coupons and lead pipes. A Scintag XDS-2000 theta-theta diffractometer with a copper X-Ray tube was used to acquire X-Ray patterns. XRD analysis was either

performed directly on the coupon surface or from scraped material that was mounted on a zero-background quartz plate in an amyl-acetate mount. JADE 6.1 software and the International Center for Diffraction Data database (1997) were used to evaluate x-ray data.

3.10 Scanning Electron Microscopy (SEM)

A Joel JSM-5300 Scanning Electron Microscope was used to analyze corrosion scale morphologies and textures. Semi-quantitative elemental data was acquired, on this instrument by energy dispersive x-ray elemental analysis (EDXA). Initially, samples were carbon coated for better imaging, but later samples were ran uncoated to allow for carbon analysis by EDXA.

3.11 Reflected Light Microscopy

A Zeiss STEMI SV 1 reflected light microscope with a mounted camera was used to analyze solid materials formed on the coupons and pipe sections.

4.0 Baseline Metal-Free Experimental Runs

Establishing the "baseline" effects of the oxidants, free chlorine and dissolved oxygen, on the chemistry of the water itself was an essential step in this study prior to running the loop apparatus system.

Two metal-free baseline experimental tests were set up to evaluate the effect of free chlorine and dissolved oxygen concentrations on the redox potential of a test water using deionized distilled water at conditions of pH 7.00, DIC 10 ppm, and $T=23^0C$. The methods for the preliminary metal-free runs were performed on a smaller scale than that of the loop apparatus system (1 liter vs. 100 liters). The smaller scale set-up provided a low-cost means to monitor, adjust, and sample the test water continually for both runs.

A one-liter cell was equipped with a stir rod, two Orion redox electrodes, a dissolved oxygen meter, and a pH electrode. The pH was continually monitored and adjusted with an on-line automatic Jenson titrator. Sodium bicarbonate was used as the source of DIC and a dilute sodium hypochlorite solution was used as the source of free chlorine. The sodium hypochlorite solution was added in 10 ml increments for the free chlorine run. The system then mixed for 10 minutes to allow the redox electrodes to equilibrate. A 10 ml sample would then be drawn out, for the chlorine run, and tested for free chlorine concentration using a Hach DR/2000 spectrophotometer.

4.1 Experimental Metal-Free Free Chlorine Run

The experimental test run indicated a direct relationship between the concentration of free chlorine and the measured redox potential (Figure 4.1). The measured redox potential rises exponentially with the addition of free chlorine concentrations ranging from 0.15 to 0.5 ppm. The redox potential remains fixed at approximately 0.87 V with free chlorine concentrations from 0.5 ppm to the end of the experimental run at 0.58 ppm free chlorine. Therefore, in this metal-free water system chemistry, the redox potential is controlled by free chlorine beginning at concentrations as low as 0.5 ppm.

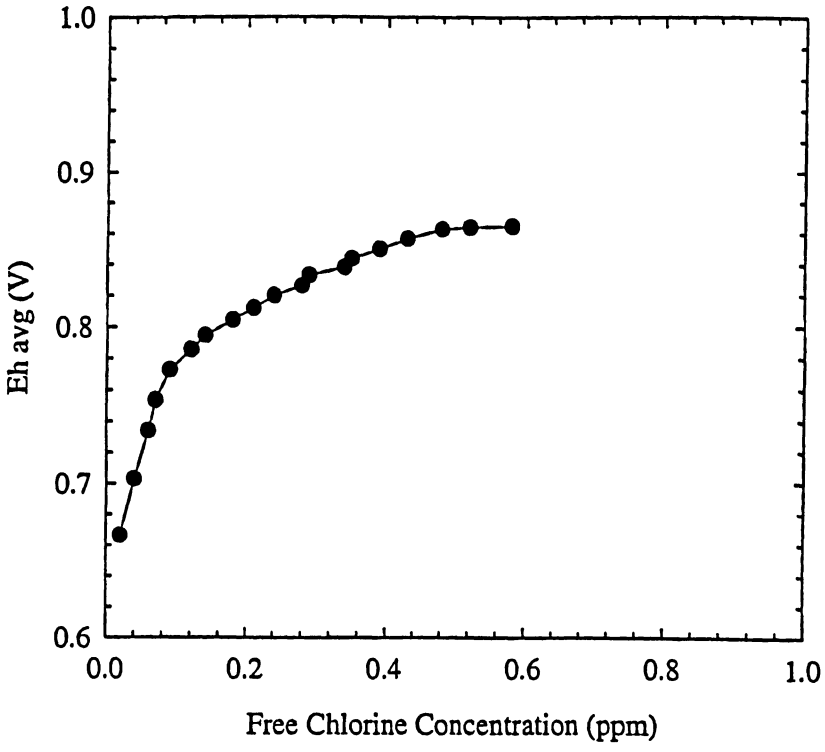

Figure 4.1 Eh vs. free chlorine concentration in distilled deionized water with dissolved inorganic carbon concentration of 10 ppm, pH at 7.00, and T= 23°C.

4.2 Experimental Metal-Free Dissolved Oxygen Run

The initial dissolved oxygen concentration was 0.4 ppm at a temperature of 23°C. The system took up atmospheric oxygen with time. Unexpectedly, the measured redox potential decreased as dissolved oxygen entered the system. This result could be due to the sluggish response of the redox electrodes in the O_2/H_2O system or the problems with electrochemically trying to measure Eh in the O_2 system discussed previously. The experiment shows, however, that Eh reaches a steady value for DO concentrations greater than approximately 4 ppm, compared to approximately 10 ppm in most tap waters and natural surficial waters.

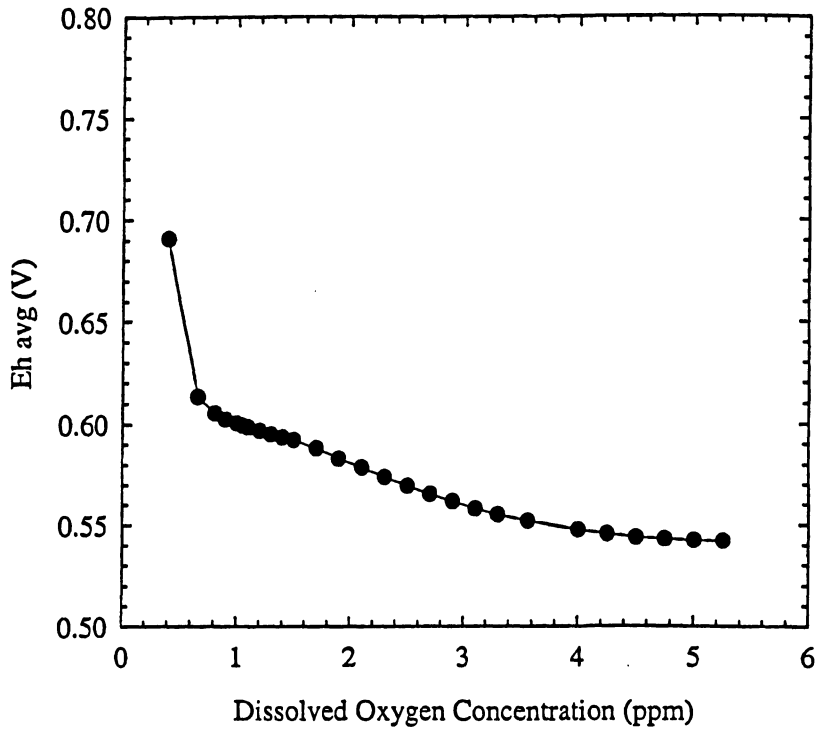

Figure 4.2 Eh vs. dissolved oxygen concentration in distilled deionized water with dissolved inorganic carbon concentration of 10 ppm, pH at 7.00, and T= 23°C.

Taken together, the chlorinated and non-chlorinated runs show that a stable Eh value is reached. For free chlorine, Eh is relatively high at about 0.85 V, whereas the non-chlorinated (dissolved oxygen) system stabilizes lower at about 0.55 V, below the theoretical boundary as shown previously in chapter 2.

5.0 Cincinnati Tap: A Case Study of Lead in Water Pipes

The Cincinnati Water Works (CWW) California Treatment facility, also known as the Miller Plant, has been ranked as one of the best in the country for water quality (CWW, 1999). However, high lead levels (>15 ppb) have been occasionally reported at the consumers' tap. The water quality leaving the facility is regularly monitored for lead and other analytes of concern and data are reported to be under the regulated action levels or below detection their limits (CDM, 2003). The source of the lead may likely come from within the extensive distribution system itself.

Focus has shifted to water chemistry as a means of reducing lead release. By maintaining a pH between 8.7 and 9.0, CWW hopes to prevent any lead carbonate species (cerussite or hydrocerussite) from going into solution and thereby contaminating the system. A serious problem with this approach is the excessive buildup of various carbonate minerals (hydrozincite, calcite, etc.) that either completely clog up the system or increase the pumping cost to the municipality.

The idea of "protective" mineral scales that form on lead pipes may actually prove to be a misnomer or a "double-edge sword" at best. In recent years, an unusual lead phase, plattnerite (PbO_2) has been identified in the CWW DS and in other municipalities nation-wide (Schock et al., 2001). Plattnerite, as discussed previously, is a rare mineral that typically forms under extremely oxidizing conditions as an oxidation product of native lead. Schock et al. (2001) noted that the presence of

plattnerite actually can be regarded as beneficial in that it forms a thin tenacious diffusion barrier that protects the lead pipe surface from reacting with the water. However, dependence on the Jade software alone for the identification of plattnerite via XRD can lead to erroneous results. The identifying peaks of plattnerite overlap those of native lead and the common lead carbonates (cerussite and hydrocerussite). When plattnerite is suspected from XRD analysis, the phases and phase relations should be closely examined by SEM and if possible TEM and an electron microprobe.

The Cincinnati Water Works' Distribution System (CWW DS) has an extensive history that may aid in unraveling the differences in texture and mineralogy of lead pipe sections recovered from known locations. Historical records have provided a rough time-line for the establishment and growth of the CWW DS.

- 1828- First iron pipe laid
  - Primitive wooden pipe distribution system
  - Reservoir of Ohio River water
- June 1839 -The City of Cincinnati took possession of the Cincinnati Water Works, assets included:
  - 3rd Street Reservoir, two pumping engines, 3.5 miles of iron and 19 miles of wooden pipe
- 1845 - Extensions to pipelines
  - New 20-inch iron supply pipe from the pumps to the reservoir
- 1846 - A new pump was installed at the Front Street Plant
- 1853 - A new and larger 3rd Street reservoir
- 1851 & 1854- Acquisition of two new steam engines
- 1866 - Eden Park reservoirs for "hilltop residences"

- 1874 - Began pumping *from/to Eden Park?*
- 1880 - 46-inch main laid from 3rd Street reservoir to Eden Park
- 1881 - Western Hills residence receive city water service
- 1890 - "auxiliary plant" became operational
- 1893 - Cumminsville pumping station
- 1884 - Eden Park Station
- 1896 - "reconstruction" of the Hunt Street Station
- January 1907 -Main Pumping Station (2526 Eastern Ave.) began serving "high pressure mains"
- November 1907 -All City water now filtered through the California filtration plant
- 1907 - Western Hills Station
  - Extension of service to the western portion of the City
  - Abandoned Eden Park and Mt. Hope pumping Stations
- 1908 - Abandoned Westwood Station
- 1912 - Two large storage tanks present on Ferguson Road
  - Western Hill station began service to Price Hill, Westwood, Cheviot, Mt. Airy, College Hill, Mt. Healthy, and Fairmount
- 1914-1915 -Two more pumping engines at the Western Hill station
- 1918 - Service main through Norwood
- 1925 - Eastern Hills reservoir
- 1927 - Mt. Airy reservoir
  - "supply" to St. Bernard
- 1930 - Severe drought
  - CWW began keeping records of consumption and filtration
- 1931 - First noted pollution: taste and odor problems + sewage
  - Chlorinators were installed at the California plant
- 1937 - New Western Hills electric pumping station
  - Improvements made to the California plant
  - Extension of "many miles" of new pipe
  - The Flood of 1937

(Hopkins et al., 1938)

5.1 Cincinnati Tap: Aqueous Data

Cincinnati Water Works' Miller Plant at California (OH) source water is 100% Ohio River water that undergoes filtration and receives free chlorine as a disinfectant. CWW also derives water from groundwater wells for its, Bolton Plant, whose output is sent to northwestern parts of the City. All of the samples in the current study are from the Miller Plant service area. Samples were analyzed for metal levels, total inorganic carbon (TIC), sulfate, phosphate, ammonia, dissolved oxygen (DO), pH, Eh, temperature, and free chlorine. Two data sets were evaluated for this study. The author sampled for three months with complete ICP data, and a Co-op student sampled for ten months with incomplete ICP data. ICP data show a fluctuation of analyte concentration that parallels storm events and seasonal changes. The dominant analyte in Cincinnati tap water is sulfate, which ranges in concentration from approximately 50 ppm to 120 ppm (Figures 5.2 and 5.3). The second most abundant analyte is the measurement of total alkalinity, reported here as ppm $CaCO_3$ (Figures 5.1 and 5.3). The concentrations of total alkalinity are closely parallel to those of sulfate (Figure 5.3). The concentration of dissolved oxygen was always recorded as saturated at the sample temperature.

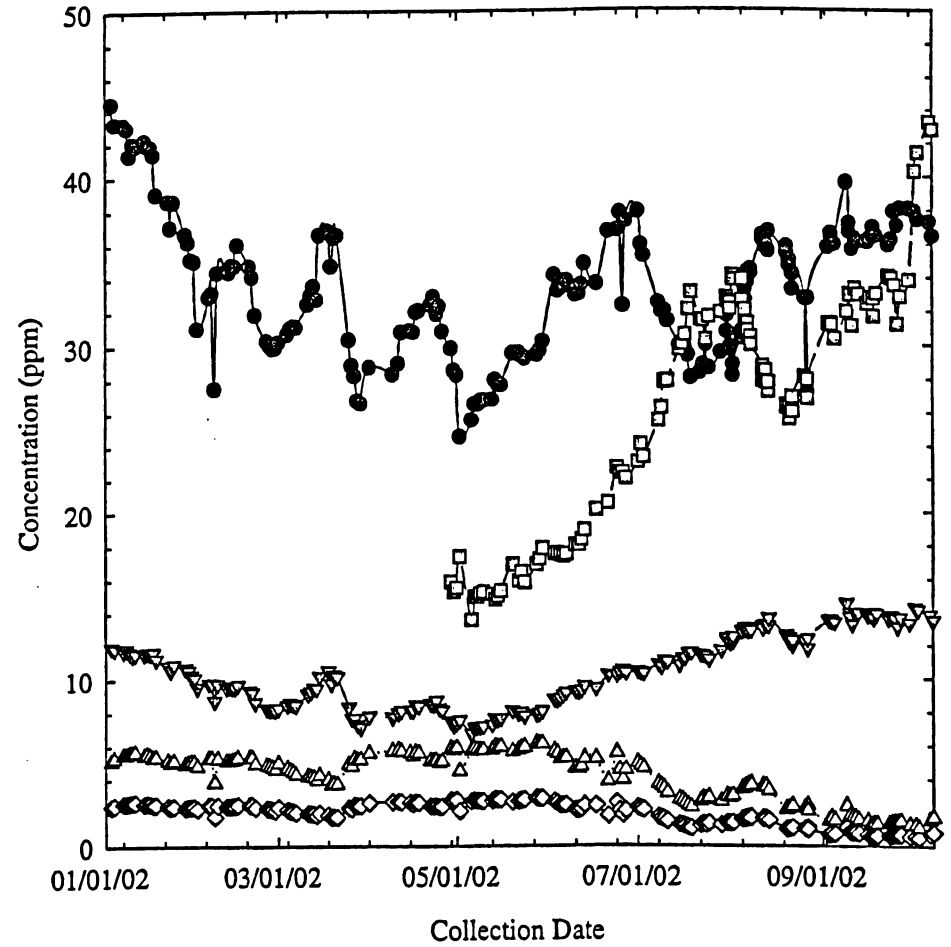

Figure 5.1 Annual Cincinnati Water Works Tap Aqueous Data of cation analytes present in concentrations greater than 1.00 ppm. Data collected by Ian LaSeke.

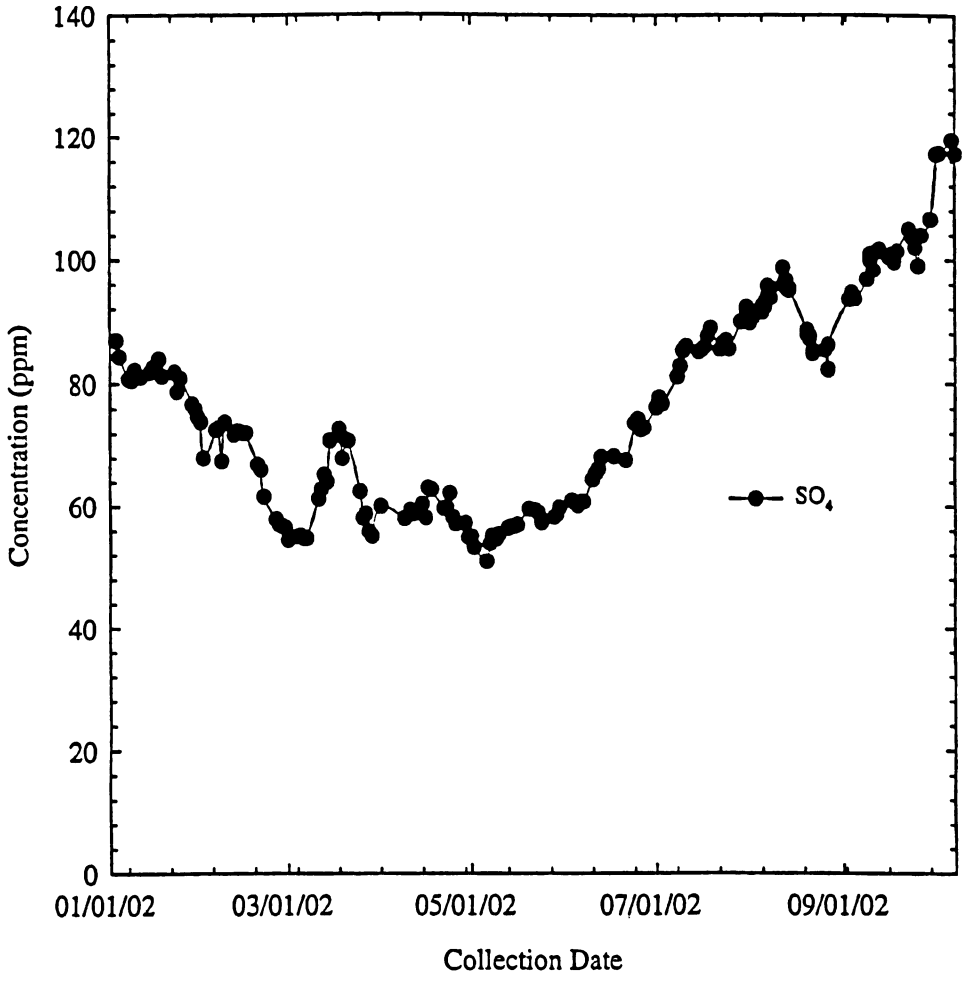

Figure 5.2 Annual Cincinnati Water Works Tap Aqueous Data of anion analyte present in concentrations greater than 1.00 ppm. Data collected by Ian LaSeke.

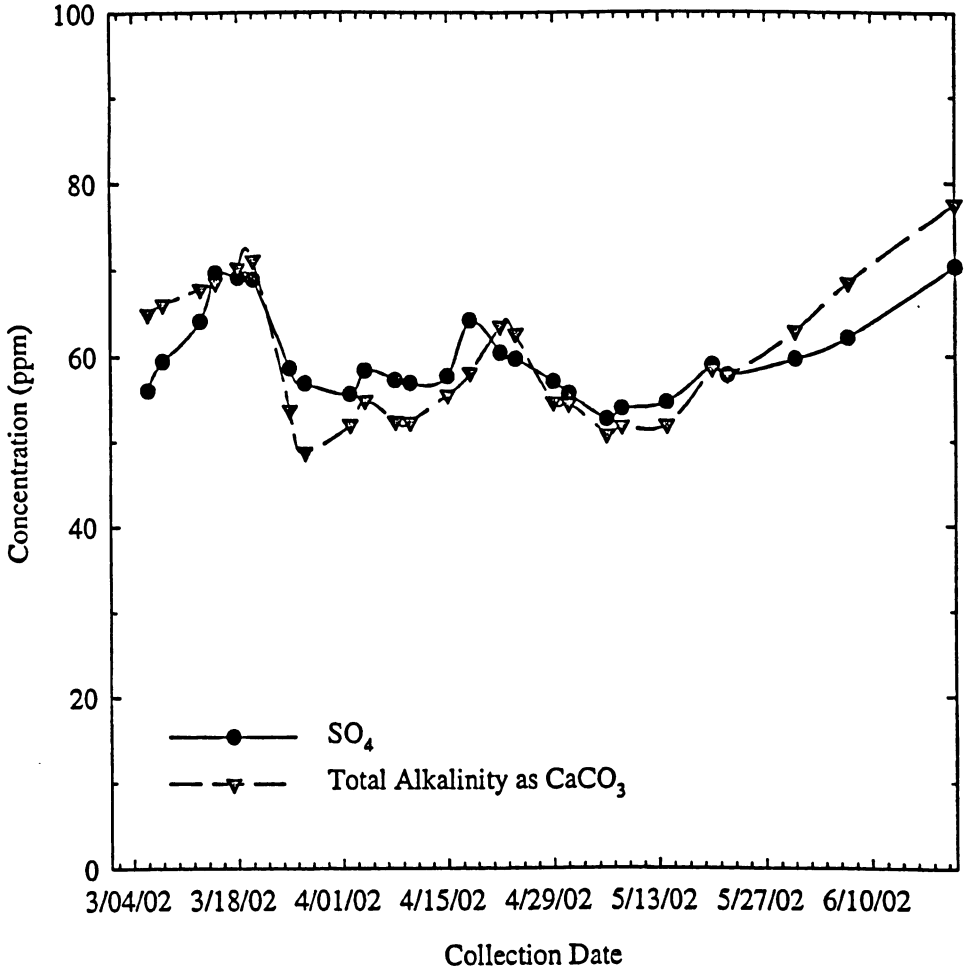

Figure 5.3 Monthly Cincinnati Water Works Tap Water Aqueous Data of anion analytes present in concentrations greater than 1.00 ppm.

The pH of the tap water samples ranged from 8.3 to 9.0. The recorded Eh and measured free chlorine concentrations appeared to be positively correlated at low concentrations of free chlorine. However, at average concentrations of free chlorine (~1.00 ppm), the Eh was relatively consistent (except for minor fluctuations in pH). Cincinnati tap water data are located in Appendix 2.

5.2 Cincinnati Tap: Solids Data

Three lead service line pipe sections were evaluated for this study. The pipes were recovered from known localities within the Cincinnati Water Works distribution system emanating from the Miller treatment plant at California, Ohio. The pipes were cut into approximately 2-inch half sections and analyzed via reflected light microscopy. The scale materials were then scraped and analyzed with x-ray powder diffraction (XRD), and scanning electron microscopy (SEM)-for two of the three samples.

Sample OHCICAT1 represents a section of the Cincinnati Water Works Distribution System (CWW DS) that is approximately 62 years old. The service line was emplaced c. 1940 based on the development of the neighborhood and historical growth of the CWW DS to that area (Hopkins et al., 1938). This sample is approximately 2.5 cm in length.

XRD analysis of sample OHCICAT1 indicated the presence of abundant hydrocerussite ($2PbCO_3Pb(OH)_2$), traces of plattnerite (PbO_2), and poorly crystalline litharge (PbO) (Table 5.1). XRD peaks cannot directly quantify the weight percent of phases present. However, the relative peak intensities of identified phases were used establish the predominant phases. The broad peaks for litharge indicate that this phase is poorly crystalline. XRD graphs and peak identification reports are in Appendix 2.

Phases	2θ and d-spacing							
Hydrocerussite	19.96 4.44	20.95 4.23	24.67 3.60	27.27 3.26	34.21 *2.61	58.62 1.57	60.49 1.52	62.53 1.48
Plattnerite	25.45 3.49	32.13 *2.78	36.26 2.47	49.18 1.85	52.29 1.68	58.92 1.56	60.60 1.52	62.46 1.48
Litharge	28.68 *3.10	Additional peaks are likely masked by overlapping peaks of other phases						

Table 5.1 Summary of powder x-ray diffraction data from OHCICAT1
* indicates the highest intensity reference peak

The interior of the pipe sample contains an orange-brown rust-colored phase, which may be litharge (PbO), plattnerite (PbO_2), or a mixture, with intermittent light tan spots, likely hydrocerussite ($2PbCO_3Pb(OH)_2$) (Figures 5.4 and 5.5). The corrosion scale exhibits desiccation-like cracks and patches where material has fallen off.

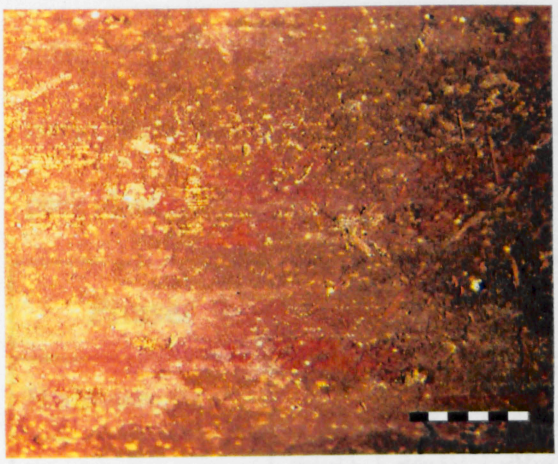

5.4)

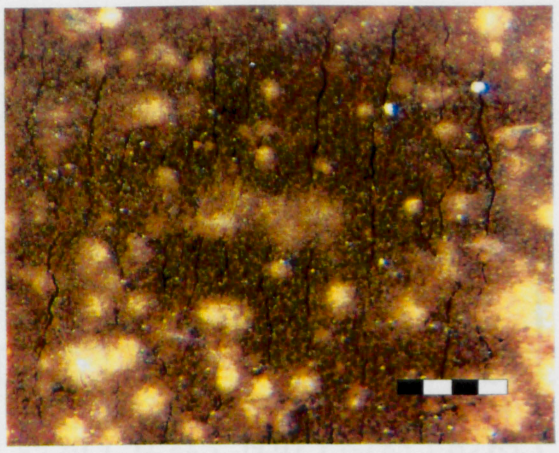

5.5)

Figure 5.4.) Photomicrograph at 10x of sample OHCICAT1.
The scale bar is 0.5 cm in length.
5.5.) Photomicrograph at 66x of sample OHCICAT1.
The scale bar is 0.5 mm in length.

Sample OHCIJUN1 represents a section of the CWW DS that is approximately 90 years old. The house was built in 1870. The Westwood neighborhood was annexed by the City in 1896 (Ahr, 1988), though the CWW DS may not have reached this area until c. 1912 (Hopkins et al., 1938). This sample is approximately 5.0 cm in length.

XRD analysis of sample OHCIJUN1 indicated the presence of abundant hydrocerussite ($2PbCO_3Pb(OH)_2$), common plattnerite (PbO_2), trace cerussite ($PbCO_3$), and poorly crystalline litharge (PbO) (Table 5.2). XRD peaks cannot

directly quantify the weight percent of phases present. However, the relative peak intensities of identified phases were used establish the predominant phases. The broad peaks for litharge indicate that this phase is poorly crystalline. XRD graphs and peak identification reports are in Appendix 1.

Phases	2θ and d-spacing							
Hydrocerussite	19.94 4.44	20.94 4.23	24.76 3.59	27.22 3.27	34.22 *2.61	58.92 1.56	60.46 1.52	62.50 1.48
Plattnerite	25.51 3.48	32.10 *2.78	36.28 2.47	49.20 1.85	52.22 1.75	59.07 1.56	60.85 1.52	62.65 1.48

Table 5.2 Summary of powder x-ray diffraction data from OHCIJUN1
* indicates the highest intensity reference peak

SEM analysis of the scraped scale was performed. SEM identified a nano-sized "crusty" to dendritic, irregular material (Figure 5.6). No other morphologies were seen. Further EDXA semi-quantitative analysis yielded lead: carbon: oxygen ratios for the abovementioned material (Table 5.3). EDXA data are shown in Appendix 1. Small amounts of iron and manganese that were found are treated as "Pb" for the purpose of calculating the weight percent ratios.

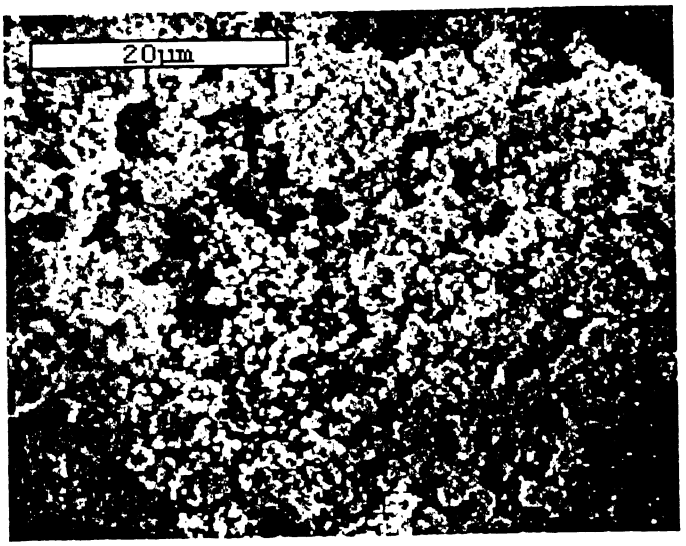

Figure 5.6

	Measured Pb	Measured C	Measured O	Likely Phase
1	78.65 %	7.52 %	10.60 %	Hydrocerussite 80:4:16
2	75.68 %	8.21 %	12.74 %	Hydrocerussite 80:4:16
3	71.95 %	10.82 %	14.94 %	Hydrocerussite 80:4:16

Table 5.3

The interior of the pipe sample consists of at least three morphologies. There is a background orange-brown rust-colored phase, possibly litharge (PbO), with numerous white and orange spots, likely hydrocerussite ($2PbCO_3Pb(OH)_2$) plus cerussite ($PbCO_3$), and dark brown to black "growths" that may be plattnerite (PbO_2). The spots and "growths" appear to be alteration products of the background

orange-brown rust-colored phase at various stages of development. The formations of spots appear to start as small orange spots and/or series of spots that alter to a white phase. This is represented in the larger white spots haloed by orange. Approximately 10 percent of these white spots contain a dark brown to black "growth" in its center. The remaining white spots may at one time have contained "growths", but the "growth" phase may had been dislodged and deposited elsewhere in the distribution system. (Figures 5.7 and 5.8).

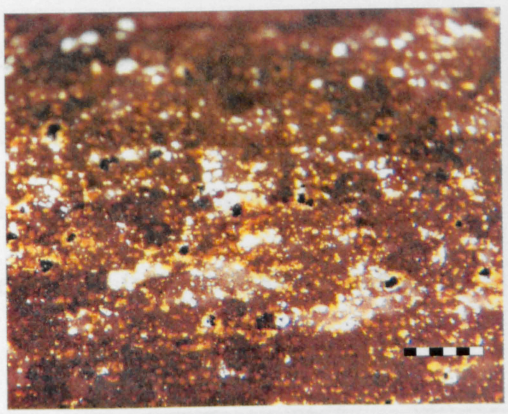

5.7)

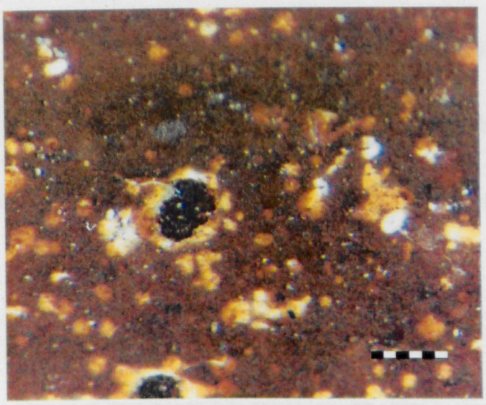

5.8)

Figure 5.7) Photomicrograph at 10x of sample OHCIJUN1.
The scale bar is 0.5 cm in length.
5.8) Photomicrograph at 50x of sample OHCIJUN1.
The scale bar is 0.5 mm in length.

Sample OHCIGIL1 represents a section of the CWW DS that is approximately 90 years old. The house was built in 1890. Historic records indicate that the Price Hill neighborhood was annexed by the City in 1870 (Ahr, 1988), though the CWW DS may not have reached this area until c. 1912 (Hopkins et al., 1938). This sample is approximately 3.75 cm in length.

XRD analysis of sample OHCIGIL1 indicated the presence of abundant plattnerite (PbO_2), and subordinate, poorly crystalline phases hydrocerussite ($2PbCO_3Pb(OH)_2$) and litharge (PbO) (Table 5.4). XRD peaks cannot directly quantify the weight percent of phases present. However, the relative peak intensities of identified phases were used establish the predominant phases. XRD graphs and peak identification reports are in Appendix 1.

Phases	2θ and d-spacing							
Plattnerite	25.44 3.49	32.10 *2.78	36.31 2.47	49.18 1.85	52.24 1.74	58.89 1.56	60.87 1.52	62.66 1.48
Litharge	28.68 *3.11	Additional peaks form shoulders at the bases of the overlapping peaks from other phases						

Table 5.4 Summary of powder x-ray diffraction data from OHCIGIL1
* indicates the highest intensity reference peak

SEM analysis of the scraped scale was performed. SEM identified a nano-sized particulate along with larger hexagonal and platy crystalline material (Figure 5.9).

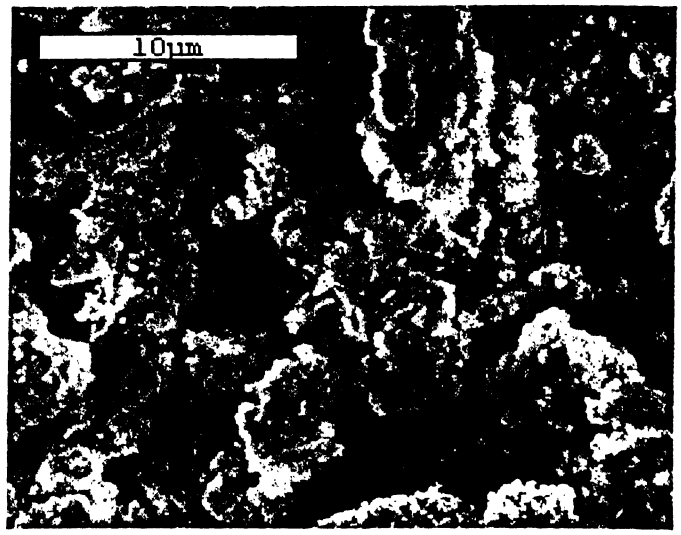

Figure 5.9

Further EDXA semi-quantitative analysis yielded lead: carbon: oxygen ratios for the abovementioned phases (Table 5.5). EDXA data are shown in Appendix 1. Small amounts of iron and manganese that were found are treated as "Pb" for the purpose of calculating the weight percent ratios.

	Morphology	**Measured Pb**	**Measured C**	**Measured O**	**Phase**
1	Platy Crystal	67.23 %	5.7 %	20.51 %	No matches
2	Nano-sized particulate	63.31 %	5.98 %	23.80 %	No matches
3	Nano-sized particulate	60.01 %	7.15 %	25.13 %	No matches

Table 5.5

Visually, the interior of the pipe sample consists of a background red-brown rust-colored phase, possibly litharge (PbO), with numerous white microcrystalline spots, likely hydrocerussite ($2PbCO_3Pb(OH)_2$), (Figure 5.10). The spots appear to be alteration products of the background red-brown rust-colored phase. Underlying the red-brown rust-colored phase is a black phase, most likely plattnerite (PbO_2). The black phase is visible where the red-brown rust colored phase has "flaked" away. The black phase also appears to be altering to the red-brown rust colored phase (Figure 5.11), based on superposition.

5.10)

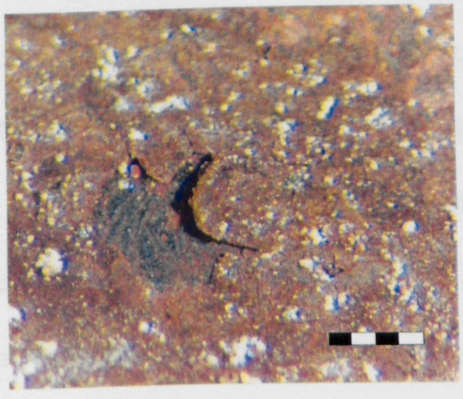

5.11)

Figure 5.10) Photomicrograph at 10x of sample OHCIGIL1.
The scale bar is 0.5 cm in length.
5.11) Photomicrograph at 66x of sample OHCIGIL1.
The scale bar is 0.5 mm in length.

5.3 Cincinnati Tap: Discussion

Pipe sections OHCIGIL1 and OHCIJUN1 are approximately the same age and both were identified as containing plattnerite by XRD among the corrosion products present (Figure 5.12). The pipe section OHCICAT1 is much younger and does not exhibit well crystallized plattnerite. Reflected light microscopy of samples OHCIJUN1 and OHCIGIL1 show strikingly different phase relationships with regard to plattnerite. OHCIJUN1 has black growths as an alteration product. OHCIGIL1 exhibits an underlying thin black layer that appears to be altering to PbO. That is, both of the samples that unquestionably contain well crystallized plattnerite appear to have formed it in different ways: OHCIGIL1 as a primary phase now being altered and OHCIJUN1, forming as a "super" oxidation product from the breakdown of hydrocerussite to cerussite and litharge and/or massicot ($PbO \rightarrow PbO_2$). If the OHCIGIL1 plattnerite formed as a primary oxidation product, this raises questions on the mechanism of formation. The pipe was laid at least 15 years before any chlorination treatment of the water. How could a dissolved oxygen system reach such high redox potentials to form plattnerite? Why don't we see plattnerite more commonly as a lead corrosion product?

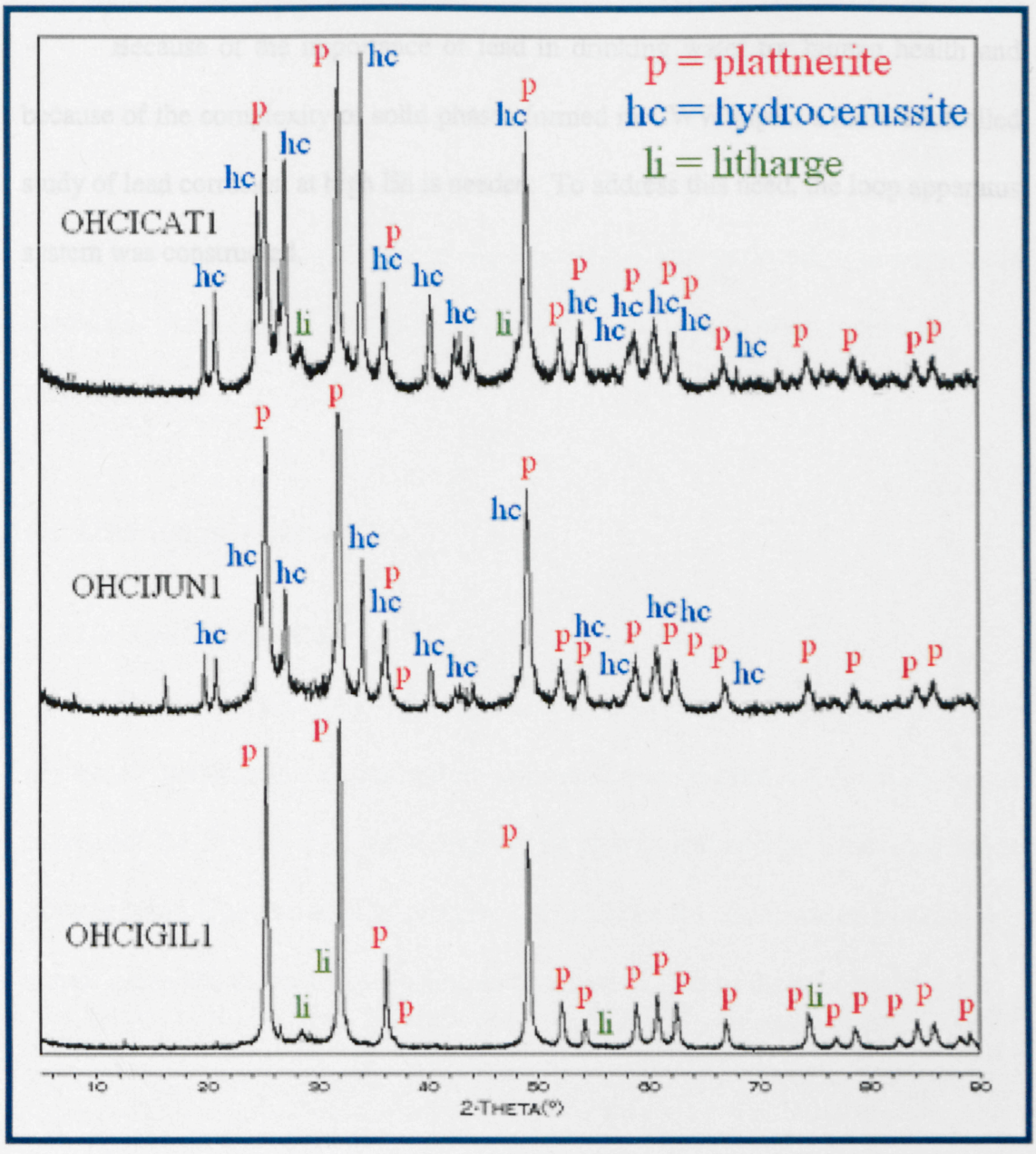

Figure 5.12 XRD patterns from the three CWW samples

Because of the importance of lead in drinking water for human health and because of the complexity of solid phases formed in CWW pipes, a more controlled study of lead corrosion at high Eh is needed. To address this need, the loop apparatus system was constructed.

6.0 LEAD RESULTS FROM THE LOOP APPARATUS

The lead behavior was studied for two separate six-month runs: Chlorinated and Non-Chlorinated (dissolved oxygen). The chlorinated run had a greater initial rate of lead release, greater initial changes in pH and Eh, produced trace amounts of metastable phases (plattnerite and minium), and more overall product than the Non-chlorinated run.

6.1 Lead System: Aqueous Data

6.1.1 Free Chlorine Run

The Eh and pH changes during the 72-hour (weekend) stagnation times were plotted at various points throughout the six month run (Figures 6.1 and 6.2). Redox curves for the first 28 days show the greatest change and exhibit a two-step redox titration curve. This two-step redox curve may indicate the initial rate of free chlorine consumption and the system switching to dissolved oxygen as the primary oxidant.

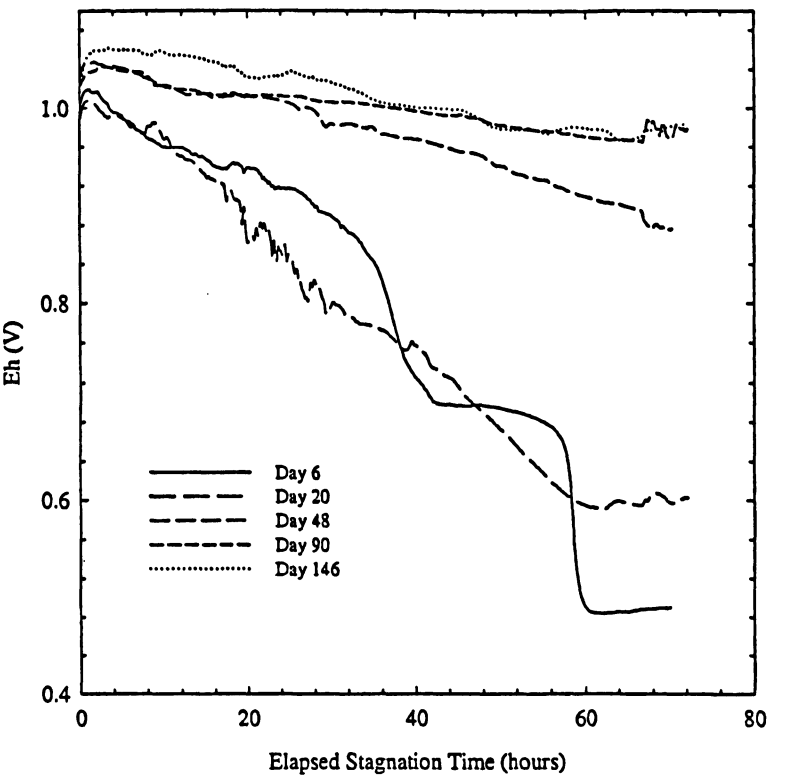

Figure 6.1 Lead 72-hour Stagnation-time Redox Profiles selected at various points throughout the 160-day study. The temperature is approximataly 23°C, pH is at 7.00, free chlorine begins at 3.00 ppm, dissolved oxygen is saturated, and dissolved inorganic carbon is 10 ppm.

(Stonesifer et al., 2002)

pH profiles during the beginning of the study to approximately day 40 showed a pronounced positive change for both the 24- and 72-hour stagnation times (Appendix 3). This positive trend in pH is greatest at day 20 and also parallels a sharp increase in measured lead levels. Lead levels reach as high as 1,100 ppb for a 24-hour stagnation time at approximately day 20 (Figure 6.3). However, the corresponding 72-hour weekend stagnation time had a much lower value (~200 ppb). By day 40, the spike pH and metal levels had "settled down" and a light tan colored

deposit was present on the bottom of both of the lead reaction cells. This deposit will be discussed in Section 6.2.1

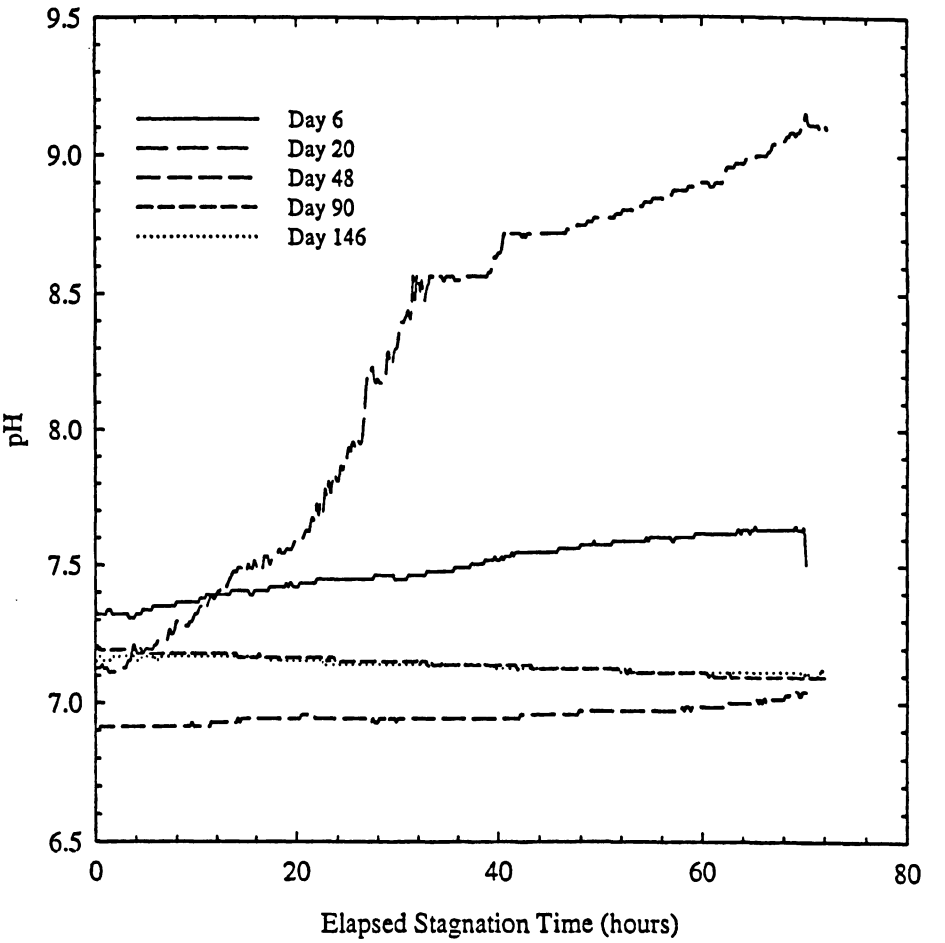

Figure 6.2 Lead 72-hour Stagnation-time pH curves selected at various points throughout the 160-day study. The temperature is approximataly 23^{0}C, pH is at 7.00, free chlorine begins at 3 ppm, dissolved oxygen is saturated, and dissolved inorganic carbon is 10 ppm.

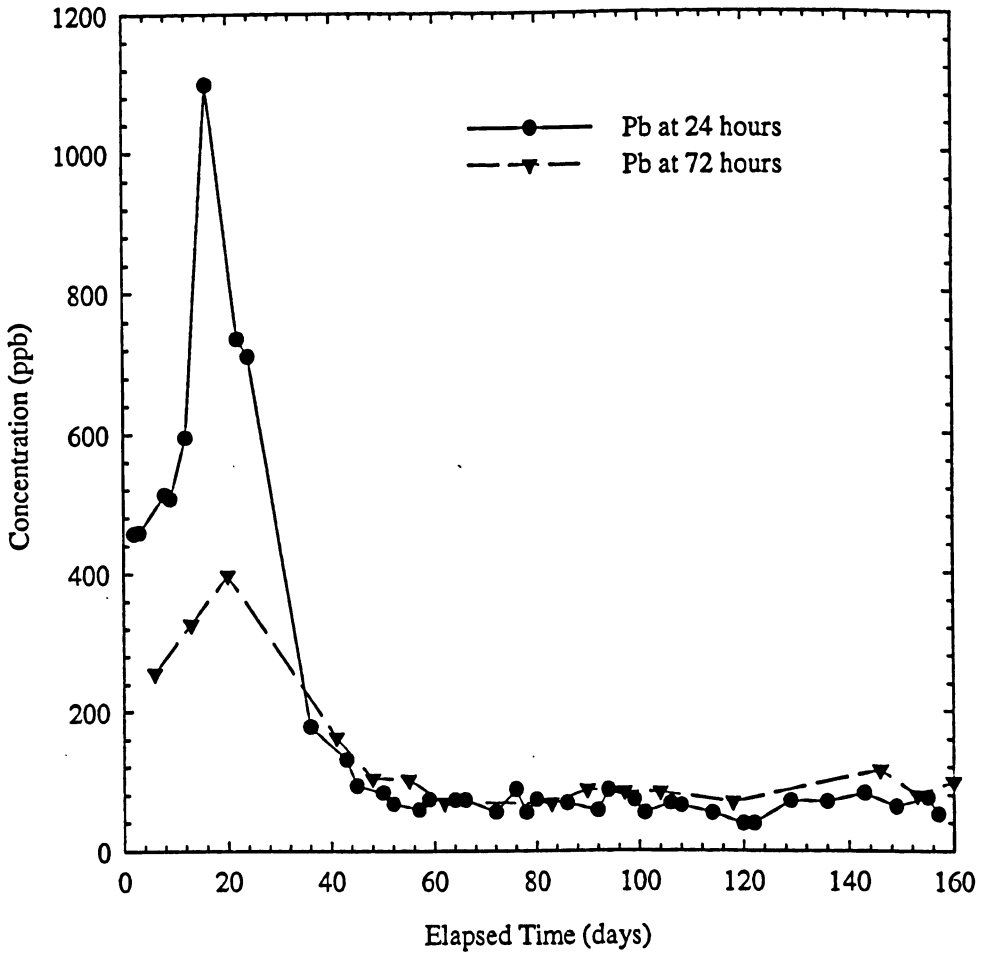

Figure 6.3 Elapsed time versus lead metal release profile for 24- and 72-hour stagnation times for Cell #1.

(Stonesifer et al., 2002)

The lead system changes behavior by day 50. The lead leaching values are lower and steady with respect to stagnation time (approximately 40 ppb for 24-hour and 80 ppb for 72-hour). There is the upward shift and leveling out of the redox curves by day 50. Also, the pronounced positive change in pH for the 72-hour

stagnation time has switched to a slightly negative change in pH. These changes may represent the aging/alteration of the rapidly formed scale deposit.

Figure 6.3 shows a pronounced peak in lead release at approximately day 20 for both 24- and 72-hour stagnation times. The peak for a 24-hour stagnation time is almost three times that of the 72-hour stagnation time. This measured behavior in metal release may represent the formation/release and settling rate of a lead particulate phase. This possibility is further addressed in the discussion section.

6.1.2 Non-Chlorinated Run

Redox profiles were steady throughout the study at ~0.480 V and there were no detectable changes or consumption of DO in the system (Figure 6.4).

6.2 Lead System: Solids Data

6.2.1 Free Chlorine Run

Reflected light microscopic examination was performed at the end of the test run on the exposed lead coupons. There are three morphologies present: small clear to white prismatic crystals, white dendritic to globular phase, and a red-brown rust colored phase(s) (Figure 6.5).

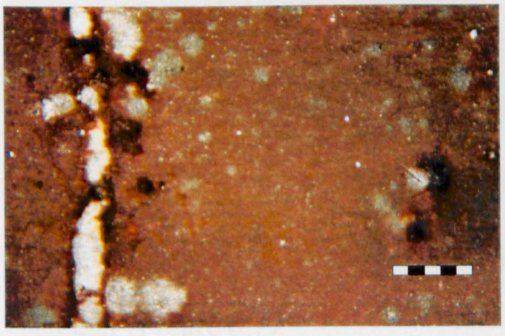

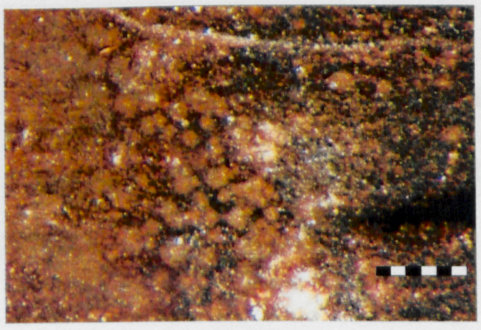

6.5) 6.6)

Figure 6.5) Photomicrograph at 8x of lead coupon Pb111.
The scale bar is 0.5 cm in length. (Stonesifer et al., 2002)
6.6) Photomicrograph at 50x of lead coupon Pb111.
The scale bar is 0.5 mm in length.

The large white clusters are cerussite crystals and form streaks downward, likely a result of nucleation and crystal growth under the influence of gravity. The streaks are from 1.5 to 1.8 cm in length and approximately 1.5 mm wide (Figure 6.5).

These clusters and streaks were the first phase(s) observed to have formed by visual inspection.

The rust-colored phase(s) is/are generally uniform in thickness and in color across the coupon, except for areas around the abovementioned white phase. The rust-colored phase(s) is/are concentrated around the white clusters and streaks. This rust-colored phase likely completely coated the streaks as an alteration product, but may have been lost during sampling.

Late small "sparkly"/microcrystalline gray spots of cerussite were identified via SEM. They appear throughout the coupons and likely formed as an alteration product of hydrocerussite and/or PbO. The spots are approximately 1.5 mm in diameter (Figure 6.7).

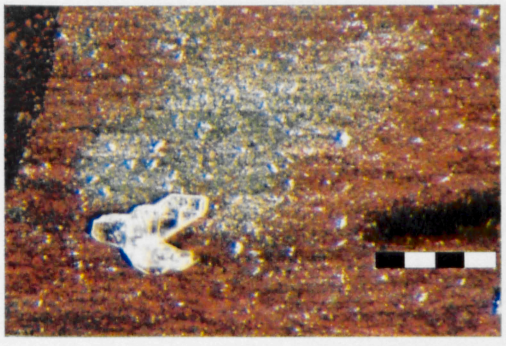

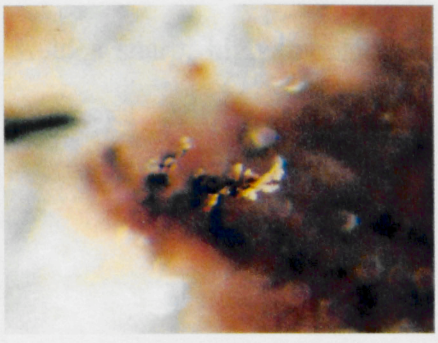

6.7) Photomicrograph at 66x of lead coupon Pb111.
The scale bar is 0.5 mm in length. (Stonesifer et al., 2002)
6.8) Photomicrograph at 66x of lead coupon Pb111.
The scale bar is 0.5 mm in length.

X-Ray Powder Diffraction (XRD) analysis was performed at day 40 for the material scraped from the bottom of cell #1. The analysis yielded five possible phases: cerussite ($PbCO_3$), hydrocerussite ($Pb_3(CO_3)_2(OH)_2$), massicot (PbO), plattnerite (PbO_2), and minium (Pb_3O_4). Visual observations of the material that had formed on the bottom of cell #1 included three distinct morphologies: a hard light tan colored uniform coating, small clear to white prismatic crystals (likely knocked off of the coupons during sampling), and small black "flecks".

XRD analysis of the lead coupons was performed at the end of the test run. No additional material had accumulated in the bottom of cell #1 since day 41. The analysis yielded cerussite ($PbCO_3$) as the dominate phase formed (Table 6.1). Other minor phases present included litharge (PbO), hydrocerussite ($2PbCO_3Pb(OH)_2$), and relic traces plattnerite (PbO_2) and minium (Pb_3O_4). It is important to note that both methods of sample preparation yield a sharp, high intensity, complete x-ray diffraction pattern of native lead.

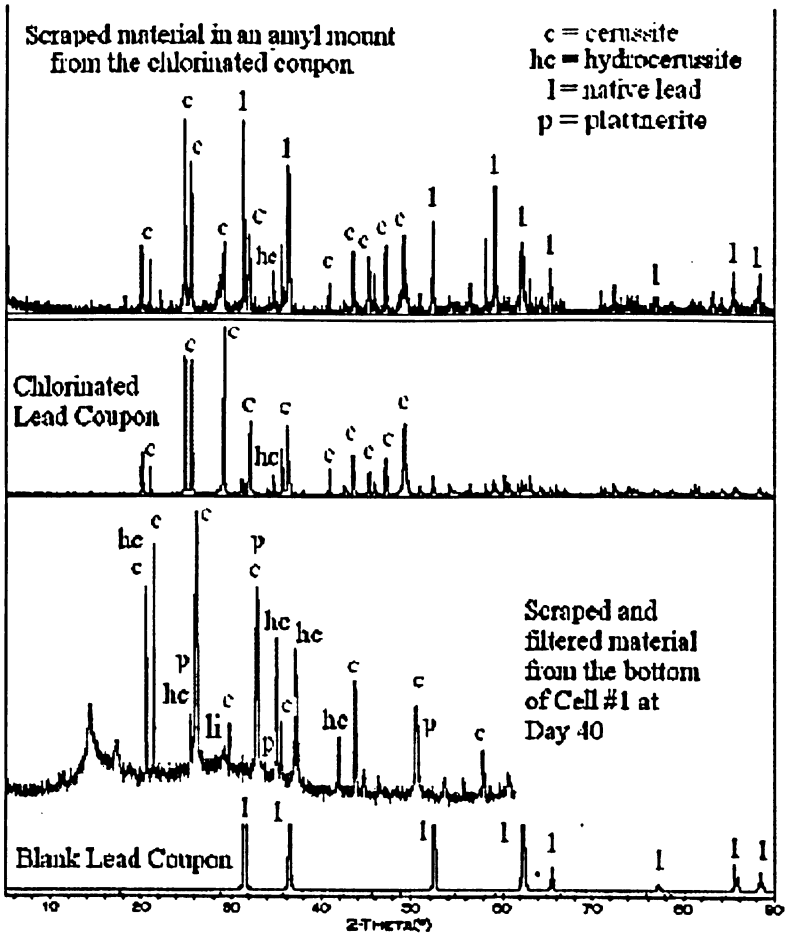

Figure 6.9

Phases	2θ and d-spacing							
Native Lead	31.32 *2.85	36.31 2.47	52.27 1.74	62.18 1.49	65.28 1.42	77.26 1.23	85.47 1.35	88.25 1.10
Cerussite	20.10 4.41	20.93 4.23	24.82 *3.58	25.52 3.48	29.08 3.06	36.16 2.48	49.02 1.85	
Hydrocerussite	Peak broadening at base of overlapping cerussite peaks						26.60 3.34	34.24 *2.61
Litharge	28.64 *3.11	31.88 2.80	48.64 1.87					

Table 6.1 Summary of powder x-ray diffraction data from Pb112 coupon
* indicates the highest intensity reference peak

Material from one lead coupon was then scraped off of the coupon, ground, and mounted with amyl-acetate onto a zero-background quartz plate. XRD analysis of the scraped lead coupon was performed to determine if any preferred orientation, pseudo-stratigraphy or relief of phases affected the results of the initial XRD analysis. No significant differences were noted except that this sample preparation method introduced native lead into the sample as a result of scraping the pure lead coupon.

SEM photomicrography was performed at the end of the test run on the lead coupons. Three distinctive morphologies were identified by SEM: striated rhombohedral crystals, thin platy crystals, and a nano-particulate/nano-crystaline material (Figure 6.10).

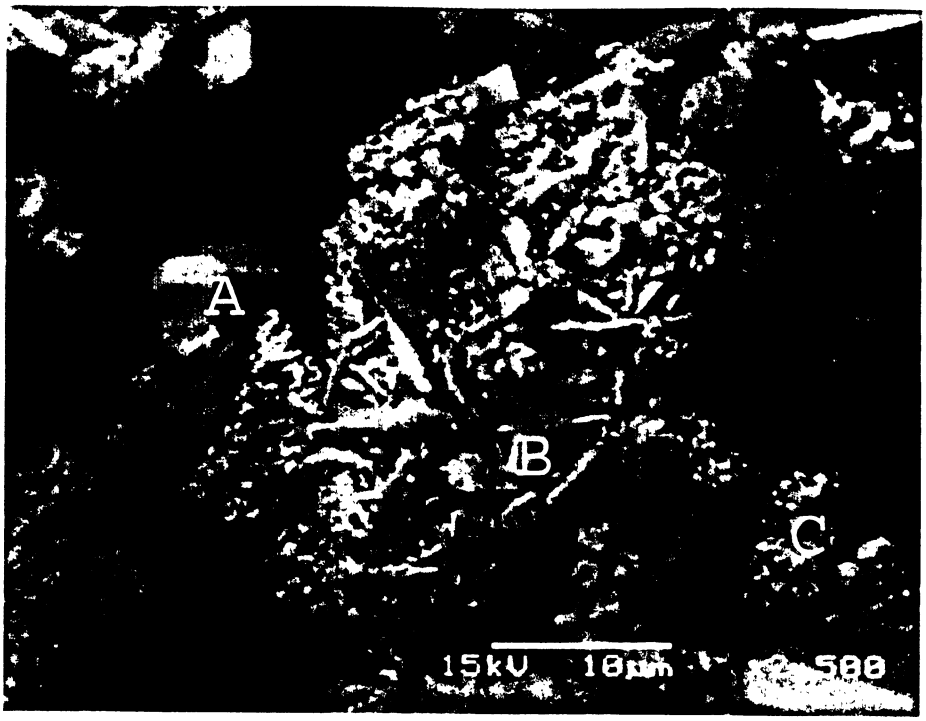

Figure 6.10 SEM back-scatter photomicrograph of the lead coupon

Further EDXA semi-quantitative analysis was attempted, but because of carbon coating of the sample, was not successful (Table 6.2).

	Morphology	Likely Phase
A	Rhombohedral striated crystals	Cerussite
B	Thin Platy crystals	Hydrocerussite (?)
C	Nanoparticulate/ Nanocrystaline material	Litharge, Plattnerite, or mixture (?)

Table 6.2

6.2.2 Non-Chlorinated Run

Reflected light microscopic analysis was performed at the end of the test run on the exposed lead coupons. The primary morphology present consisted of small white prismatic crystals (Figure 6.11). Other phases included a yellow-orange rust-colored phase and a red-brown rust colored phase. Additional lesser phases present included a metallic copper-colored iridescent phase, monoclinic prismatic blue crystals, blue spots, a teal-green phase, and a fluorescent-yellow-green botryoidal phase. All of are likely the result of contamination due to user error based on aqueous data beyond Day 100 that indicated the presence of iron and copper in the pure lead system. Erratic results beyond Day 100 are also seen in the non-chlorine red brass system (section 7.1.2). The most likely explanation is that the proper standard operating procedure for system operation was not implemented regularly. The system likely lost hydrolic head and back-flow occurred from all reaction cells to the pure tank water prior to the daily system flush. As a result, the solution data beyond day 100 have to be treated with caution, but are still useable because the amount of cross-contamination is relativity small.

6.11)

6.12)

Figure 6.11) Photomicrograph at 10x of lead coupon Pb112.
The scale bar is 0.5 cm in length.
6.12) Photomicrograph at 66x of lead coupon Pb112.
The scale bar is 0.5 mm in length.

The coupons are dominated by microcrystalline gray to white uniform coating of cerussite. There are several random globular growths of cerussite on the coupon that have been lightly coated with a very fine-grained rust-colored particulate. The growths are approximately 0.3 mm in diameter (Figure 6.12).

XRD analysis of the lead coupons was performed at the end of the test run. The analysis yielded cerussite ($PbCO_3$) as the dominate phase. Other minor phases present included litharge (PbO), and trace hydrocerussite ($2PbCO_3Pb(OH)_2$).

Phases	2θ and d-spacing							
Native Lead	32.08 *2.78	36.21 2.47	52.31 1.74	62.23 1.49	65.28 1.42	77.26 1.23	85.47 1.35	88.25 1.10
Cerussite	20.14 4.40	20.98 4.23	24.88 *3.57	25.54 3.48	29.14 3.06	36.21 2.47	49.18 1.85	
Hydrocerussite	Peak broadening at base of overlapping cerussite peaks						34.27 *2.61	
Litharge	28.66 *3.11	31.36 2.84	48.72 1.86					

Table 6.3 Summary of powder x-ray diffraction data from Pb211 coupon
* indicates the highest intensity reference peak

Evenly distributed rhombohedral to tabular crystals were identified via SEM. The even distribution of crystals also exhibited a peculiar preferred orientation in patches (Figure 6.13). These patches of aligned crystals form a swirl-like pattern on a larger scale and may have formed in response to currents present during the daily flush of the system. A less common, submicron-scale late phase was also observed (Figure 6.14).

6.13

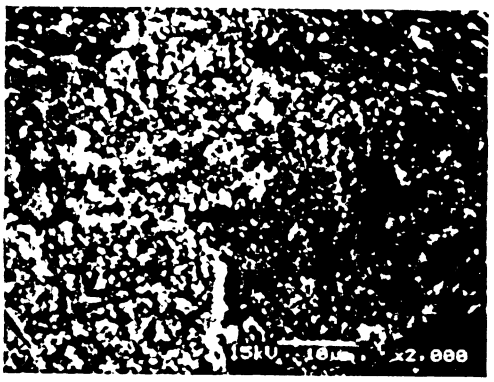

6.14

Figure 6.13) SEM Photomicrograph of lead coupon Pb112.
6.14) SEM Photomicrograph of lead coupon Pb112.

7.0 RED BRASS RESULTS FROM THE LOOP APPARTUS

Brass fixtures within the distribution system and brass household plumbing materials provide another source of lead. A comparison can be made between pure lead and brass for the chlorinated and non-chlorinated systems in terms of the metals released into solution and the corrosion products formed. Brasses include various combinations of copper, ± zinc, ± lead, ± tin. The red brass chosen for this study represents a typical, commonly used "garden variety" brass with an average composition of 78% copper, 11% zinc, 7% lead, 3% tin, and ~1% of iron. The manufactures' solids analysis of metal used for the coupons installed in the loop apparatus system are presented in Appendix 6.

The lead behavior in brass was similar for two separate six-month runs: Chlorinated and Non-Chlorinated (dissolved oxygen). Both runs had an initial elevated lead release values (300 and 200 ppb, respectively) that rapidly dropped off by day 20. A difference between the lead levels released into solution occurred beyond day 20. The chlorinated run yielded overall higher lead values for 24- and 72-hour stagnation times. No lead-containing corrosion products were observed for either run.

Given that copper comprises ~78% of the red brass composition, the overall behavior of the brass system is strongly influenced by the copper chemistry. The copper behavior was different for two separate six-month runs: Chlorinated and Non-Chlorinated (dissolved oxygen). The 24- and 72-hour stagnation copper levels were

approximately the same throughout the chlorinated run. The non-chlorinated 24- and 72-hour stagnation copper levels do parallel each other, though, not on the same scale. The 72-hour copper levels are approximately three times the values for the 24-hour stagnation metal levels. In addition, the chlorinated run produced more overall corrosion product (including malachite) than the non-chlorinated run (only trace amounts of cuprite).

7.1 Red Brass System: Aqueous Data

7.1.1 Free Chlorine Run

Copper metal leaching levels reached a maximum value of approximately 1,100 ppb by day 20 and dissipated by approximately day 40 to declining values that ranged from 380 to 200 ppb. There were no significant differences between the copper metal leaching values for 24- and 72-hour stagnation times (Figure 7.1). Lead metal leaching values were greatest at the beginning of the study at 280 ppb and declined by day 15 to an average of ~40 ppb for a 24-hour stagnation time, and an average of ~70 ppb for a 72-hour stagnation time. Zinc metal leaching values were relatively steady throughout the study. However, zinc concentrations differed significantly with respect to stagnation-times: ~300 ppb for 24-hour stagnation times, ~400 ppb for 72-hour stagnation times, and ~500 ppb for the occasional 95-hour stagnation time.

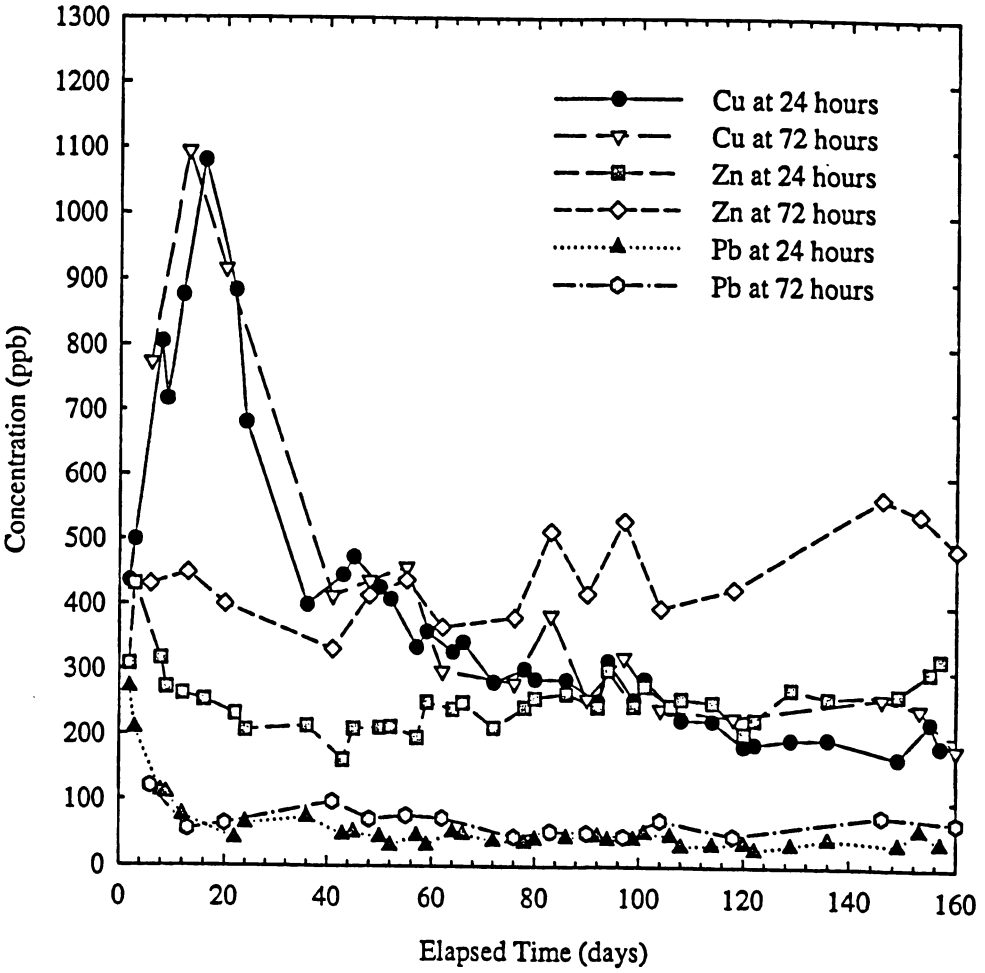

Figure 7.1 Red Brass Free Chlorine Run: Elapsed time versus copper, zinc, and lead metal release profiles for 24 and 72 hour stagnation times for Cell #8.

(Stonesifer et al., 2002)

pH had no significant relative change until approximately day 55. From day 55 through the end of the study, the relative change in pH was +0.05 for 24-hour stagnation times, +0.11 for 72-hour stagnation times, and +0.20 for the occasional 95-hour stagnation time. The redox curves represented a mixed potential and did not become stable for any 72-hour stagnation time.

7.1.2 Non-Chlorinated Run

There were significant differences between the copper metal leaching values for 24- and 72-hour stagnation times (Figure 7.2). Copper metal leaching levels for the 72-hour stagnation time reached a maximum value of approximately 400 ppb by day 35. The 24-hour stagnation times yielded a maximum copper concentration of 200 ppb on the first day of the study. Lead metal leaching values were greatest at the beginning of the study at 200 ppb and declined by day 40 to an average of ~10 ppb for a 24-hour stagnation time and an average of ~20 ppb for a 72-hour stagnation time. Zinc metal leaching values were relatively steady throughout the study. However, zinc concentrations differed significantly with respect to stagnation-times: ~40 ppb for 24-hour stagnation times, and ~80 ppb for 72-hour stagnation times.

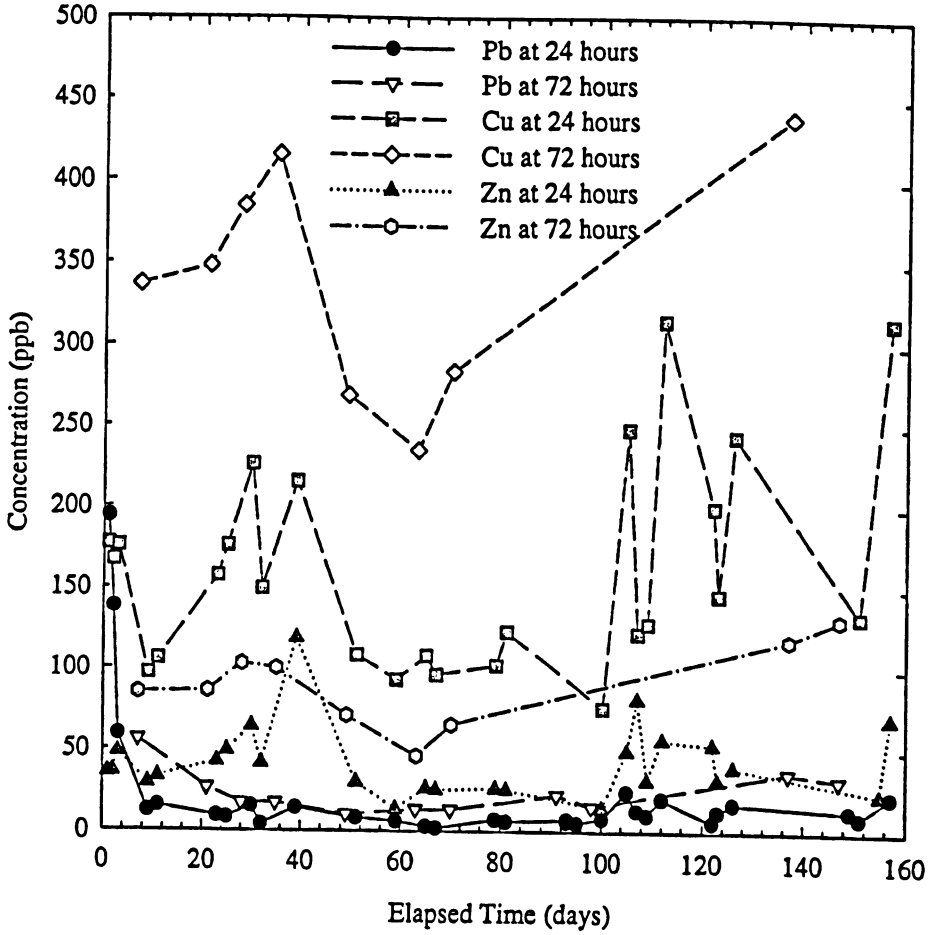

Figure 7.2 Red Brass Non-Chlorinated Run: Elapsed time versus copper, zinc, and lead metal release profiles for 24and 72 hour stagnation times for Cell #7.

The aqueous data appear to be erratic beyond day 100 of the study. Day 100 also corresponds with a change in the apparatus operator from the author to laboratory Co-op students. Due to the lack of recorded laboratory notes beyond day 100, this data will be omitted from interpretation.

The redox curves were stable at approximately 0.480 V for a 72-hour stagnation time throughout the run and there were no detectable changes or consumption of DO in the system .

7.2 Red Brass System: Solids Data

7.2.1 Free Chlorine Run

Traditional light microscopy examination was performed at the end of the test run on the exposed brass coupons. There were two predominant phases present and they were identified by XRD: small olive-green to brown microcrystalline cuprite and a green druzy to botryoidal malachite (as identified by XRD).

The olive-green to brown microcrystalline cuprite phase was generally uniform in thickness and in color across the coupon. However, only approximately 10% of the cuprite was exposed on the coupon surface area. Overlying the cuprite were druzy and/or botryoidal masses of malachite. The globular botryoidal malachite ranged in size from 0.15 to 0.02 mm in diameter. The overall distribution of the malachite scale was uniform with coverage ranging from ~80 to 90% of the coupon surface area.

XRD analysis of the brass coupons was performed at the end of the test run. The analysis yielded two predominate phases: cuprite (Cu_2O) and malachite ($Cu_2(CO_3)OH_2$) (Table 7.1).

Phases	2θ and d-spacing					
Malachite	14.82 5.97	17.59 5.03	24.10 3.68	31.32 2.85	32.28 2.77	35.90 2.49
Cuprite	36.44 *2.46	42.38 2.13	61.43 1.50	73.40 1.28		
Native Copper	42.93 *2.10	49.82 1.82				

Table 7.1 Summary of powder x-ray diffraction data from the chlorinated red brass coupon. * indicates the highest intensity reference peak

7.2.2 Non-Chlorinated Run

XRD analysis of the brass coupons was performed at the end of the test run. The analysis yielded two phases: cuprite (Cu_2O) and copper. A thin "film" of cuprite had formed that lessened the intensity of the copper peaks when compared to the XRD analysis of an unexposed brass coupon (Table 7.2).

Phases	2θ and d-spacing		
Native Copper	42.91 *2.10	49.84 1.82	
Cuprite	36.48 *2.46	52.30 1.74	73.47 1.28

Table 7.2 Summary of powder x-ray diffraction data from non-chlorinated red brass coupon. * indicates the highest intensity reference peak

8.0 DISCUSSION

The results of this study indicate that the presence of an oxidant and its concentration do have a direct relationship to the rate of corrosion. An initial "protective" corrosion scale forms in approximately forty days in both the chlorinated and non-chlorinated systems. The differences between the systems resulted from the initial phases that form and the rate of their further alteration. The differences in phases formed and rates of formation indicate not only a thermodynamic control but also, a strong kinetic control.

8.1 Aqueous Results

Aqueous results are not consistent with the prevailing Kuch and Wagner (1983) diffusion-based stagnation model. This model states that with a given water chemistry and lead pipe length and diameter (surface area to water volume ratio), the amount of lead released into solution can be calculated. Their stagnation model indicates that lead release stabilizes to a constant concentration after approximately 16 hours of stagnation regardless of pipe diameter or alkalinity (their pH ranged from 6.8 to 7.2). Stagnation data collected during our study did not exhibit this behavior.

Two profiling periods were performed during the chlorinated run of our study: at day 30 and at day 120 into the study (Figures 8.1 and 8.2). Lead release measured from day 30 in the study reflected a peak after 20 hours of stagnation followed by a reversal/decline of lead values for 72- and 95- hour stagnation times. Profiling at day 120 into the study yielded a more stable system. However, lead release levels steadily rose with increased stagnation time and did not reach a fixed concentration up to a 95-hour stagnation time. Both profiling periods also showed a continued decline in Eh with increased stagnation time. This alone suggests that reaction rates are changing well beyond 95-hours of stagnation.

In figure 8.1, Eh falls steadily, paralleled by a fall in free chlorine residual. Therefore, some reaction is consuming oxidant, in this case free chlorine. At the same time, lead levels rise in solution, but then fall. The early rise coupled with Eh fall is most simply interpreted as the oxidation of native lead ($Pb^0 \rightarrow Pb^{2+}$). The subsequent fall in lead concentration would then be a result of precipitation of a lead oxide or carbonate. However, because Eh continues to fall, new release of Pb^{2+} from the oxidation of native lead must still be continuing.

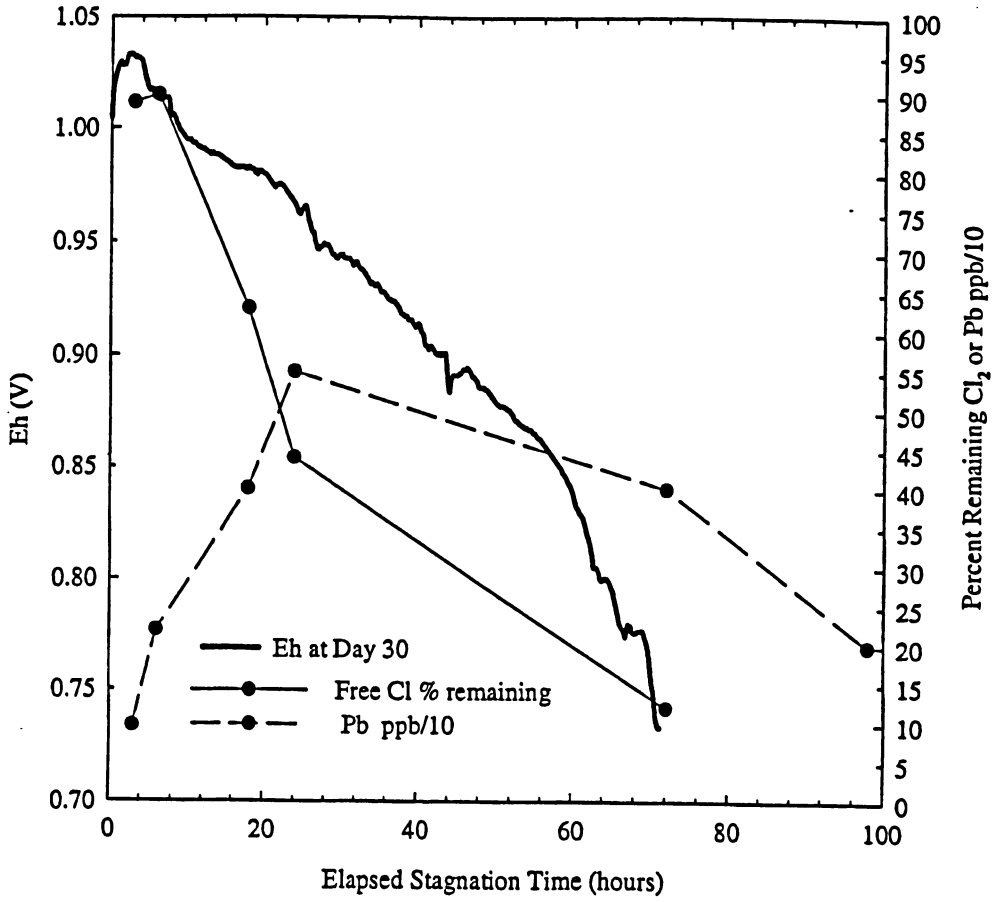

Figure 8.1 Lead profile at 30 days into the free chlorine run . Elapsed stagnation time versus the percent remaining of free chlorine and lead metal release with respect to the redox potential. Temperature is approximately 23°C, pH is at 7.00, free clorine begins at 3 ppm, and dissolved inorganic carbon is 10 ppm. The concentration of lead for 18-, 24-,72 and 95-hour stagnation times are above twice the dection limit (>200 ppb) for the Palintest method and are shown here from ICP data.

Figure 8.3 shows the same variables plus dissolved oxygen for the system after ageing for 120 days. Note Eh and free chlorine concentration fall steadily throughout the stagnation time, again indicating conversion of native lead to Pb^{2+}. Measurement of dissolved oxygen shows no significant fall, so that the oxidant in this case is free chlorine, not oxygen. Lead rises steeply in the beginning, then slows

as in the 30 day trial, but in this case a renewal of lead release is seen after 60 hours of stagnation. One possibility is that the initial precipitate causing the "leveling off" of the lead release rate is plattnerite (PbO2), which is highly insoluble at high Eh. Though, when the Eh falls below 1.00 V, this phase became soluble and began releasing extra Pb^{2+}.

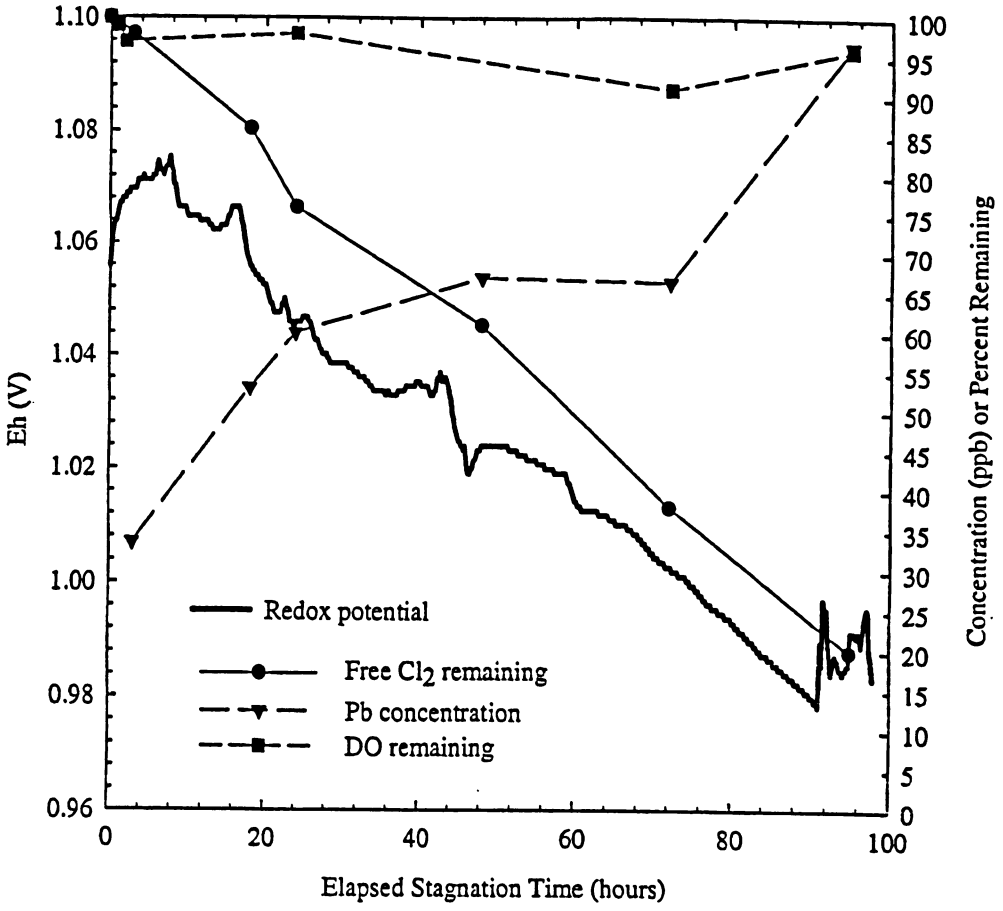

Figure 8.2 Lead profile at 120 days into the free chlorine run. Elapsed stagnation time versus the percent remaining of free chlorine and dissolved oxygen, and concentration of lead with respect to the redox potential. Temperature is approximataly 23°C, pH is at 7.00, free clorine begins at 3 mg/L, and dissolved inorganic carbon is 10 ppm.

In a diffusion controlled system, the rate of lead release from a flat plate should be proportional to the time. Therefore, lead release rates in the stagnation profiles should plot as straight lines vs. the square root of elapsed stagnation time should produce a linear trend (Maynard, 1976 and Crank, 1956). The equation for diffusion from Crank (1970) is:

$$\partial C/\partial t = D\,(\partial^2 C/\partial x^2)$$

Where C is the Pb concentration,
t is the time,
D is the diffusion coefficient, and
x is the radial position (for radial diffusion)

If $x=0$ and $x \rightarrow \infty$
$C=0$ and $C \rightarrow C_i$.

Then

$$C = C_i \operatorname{erf}(x/2\sqrt{(Dt)}) \qquad \text{(Berner, 1971)}$$

where erf is the error function: $(2/\sqrt{\pi}) \int_0^{\nu} \exp(-\epsilon^2)\, d\epsilon$ and
Ci represents the change in concentration.

If we assume that D is constant, fix the value "x" to equal 1,
then the equation can be simplified to,

$$C = Ci \operatorname{erf}(1/2\sqrt{(t)}).$$

Plotting this equation with respect to increasing stagnation time yields Figure 8.3.

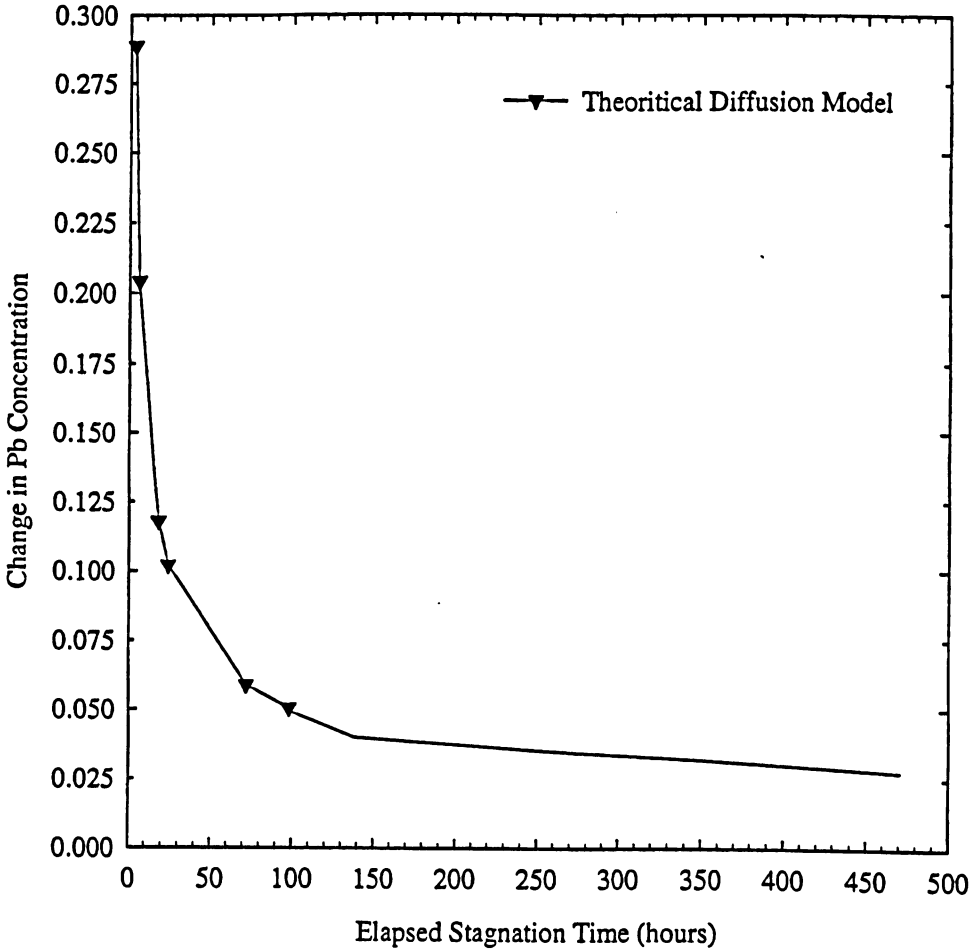

Figure 8.3 Theoritical Diffusion Model Curve of the elapsed stagnation time versus the change in concentration of lead metal release.

In contrast to figure 8.3, which decreases monotonically, the data from the two profiling periods in the chlorinated run indicate at least two parabolic curves (Figures 8.4 and 8.5), the sum of which do not change monotonically.

The profile at Day 30 initially shows a steady increase in pH as a positive change in lead release occurs. An abrupt change in mechanism occurs at approximately 20 hours of stagnation. The sudden change is reflected by a sudden rise in the rate of pH increase coupled with an extreme negative change in lead release. The diffusion controlled model (figure 8.3) may explain behaviors beyond 20 hours of stagnation (figure 8.4), but cannot model the behavior for the entire time range.

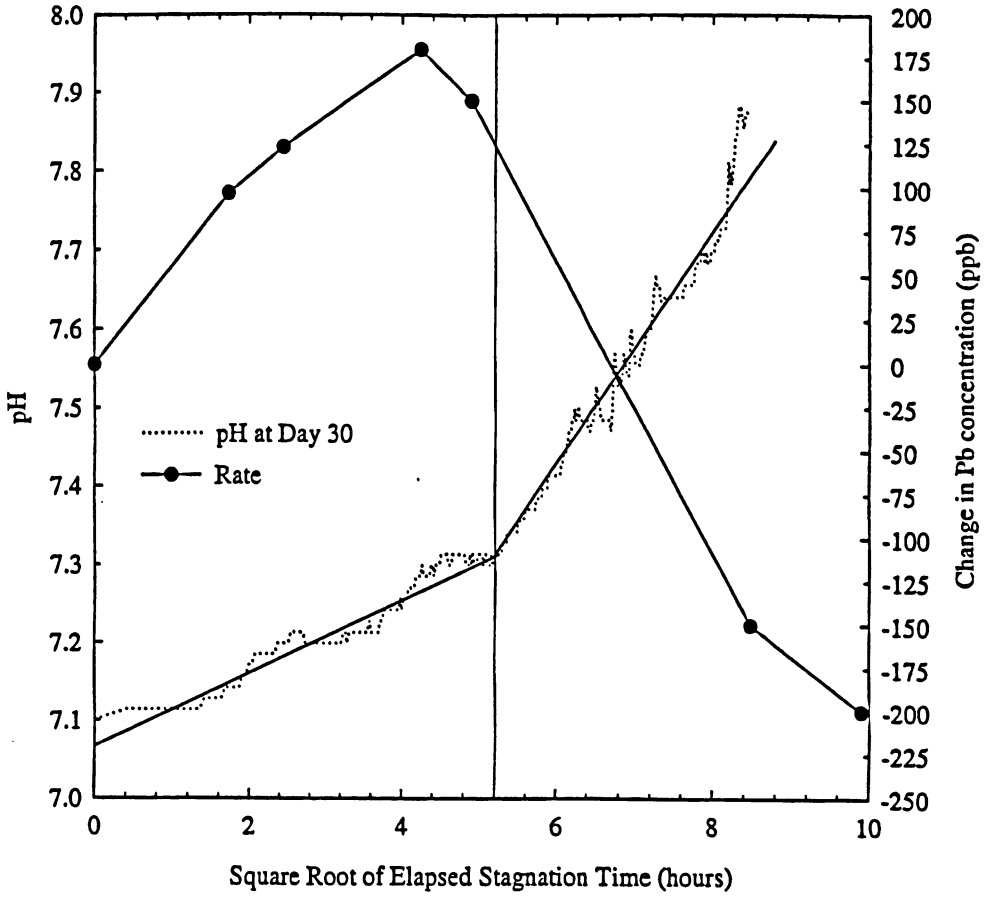

Figure 8.4 Lead Rate Profile at 30 days into the free chlorine run . The square root of the elapsed stagnation time versus the change in concentration of lead metal release with respect to the measured pH. Temperature is approximately 23°C, pH begins at 7.00, and dissolved inorganic carbon is 10 ppm.

The profile at Day 120 shows a parallel hyperbolic behavior between the pH and lead release up to 72 hours of stagnation (Figure 8.5). An abrupt change in mechanism occurs at approximately 72 hours of stagnation. The sudden change is reflected by a sudden rise in the rate of pH decrease coupled with an extreme positive change in lead release.

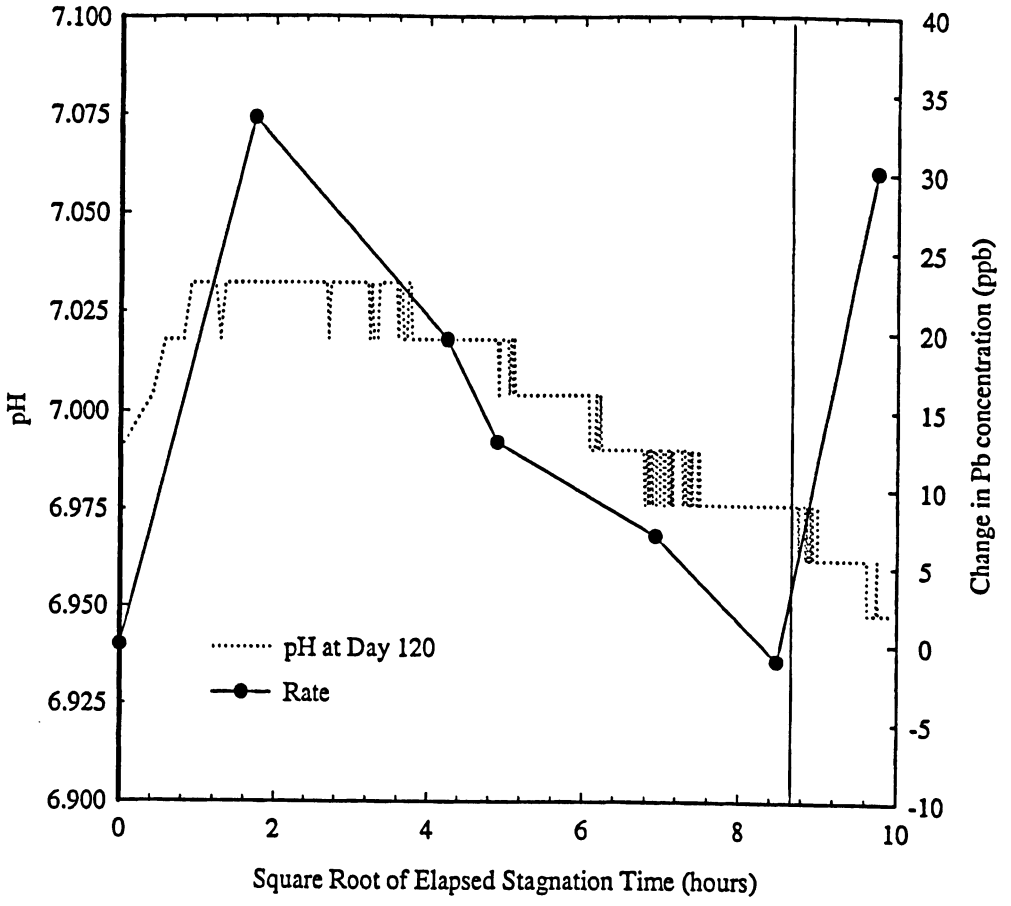

Figure 8.5 Lead Rate Profile at 120 days into the free chlorine run . The square root of the elapsed stagnation time versus the change in concentration of lead metal release with respect to the measured pH. Temperature is approximately 23°C, pH is at 7.00, and dissolved inorganic carbon is 10.00 ppm.

The data are more consistent with a combination of surface reaction models This model was derived on an assumption of a rapid adsorption "equilibrium" followed by a slow chemical reaction (Laidler and Meiser, 1999). The adsorption rate may actually exhibit the greatest initial kinetic control on lead release.

8.2 Eh and pH Reaction Paths

Figure 8.6 depicts the measured 72-hour Eh-pH reaction paths with time for the free chlorine system and the dissolved oxygen system superimposed on the Eh-pH diagram for lead. The numbered circles indicate the sequential timing of paths of the chlorinated lead system: #1 = Day 6, #2 = Day 10, #3 = Day 20, and #4 = Day 50. The "X" on the figure represents the pH-Eh space in which the lead dissolved oxygen system occupied for the entire length of the six-month run.

In table 8.1, the likely reactions producing the Eh-pH changes are given. The first reaction, the oxidation of native lead, continues throughout all the observations as shown by the Eh profiles with time (Figures 8.1 and 8.2). Reaction B, the formation of cerussite ($PbCO_3$) is well-documented by solids recovered at Day 40. The similar solids were also seen to have formed in the Day 6 (#1) and Day 10 (#2) runs. Therefore it is likely that the reaction was occurring throughout the entirety of the chlorinated run. Reaction #3, the precipitation of plattnerite, is likely the fastest reaction in the early reaction paths as a result of the initially very high Eh values, but is quickly followed as Eh falls by reactions like D and E, which make relatively soluble oxides and result in an increase lead levels. Reaction E is based on the observation of hydrocerussite in the solids at day 40 and F on the absence of this

phase at the end of the experiment. Reaction G is required because litharge is greatly subordinate to cerussite in the final products.

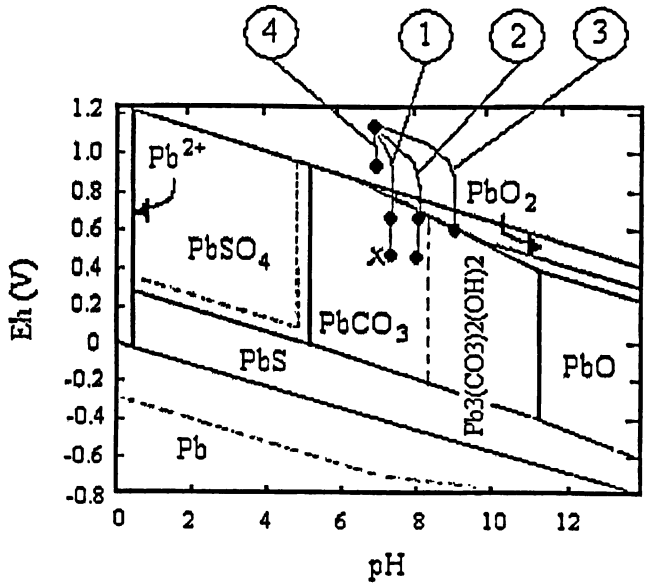

Figure 8.6 Measured reaction paths from the pure lead system. 1=Day 6, 2=Day 10, 3=Day 20, and 4=Day 50 in the chlorinated run (plotted on Brookins, 1988). The assumed activities of dissolved species include Pb= $10^{-6,-8}$, C= 10^{-3}, S=10^{-3}

Fig. 8.6 Pathway	Reaction	Significant reaction ?	Rxn. ID
#1→#4	$Pb_{(s)} \leftrightarrow Pb^{2+} + 2e^-$	Yes	A
#1→#4	$Pb^{2+} + HCO_3^- \leftrightarrow PbCO_{3\,(s)} + H^+$	Yes	B
#1→#3	$Pb^{2+} + 2H_2O \leftrightarrow PbO_{2(s)} + 4H^+ + 2e^-$	No	C
#2→#3	$3PbO_{2(s)} + 2H_2O + 4e^- \leftrightarrow Pb_3O_{4(s)} + 4OH^-$	No	D
#2→#3	$Pb_3O_{4(s)} + H_2O + 2e^- \leftrightarrow 3PbO_{(s)} + 2OH^-$	No	E
#2→#3	$Pb_3(CO_3)_2(OH)_{2\,(s)} \leftrightarrow 2PbCO_{3\,(s)} + H_2O + PbO_{(s)}$	Yes	F
#4	$PbO + HCO^- \leftrightarrow PbCO_{3\,(s)} + OH^-$	No	G

Table 8.1 Reactions from the chlorinated lead system, their significance, and relative timing (Figure 8.6).

The reactions for the non-chlorinated run appear to be the same except that there were no odd metastable phases formed initially. The non-chlorinated run had a significant slower rate of scale formation. The initial and dominant phase appeared to be cerussite ($PbCO_3$) with trace hydrocerussite and PbO. No measurable consumption of dissolved oxygen was noted within the detection limits of the Hach DO meter.

8.3 Comparison of Experimental Results with the CWW Pipe Samples

Both CWW pipes and the experimental system produced multiple phases including lead oxides and lead carbonates. The difference lies in the species of carbonate and oxide formed. The CWW pipes contain hydrocerussite and plattnerite. The experimental system produces cerussite with trace amounts of relic initial phases. This difference of dominant phase(s) present is likely the difference in pH under which the phases formed. The CWW pipes are at a higher pH than the experimental system (~9 vs. 7.00, respectively). At pH values greater than approximately 8, hydrocerussite is the more stable lead carbonate. The presence of plattnerite in the CWW samples, is again, a result of a higher pH. The stability field of plattnerite is much larger at higher pHs. At pH 7, the stability field for plattnerite consists of only a narrow sliver of Eh-pH space and is not likely to remain stable for very long under dynamic conditions.

The solid phases formed in CWW pipes and the experimental system are comparable in the crystallite sizes and textures present. Both systems produce a nano-crystaline / nano-particulate. This is significant in that such small sizes yield large surface areas, and larger surface areas allow for faster reactions. This was illustrated with the aging of the experimental system. At Day 40, solids were recovered from the bottom of the reaction cell.

9.0 Conclusions

- Test loop system did not produce any significant plattnerite at pH 7. However, plattnerite did form as an intermediate at higher pHs.

- Plattnerite can form by direct precipitation, but is likely to redissolve or convert to Pb^{2+} compounds as Eh falls, unless the free chlorine residual is maintained at high levels.

- Real-time continual data collection of Eh and pH provide a means to determine the dominant phase forming reaction and its relative rate.

- SEM analysis of test coupons and of samples from CWW DS show nano-sized particulate lead phases. These loosely adherent particles may be the primary source of elevated measured lead levels.

- The difference in phases formed in the CWW DS vs. those formed in the experimental system is a result of the differing pH (~9 vs. 7.00, respectively). This difference in pH dictates which mineral stability field(s) Eh will move through upon consumption of oxidant.

10.0 AREAS FOR FURTHER STUDY

- Further study on the controls of the co-existents of the lead carbonates.
- There are no practical means to measure the speciation and oxidation states of the ions present (such as the case for Pb^{2+} vs. Pb^{4+})
- Parameters that affect oxidation rates, scale formation and alteration need to be further studied
- Run the loop apparatus at different pHs and concentrations of free chlorine to further constrain rates.
- Although free chlorine is a commonly used disinfectant, some municipalities use ozonation, addition of chloramines, etc. to disinfect the water. The corrosion products and rates have not been thoroughly established. The loop apparatus should be systematically ran with different disinfectants and varying pHs.
- Further investigation is needed to address the formation of primary plattnerite from native lead in drinking water distribution systems. Such study should include the historical source of lead used, the means of manufacture of lead pipe (past and present), expanding the number of samples, and implementing more precise analytical techniques (such as tunneling electron microscopy TEM) to analyze the nano-crystaline/nano-particulatescale product.

REFERENCES

Ahr, N. J. (ed.), 1988. Cincinnati: An Urban History Sourcebook. Produced by the Cincinnati Historical Society as a Greater Cincinnati Bicentennial Commission Project. 88 pages.

Allen, H. E. and Hunt, D. T. E. 1981. Chemical Speciation: Measurement and Significance of Complexation. Proceedings of Water Industry International Conference, Brighton, UK. pp. 99-103.

Bethke, C. M. 1996. Geochemical Reaction Modeling Concepts and Applications, University of Illinois Urbana-Champaign, Oxford University Press. 397 pages.

Breck, W. G. 1974. Redox Levels In The Sea, *In* The Sea: Ideas and Observations on Progress in the Study of the Seas. Goldberg, E. D. ed. Vol. 5, Marine Chemistry. pp. 153-179.

Bricker, O. P. 1982. Redox Potential: Its Measurement and Importance in Water Systems. *In* Water Analysis, Vol. 1, pp. 55-83.

Brookins, D. 1988. Eh-pH Diagrams for Geochemistry. Springer-Verlag Berlin Heidelberg. 176 pages.

Escher, A. and Watt, W. 1976. Geology of Greenland. The Geological Survey of Greenland. Copenhagen, Denmark. 603 pages.

Guilbert, J. and Park, C. Jr. 1986. The Geology of Ore Deposits. W. H. Freeman and Company. 985 pages.

Harmon, S., 1998. Precipitation of Lead Minerals in Service Lines: An Example From the Water Utility of Hopkinton, Massachusetts. Thesis: The University of Cincinnati, Department of Geology. 124 pages.

Hopkins, H. L, Woodward, E. S., and Alsberg, H. G. 1938. They Built a City- 150 Years of Industrial Cincinnati, Works Progress Administration, Published by the Cincinnati Post. 402 pages.

Karup-Moller, S. 1975. On the occurrence of the native lead, litharge, hydrocerussite and plattnerite within the Ilimaussaq alkaline intrusion in South Greenland. *In*: Contribution to the mineralogy of Ilimaussaq.

Kuch, A. and Wagner, I. 1983. A Mass Transfer Model to Describe Lead Concentrations in Drinking Water. Water Research, Vol. 17, No. 10, pp. 1303-1307.

Laidler, K. J. and Meiser, J. H. 1999. Physical Chemistry 3rd Ed. Houghton Mifflin Company. 1019 pages.

Langmuir, D. 1997. Aqueous Environmental Geochemistry. Prentice-Hall, Inc. 600 pages.

Lytle, D. A. and Schock M. R. 1996. Stagnation Time, Composition, pH, and Orthophosphate Effects on Metal Leaching from Brass. ORD, USEPA, Washington, D.C.

Lytle, D. A. and Schock M. R. 2000. Impact of Stagnation Time on Metal Dissolution From Plumbing Materials in Drinking Water. Journal of Water Supply: Research and Technology-AQUA. Vol. 49.5. p. 243-257.

Morel, F. M. M. and Hering, J. G. 1993. Principles and Applications of Aquatic Chemistry, A Wiley Interscience Publication. 588 pages.

Pankow, J. F. 1991. Aquatic Chemistry Concepts. Lewis Publishers. p. 683.

Rose-Hansen, J. and Sorensen, H. 2002. Geology of the Lujavrites from the Ilimaussaq alkaline complex. Danish Polar Center, Copenhagen, Denmark. 58 pages.

Schock, M. R., Harmon, S. M., Swertfeger, J., and Lohmann, R. 2001. Tetravalent Lead: A Hitherto Unrecognized Control of Tap Water Lead Contamination. American Water Works Association Water Quality Technology Conference Proceedings, November 2001.

Schock, M. R., Wagner, I., Oliphant, R. J. 1996. Corrosion and Solubility of Lead in Drinking Water. *In* Internal Corrosion of Water Distribution Systems, Cooperative Research Report, 2nd Edition, American Water Works Association Research Foundation. Pp. 131-230.

Stonesifer, K. K., Lytle, D. A., and Schock, M. R. 2002. Oxidant and Redox Potential Effects on the Corrosion of Distribution System Materials. American Water Works Association Water Quality Technology Conference Proceedings, November 2002.

Stumm, W. and Morgan, J. J. 1996. Aquatic Chemistry: Chemical Equilibra and Rates in Natural Waters 3rd Ed. John Wiley & Sons, Inc. 1022 pages.

APPENDIX 1

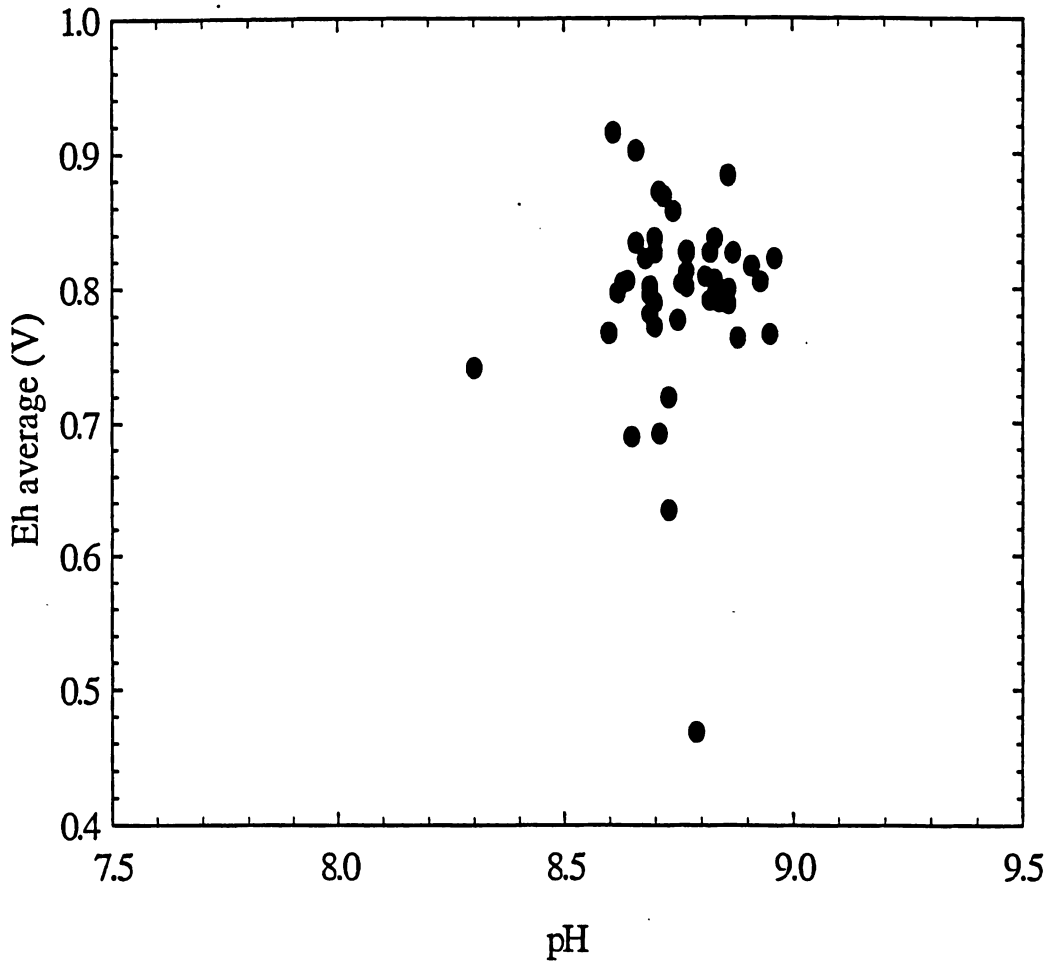

Appendix 1 Eh vs. pH for Cincinnati tap water.

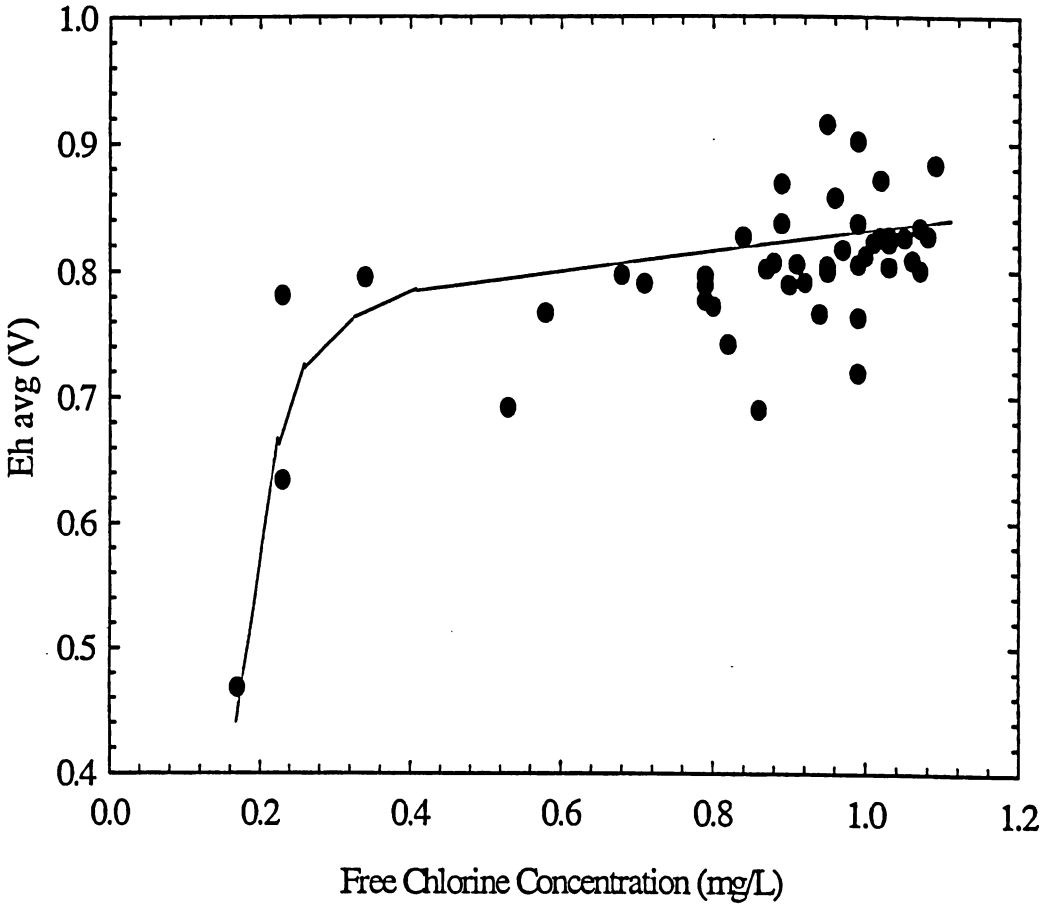

Appendix 1 Eh vs. Free chlorine concentration in Cincinnati Tap Water.

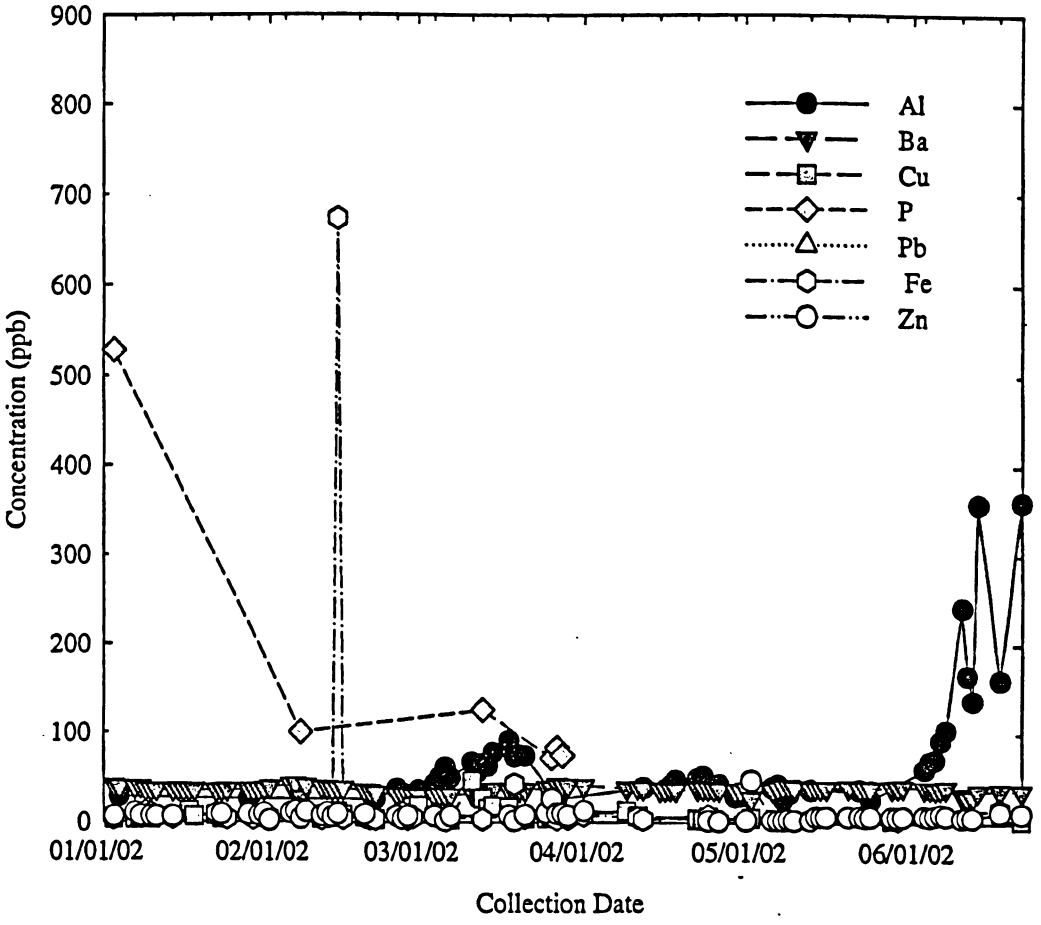

Appendix 1 Cincinnati Water Works Tap Water Aqueous Data of analytes present in concentrations relevant to the ppb scale. Data colledted by Ian S.

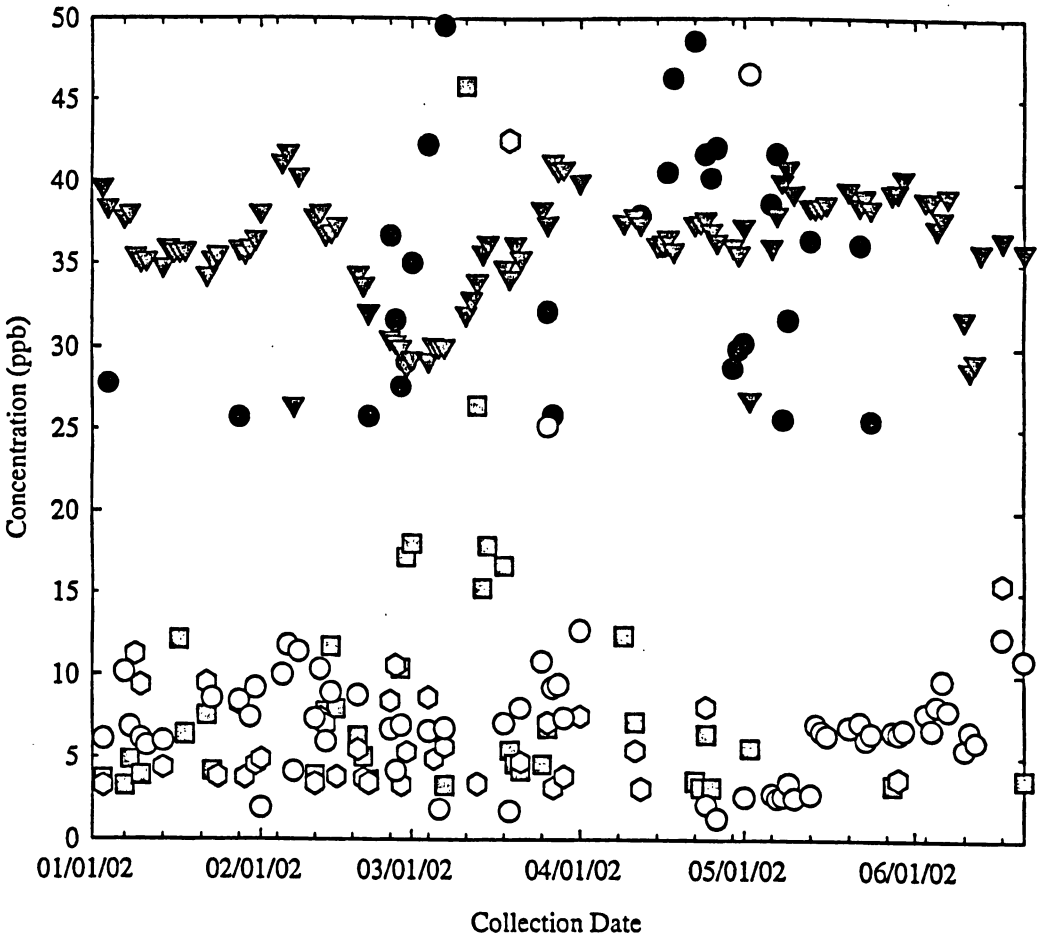

Appendix 1 Cincinnati Water Works Tap Water Aqueous Data of analytes present in concentrations relevant to a smaller ppb scale. Data colledted by Ian S.

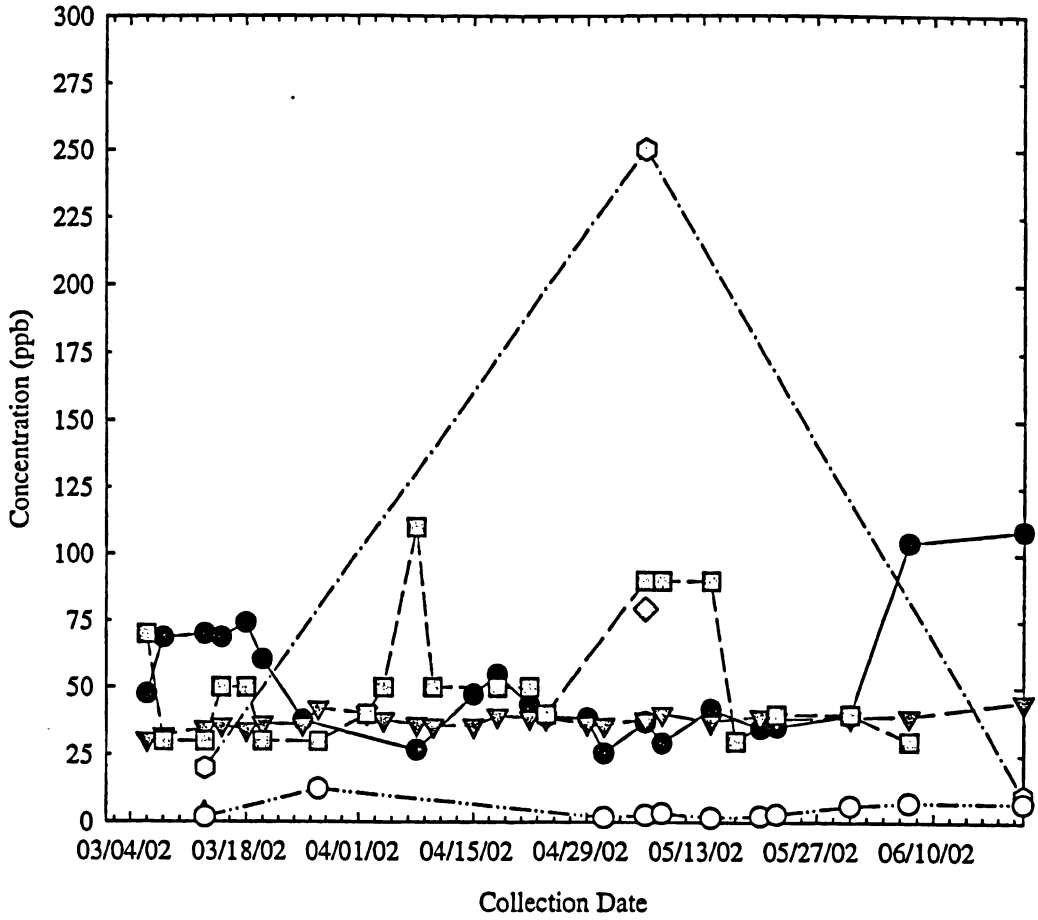

Appendix 1 Cincinnati Water Works Tap Water Aqueous Data of analytes present in concentrations relevant to the ppb scale.

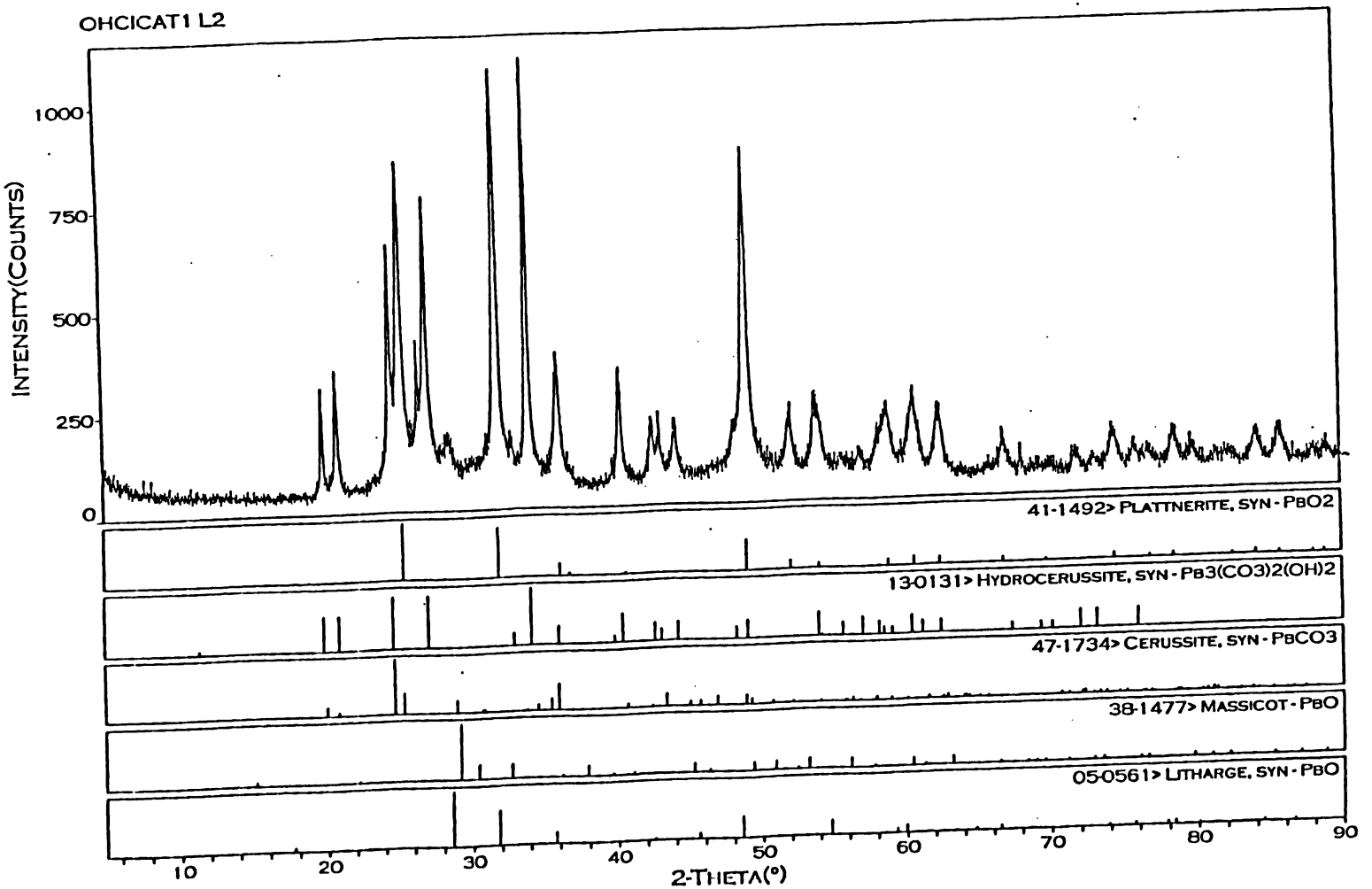
OHCICAT1 L2
INTENSITY(COUNTS)
1000
750
500
250
0
41-1492> PLATTNERITE, SYN - PBO2
13-0131> HYDROCERUSSITE, SYN - PB3(CO3)2(OH)2
47-1734> CERUSSITE, SYN - PBCO3
38-1477> MASSICOT - PBO
05-0561> LITHARGE, SYN - PBO
10
20
30
40
50
60
70
80
90
2-THETA(°)

[MS30203A.RAW] OHCICAT1 L2 | PEAK ID REPORT

SCAN: 5.0/90.0/0.01/5(SEC), CU(35KV,40MA), I(MAX)=1105, 02/04/03 02:42

PEAK: 15-PTS/PARABOLIC FILTER, THRESHOLD=3.0, CUTOFF=0.1%, BG=3/1.0, PEAK-TOP=SUMMIT

NOTE: INTENSITY = COUNTS, 2T(0)=0.0(°), WAVELENGTH TO COMPUTE D-SPACING = 1.54056A (CU/K-...

#	2-THETA	D(A)	HEIGHT	I%(H)	PHASE ID	D(A)··	I%	(H K L)	2-THETA
1	7.778	11.3573	44	4.4					
2	8.268	10.6845	41	4.1					
3	19.960	4.4446	251	25.3	CERUSSITE, ...	4.4311	15.0	(1 1 0)	20.022
4	20.680	4.2915	36	3.6	CERUSSITE, ...	4.2641	5.0	(0 2 0)	20.814
5	20.951	4.2366	288	29.0	HYDROCER...	4.2500	60.0	(0 1 2)	20.884
6	24.381	3.6478	112	11.3					
7	24.541	3.6245	187	18.8					
8	24.671	3.6056	387	39.0	HYDROCER...	3.6100	90.0	(1 0 4)	24.640
9	24.741	3.5956	576	58.0	CERUSSITE, ...	3.5986	100.0	(1 1 1)	24.720
10	24.950	3.5659	262	26.4					
11	25.131	3.5407	215	21.7	CERUSSITE, ...	3.5081	37.0	(0 2 1)	25.367
12	25.450	3.4969	678	68.3	PLATTNERITE...	3.5000	100.0	(1 1 0)	25.427
13	26.691	3.3372	241	24.3					
14	27.270	3.2676	609	61.3	HYDROCER...	3.2900	90.0	(0 1 5)	27.080
15	27.499	3.2409	118	11.9					
16	28.687	3.1092	67	6.7	LITHARGE, SYN	3.1150	100.0	(1 0 1)	28.633
17	28.797	3.0977	64	6.4					
18	28.920	3.0848	60	6.0	CERUSSITE, ...	3.0792	21.0	(0 0 2)	28.973
19	32.139	2.7827	869	87.5	PLATTNERITE...	2.7970	88.0	(1 0 1)	31.971
20	33.003	2.7119	53	5.3	HYDROCER...	2.7150	20.0	(1 0 7)	32.964
21	33.111	2.7033	45	4.5					
22	33.912	2.6412	105	10.6	CERUSSITE, ...	2.6476	1.0	(1 0 2)	33.829
23	34.210	2.6189	993	100.0	HYDROCER...	2.6230	100.0	(1 1 0)	34.155
24	35.740	2.5102	40	4.0	LITHARGE, SYN	2.5100	18.0	(0 0 2)	35.743
25	35.920	2.4980	78	7.9	CERUSSITE, ...	2.4940	46.0	(0 2 2)	35.980
26	36.131	2.4840	239	24.1	MASSICOT	2.4803	1.0	(2 1 0)	36.186
27	36.260	2.4754	271	27.3	PLATTNERITE...	2.4800	21.0	(2 0 0)	36.190
28	36.419	2.4649	160	16.1					
29	36.519	2.4584	110	11.1					
30	40.480	2.2266	275	27.7	HYDROCER...	2.2310	50.0	(2 0 2)	40.396
31	42.472	2.1266	78	7.9	LITHARGE, SYN	2.1240	1.0	(1 0 2)	42.527
32	42.651	2.1181	138	13.9	HYDROCER...	2.1200	30.0	(0 2 4)	42.611
33	42.759	2.1130	129	13.0					
34	43.170	2.0938	140	14.1	HYDROCER...	2.0990	20.0	(1 0 10)	43.058
35	44.251	2.0452	124	12.5	HYDROCER...	2.0460	30.0	(2 0 5)	44.232
36	44.369	2.0400	108	10.9					
37	48.271	1.8838	118	11.9	HYDROCER...	1.8840	20.0	(0 2 7)	48.266
38	49.180	1.8511	720	72.5	CERUSSITE, ...	1.8482	8.0	(0 2 3)	49.262
39	49.349	1.8451	461	46.4	MASSICOT	1.8452	12.0	(0 2 2)	49.349
40	49.570	1.8375	208	20.9					
41	52.170	1.7518	116	11.7	CERUSSITE, ...	1.7517	1.0	(0 4 2)	52.175
42	52.231	1.7499	132	13.3					
43	52.299	1.7478	154	15.5	MASSICOT	1.7439	1.0	(3 1 0)	52.424

[MS30203A.RAW] OHCICAT1 L2 — PEAK ID REPORT

SCAN: 5.0/90.0/0.01/5(SEC), CU(35KV,40MA), I(MAX)=1105, 02/04/03 02:42

PEAK: 15-PTS/PARABOLIC FILTER, THRESHOLD=3.0, CUTOFF=0.1%, BG=3/1.0, PEAK-TOP=SUMMIT

NOTE: INTENSITY = COUNTS, 2T(0)=0.0(°), WAVELENGTH TO COMPUTE D-SPACING = 1.54056A (CU/K-...

#	2-THETA	D(A)	HEIGHT	I%(H)	PHASE ID	D(A)	I%	(H K L)	2-THETA
44	53.960	1.6978	174	17.5	HYDROCER...	1.6960	40.0	(1 2 2)	54.024
45	54.129	1.6929	168	16.9	CERUSSITE, ...	1.6938	1.0	(3 1 0)	54.098
46	54.240	1.6897	148	14.9					
47	54.309	1.6878	127	12.8					
48	54.450	1.6837	105	10.6					
49	55.385	1.6575	34	3.4					
50	55.851	1.6448	33	3.3	CERUSSITE, ...	1.6458	1.0	(2 4 0)	55.812
51	56.613	1.6244	33	3.3	CERUSSITE, ...	1.6188	1.0	(1 5 0)	56.829
52	56.996	1.6144	45	4.5	CERUSSITE, ...	1.6188	1.0	(1 5 0)	56.829
53	57.061	1.6127	42	4.2	HYDROCER...	1.6130	30.0	(1 2 5)	57.050
54	58.329	1.5807	73	7.4	HYDROCER...	1.5840	20.0	(0 1 14)	58.194
55	58.629	1.5733	112	11.3	HYDROCER...	1.5760	10.0	(1 1 12)	58.518
56	58.920	1.5662	136	13.7	PLATTNERITE...	1.5670	9.0	(3 1 0)	58.887
57	58.920	1.5662	136	13.7					
58	59.009	1.5641	121	12.2	CERUSSITE, ...	1.5647	3.0	(1 5 1)	58.980
59	59.150	1.5607	90	9.1	HYDROCER...	1.5620	10.0	(2 0 11)	59.094
60	60.492	1.5292	107	10.8	HYDROCER...	1.5300	30.0	(2 1 7)	60.457
61	60.601	1.5267	129	13.0	PLATTNERITE...	1.5253	12.0	(1 1 2)	60.663
62	60.819	1.5218	175	17.6					
63	60.931	1.5192	148	14.9					
64	61.165	1.5140	88	8.9	HYDROCER...	1.5130	20.0	(3 0 0)	61.209
65	62.229	1.4906	61	6.1					
66	62.460	1.4857	142	14.3	PLATTNERITE...	1.4856	10.0	(3 0 1)	62.463
67	62.531	1.4841	156	15.7	HYDROCER...	1.4850	20.0	(3 0 3)	62.491
68	62.670	1.4812	153	15.4	CERUSSITE, ...	1.4832	2.0	(3 1 2)	62.577
69	62.889	1.4765	67	6.7	CERUSSITE, ...	1.4767	4.0	(3 3 0)	62.884
70	66.033	1.4137	32	3.2					
71	66.658	1.4019	52	5.2	LITHARGE, SYN	1.4050	5.0	(2 2 0)	66.493
72	66.869	1.3980	59	5.9	PLATTNERITE...	1.3986	6.0	(2 0 2)	66.837
73	67.021	1.3952	88	8.9					
74	67.407	1.3882	42	4.2	HYDROCER...	1.3880	10.0	(2 1 10)	67.415
75	68.201	1.3739	62	6.2	MASSICOT	1.3704	1.0	(4 0 0)	68.398
76	69.325	1.3544	30	3.0	HYDROCER...	1.3530	10.0	(1 1 15)	69.405
77	69.491	1.3515	29	2.9	MASSICOT	1.3501	1.0	(1 2 3)	69.574
78	70.373	1.3367	32	3.2	HYDROCER...	1.3400	10.0	(1 2 11)	70.176
79	71.752	1.3144	56	5.6					
80	71.970	1.3109	55	5.5	HYDROCER...	1.3090	30.0	(2 2 0)	72.094
81	72.167	1.3079	50	5.0	CERUSSITE, ...	1.3080	3.0	(1 3 4)	72.155
82	73.153	1.2926	34	3.4	HYDROCER...	1.2920	30.0	(2 2 3)	73.195
83	74.420	1.2737	96	9.7	PLATTNERITE...	1.2739	8.0	(3 2 1)	74.409
84	74.559	1.2717	84	8.5	PLATTNERITE...	1.2739	8.0	(3 2 1)	74.409
85	74.700	1.2697	76	7.7	CERUSSITE, ...	1.2702	1.0	(1 5 3)	74.665
86	74.950	1.2660	34	3.4	CERUSSITE, ...	1.2629	1.0	(2 2 4)	75.172

[MS30203A.RAW] OHCICAT1 L2 — PEAK ID REPORT

SCAN: 5.0/90.0/0.01/5(SEC), CU(35KV,40MA), I(MAX)=1105, 02/04/03 02:42

PEAK: 15-PTS/PARABOLIC FILTER, THRESHOLD=3.0, CUTOFF=0.1%, BG=3/1.0, PEAK-TOP=SUMMIT

NOTE: INTENSITY = COUNTS, 2T(O)=0.0(°), WAVELENGTH TO COMPUTE D-SPACING = 1.54056A (CU/K-...

#	2-THETA	D(A)	HEIGHT	I%(H)	PHASE ID	D(A)	I%	(H K L)	2-THETA
87	75.940	1.2520	48	4.8	HYDROCER...	1.2510	30.0	(3 1 2)	76.010
88	77.269	1.2337	32	3.2					
89	78.369	1.2191	61	6.1	LITHARGE, SYN	1.2190	5.0	(3 1 1)	78.380
90	78.439	1.2182	60	6.0	PLATTNERITE...	1.2179	5.0	(2 2 2)	78.465
91	78.591	1.2163	80	8.1	CERUSSITE, ...	1.2154	1.0	(4 2 1)	78.659
92	78.809	1.2134	65	6.5	CERUSSITE, ...	1.2130	1.0	(3 5 0)	78.845
93	78.939	1.2118	36	3.6					
94	79.548	1.2040	32	3.2					
95	79.779	1.2011	61	6.1	MASSICOT	1.2017	4.0	(1 3 3)	79.735
96	79.928	1.1992	44	4.4	MASSICOT	1.2017	4.0	(1 3 3)	79.735
97	80.047	1.1978	44	4.4	LITHARGE, SYN	1.1977	1.0	(1 0 4)	80.052
98	82.431	1.1690	32	3.2	PLATTNERITE...	1.1683	2.0	(3 3 0)	82.496
99	84.179	1.1492	72	7.3	CERUSSITE, ...	1.1497	1.0	(4 2 2)	84.135
100	84.308	1.1477	73	7.4	CERUSSITE, ...	1.1497	1.0	(4 2 2)	84.135
101	84.430	1.1464	65	6.5	LITHARGE, SYN	1.1462	2.0	(1 1 4)	84.448
102	85.399	1.1359	34	3.4	MASSICOT	1.1379	2.0	(1 1 4)	85.207
103	85.612	1.1336	65	6.5					
104	85.760	1.1320	77	7.8	PLATTNERITE...	1.1327	4.0	(4 1 1)	85.693
105	85.822	1.1313	72	7.3					
106	85.950	1.1300	82	8.3	CERUSSITE, ...	1.1279	1.0	(3 5 2)	86.144
107	86.809	1.1210	32	3.2	LITHARGE, SYN	1.1232	2.0	(3 1 2)	86.596
108	88.256	1.1063	31	3.1	CERUSSITE, ...	1.1068	1.0	(4 4 0)	88.207
109	88.628	1.1026	32	3.2	MASSICOT	1.1008	3.0	(4 2 2)	88.810
110	89.089	1.0981	48	4.8					

LINE SHIFTS OF INDIVIDUAL PHASES:

PDF#41-1492 - PLATTNERITE, SYN <2T(O) = 0.0, D/D(O) = 1.0>

PDF#13-0131 - HYDROCERUSSITE, SYN <2T(O) = 0.0, D/D(O) = 1.0>

PDF#47-1734 - CERUSSITE, SYN <2T(O) = -0.06, D/D(O) = 1.0>

PDF#38-1477 - MASSICOT <2T(O) = 0.12, D/D(O) = 1.0>

PDF#05-0561 - LITHARGE, SYN <2T(O) = 0.0, D/D(O) = 1.0>

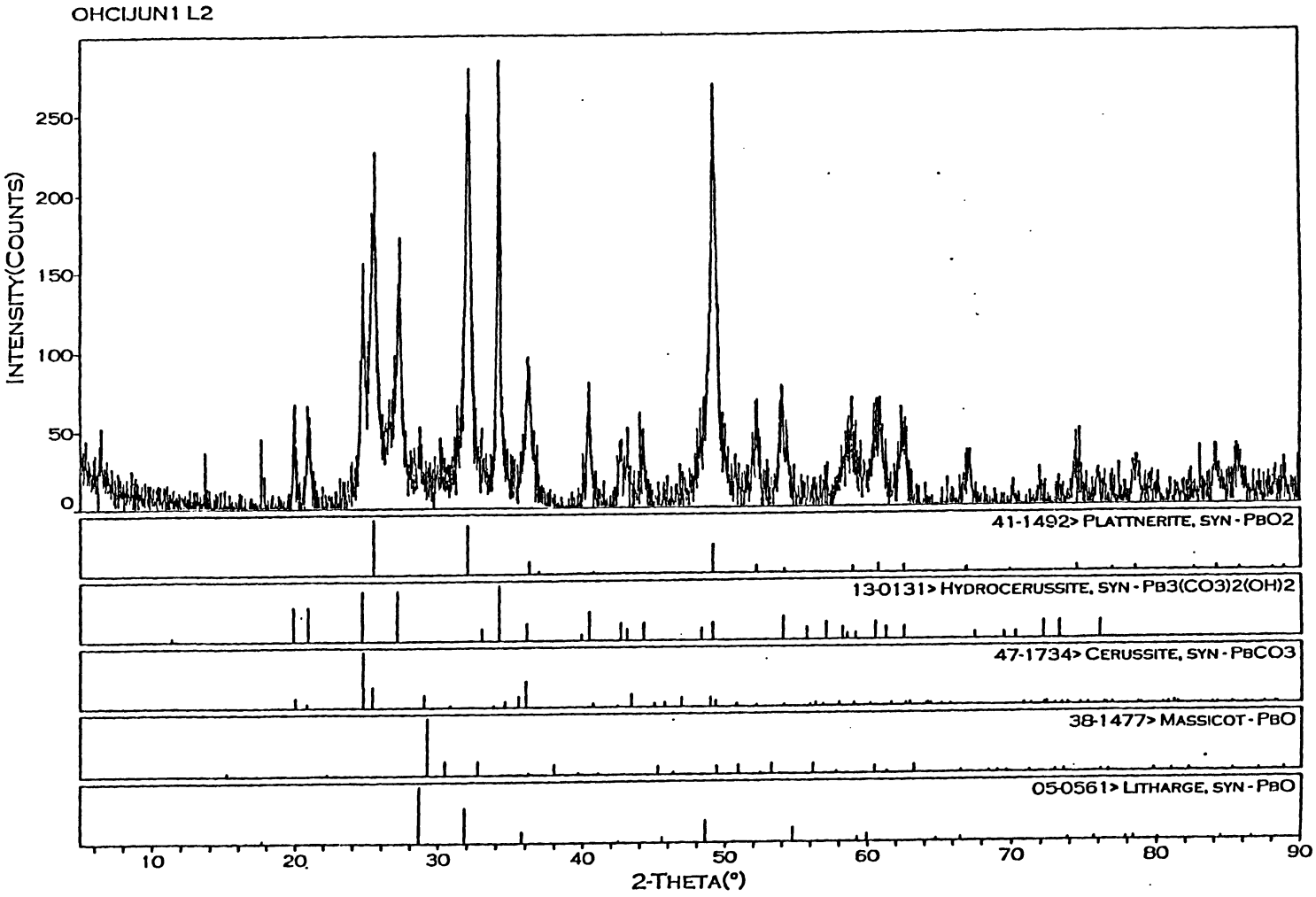
OHCIJUN1 L2
INTENSITY(COUNTS)
250
200
150
100
50
0
41-1492> PLATTNERITE, SYN - PBO2
13-0131> HYDROCERUSSITE, SYN - PB3(CO3)2(OH)2
47-1734> CERUSSITE, SYN - PBCO3
38-1477> MASSICOT - PBO
05-0561> LITHARGE, SYN - PBO
10
20
30
40
50
60
70
80
90
2-THETA(°)

[MS30130A.RAW] OHCIJUN1 L2 | PEAK ID REPORT

SCAN: 5.0/90.0/0.02/3(SEC), CU(35KV,40MA), I(MAX)=285, 01/30/03 12:47

PEAK: 15-PTS/PARABOLIC FILTER, THRESHOLD=3.0, CUTOFF=0.1%, BG=3/1.0, PEAK-TOP=SUMMIT

NOTE: INTENSITY = COUNTS, 2T(O)=0.0(°), WAVELENGTH TO COMPUTE D-SPACING = 1.54056A (CU/K-...

#	2-THETA	D(A)	HEIGHT	I%(H)	PHASE ID	D(A)	I%	(H K L)	2-THETA
1	6.475	13.6384	34	12.7					
2	19.960	4.4447	58	21.6	CERUSSITE, ...	4.4311	15.0	(1 1 0)	20.022
3	20.884	4.2501	52	19.4	HYDROCER...	4.2500	60.0	(0 1 2)	20.884
4	23.965	3.7101	23	8.6					
5	24.720	3.5985	141	52.6	CERUSSITE, ...	3.5986	100.0	(1 1 1)	24.720
6	25.503	3.4899	176	65.7	PLATTNERITE...	3.5000	100.0	(1 1 0)	25.427
7	26.820	3.3214	56	20.9					
8	27.258	3.2690	152	56.7	HYDROCER...	3.2900	90.0	(0 1 5)	27.080
9	27.656	3.2228	29	10.8					
10	28.680	3.1101	35	13.1	LITHARGE, SYN	3.1150	100.0	(1 0 1)	28.633
11	28.796	3.0978	25	9.3					
12	28.809	3.0964	25	9.3	CERUSSITE, ...	3.0792	21.0	(0 0 2)	28.973
13	30.213	2.9556	23	8.6	MASSICOT	2.9346	24.0	(0 2 0)	30.435
14	31.316	2.8540	47	17.5					
15	32.100	2.7861	252	94.0	PLATTNERITE...	2.7970	88.0	(1 0 1)	31.971
16	34.199	2.6197	268	100.0	HYDROCER...	2.6230	100.0	(1 1 0)	34.155
17	36.299	2.4728	80	29.9	PLATTNERITE...	2.4800	21.0	(2 0 0)	36.190
18	39.989	2.2527	30	11.2	HYDROCER...	2.2610	10.0	(0 2 1)	39.837
19	40.420	2.2297	73	27.2	HYDROCER...	2.2310	50.0	(2 0 2)	40.396
20	42.740	2.1139	36	13.4	HYDROCER...	2.1200	30.0	(0 2 4)	42.611
21	43.156	2.0945	42	15.7	HYDROCER...	2.0990	20.0	(1 0 10)	43.058
22	44.258	2.0449	39	14.6	HYDROCER...	2.0460	30.0	(2 0 5)	44.232
23	48.256	1.8844	53	19.8	HYDROCER...	1.8840	20.0	(0 2 7)	48.266
24	48.520	1.8747	57	21.3	LITHARGE, SYN	1.8720	37.0	(1 1 2)	48.595
25	49.119	1.8533	244	91.0	PLATTNERITE...	1.8559	52.0	(2 1 1)	49.044
26	49.476	1.8407	111	41.4	MASSICOT	1.8452	12.0	(0 2 2)	49.349
27	49.995	1.8228	42	15.7					
28	50.198	1.8159	28	10.4					
29	50.699	1.7991	21	7.8	CERUSSITE, ...	1.7976	3.0	(2 2 2)	50.746
30	51.936	1.7592	35	13.1	PLATTNERITE...	1.7534	12.0	(2 2 0)	52.119
31	52.162	1.7521	57	21.3	CERUSSITE, ...	1.7517	1.0	(0 4 2)	52.175
32	53.878	1.7002	55	20.5	HYDROCER...	1.6960	40.0	(1 2 2)	54.024
33	54.059	1.6950	69	25.7	PLATTNERITE...	1.6941	6.0	(0 0 2)	54.089
34	54.324	1.6873	46	17.2	CERUSSITE, ...	1.6938	1.0	(3 1 0)	54.098
35	58.718	1.5711	46	17.2	PLATTNERITE...	1.5670	9.0	(3 1 0)	58.887
36	58.940	1.5657	55	20.5	CERUSSITE, ...	1.5647	3.0	(1 5 1)	58.980
37	59.205	1.5593	41	15.3	LITHARGE, SYN	1.5580	6.0	(2 0 2)	59.261
38	60.480	1.5295	53	19.8	HYDROCER...	1.5300	30.0	(2 1 7)	60.457
39	60.662	1.5253	54	20.1	PLATTNERITE...	1.5253	12.0	(1 1 2)	60.663
40	60.933	1.5192	53	19.8					
41	62.161	1.4921	32	11.9					
42	62.358	1.4878	55	20.5	PLATTNERITE...	1.4856	10.0	(3 0 1)	62.463
43	62.659	1.4814	46	17.2	CERUSSITE, ...	1.4832	2.0	(3 1 2)	62.577

[MS30130A.RAW] OHCIJUN1 L2 | PEAK ID REPORT

SCAN: 5.0/90.0/0.02/3(SEC), CU(35KV,40MA), I(MAX)=285, 01/30/03 12:47

PEAK: 15-PTS/PARABOLIC FILTER, THRESHOLD=3.0, CUTOFF=0.1%, BG=3/1.0, PEAK-TOP=SUMMIT

NOTE: INTENSITY = COUNTS, 2T(O)=0.0(°), WAVELENGTH TO COMPUTE D-SPACING = 1.54056A (CU/K-...

#	2-THETA	D(A)	HEIGHT	I%(H)	PHASE ID	D(A)	I%	(H K L)	2-THETA
44	66.739	1.4004	17	6.3	PLATTNERITE...	1.3986	6.0	(2 0 2)	66.837
45	66.999	1.3956	32	11.9					
46	66.999	1.3956	32	11.9					
47	70.102	1.3412	16	6.0	HYDROCER...	1.3400	10.0	(1 2 11)	70.176
48	74.458	1.2732	32	11.9	PLATTNERITE...	1.2739	8.0	(3 2 1)	74.409
49	74.709	1.2695	44	16.4	CERUSSITE, ...	1.2702	1.0	(1 5 3)	74.665
50	78.408	1.2186	20	7.5	LITHARGE, SYN	1.2190	5.0	(3 1 1)	78.380
51	78.682	1.2151	24	9.0	CERUSSITE, ...	1.2154	1.0	(4 2 1)	78.659
52	78.853	1.2129	18	6.7	CERUSSITE, ...	1.2130	1.0	(3 5 0)	78.845
53	84.056	1.1505	28	10.4	PLATTNERITE...	1.1503	6.0	(3 1 2)	84.078
54	85.609	1.1336	30	11.2					
55	85.720	1.1324	28	10.4	PLATTNERITE...	1.1327	4.0	(4 1 1)	85.693
56	85.875	1.1308	25	9.3					
57	88.337	1.1055	18	6.7	CERUSSITE, ...	1.1053	1.0	(1 7 2)	88.358

LINE SHIFTS OF INDIVIDUAL PHASES:

PDF#41-1492 - PLATTNERITE, SYN <2T(O) = 0.0, D/D(O) = 1.0>

PDF#13-0131 - HYDROCERUSSITE, SYN <2T(O) = 0.0, D/D(O) = 1.0>

PDF#47-1734 - CERUSSITE, SYN <2T(O) = -0.06, D/D(O) = 1.0>

PDF#38-1477 - MASSICOT <2T(O) = 0.12, D/D(O) = 1.0>

PDF#05-0561 - LITHARGE, SYN <2T(O) = 0.0, D/D(O) = 1.0>

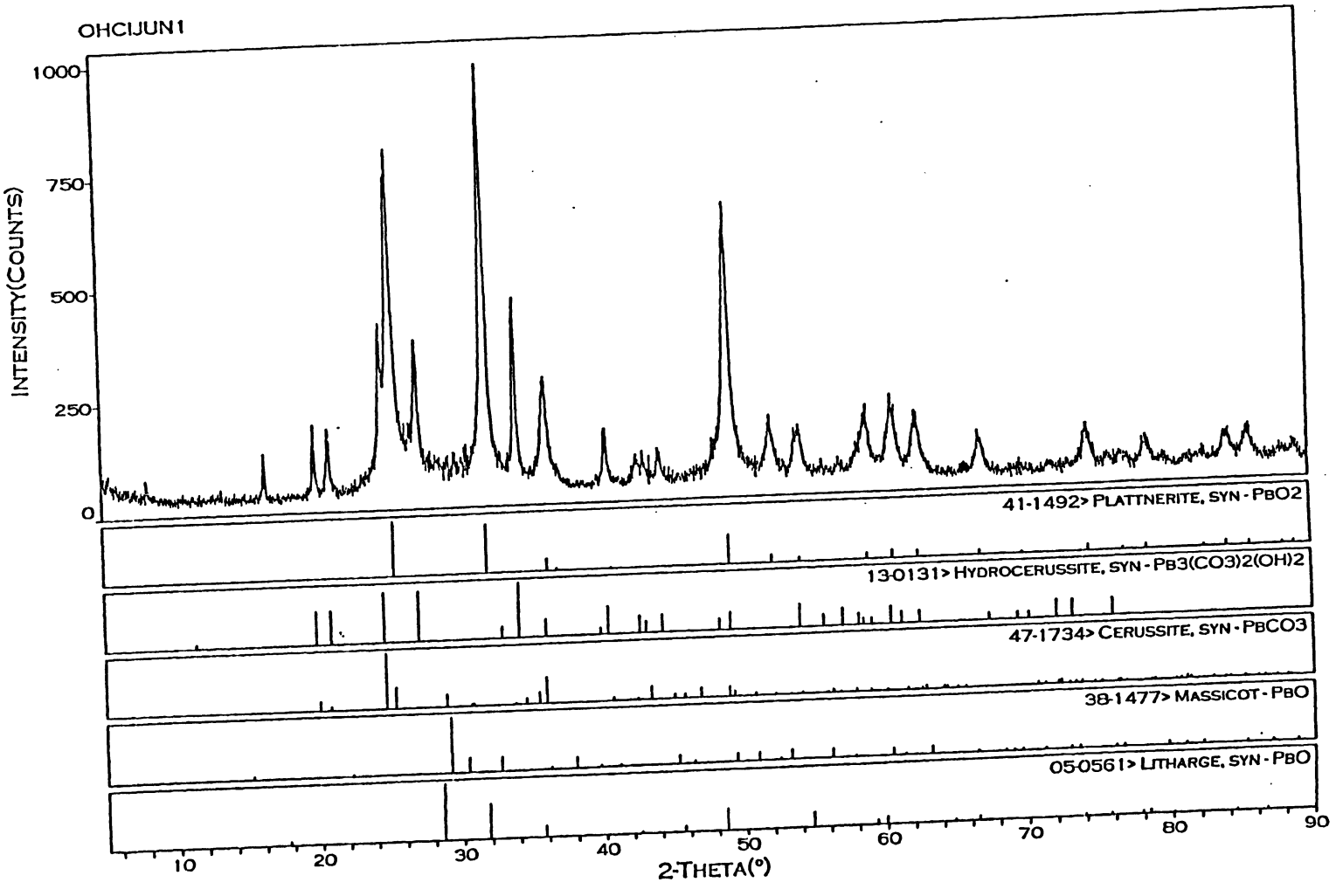
OHCIJUN1
INTENSITY(COUNTS)
1000
750
500
250
0
41-1492> PLATTNERITE, SYN - PBO2
13-0131> HYDROCERUSSITE, SYN - PB3(CO3)2(OH)2
47-1734> CERUSSITE, SYN - PBCO3
38-1477> MASSICOT - PBO
05-0561> LITHARGE, SYN - PBO
10
20
30
40
50
60
70
80
90
2-THETA(°)

[MS30129A.RAW] OHCIJUN1 | PEAK ID REPORT

SCAN: 5.0/90.0/0.02/3(SEC), CU(35KV,40MA), I(MAX)=984, 01/29/03 18:09

PEAK: 15-PTS/PARABOLIC FILTER, THRESHOLD=3.0, CUTOFF=0.1%, BG=3/1.0, PEAK-TOP=SUMMIT

NOTE: INTENSITY = COUNTS, 2T(O)=0.0(°), WAVELENGTH TO COMPUTE D-SPACING = 1.54056A (CU/K-...

#	2-THETA	D(A)	HEIGHT	I%(H)	PHASE ID	D(A)	I%	(H K L)	2-THETA
1	5.523	15.9876	30	3.4					
2	13.364	6.6200	24	2.7					
3	16.359	5.4139	99	11.2					
4	19.940	4.4490	151	17.1	CERUSSITE, ...	4.4311	15.0	(1 1 0)	20.022
5	20.944	4.2380	139	15.8	HYDROCER...	4.2500	60.0	(0 1 2)	20.884
6	24.244	3.6681	66	7.5					
7	24.760	3.5928	338	38.4	CERUSSITE, ...	3.5986	100.0	(1 1 1)	24.720
8	25.519	3.4877	643	73.0	PLATTNERITE...	3.5000	100.0	(1 1 0)	25.427
9	26.718	3.3338	55	6.2					
10	27.221	3.2733	254	28.8	HYDROCER...	3.2900	90.0	(0 1 5)	27.080
11	29.918	2.9841	34	3.9					
12	32.100	2.7861	881	100.0	PLATTNERITE...	2.7970	88.0	(1 0 1)	31.971
13	34.220	2.6182	382	43.4	HYDROCER...	2.6230	100.0	(1 1 0)	34.155
14	36.280	2.4741	220	25.0	PLATTNERITE...	2.4800	21.0	(2 0 0)	36.190
15	37.077	2.4227	50	5.7	PLATTNERITE...	2.4370	2.0	(1 1 1)	36.852
16	40.423	2.2296	118	13.4	HYDROCER...	2.2310	50.0	(2 0 2)	40.396
17	42.636	2.1188	52	5.9	HYDROCER...	2.1200	30.0	(0 2 4)	42.611
18	42.816	2.1103	41	4.7					
19	43.102	2.0970	52	5.9	HYDROCER...	2.0990	20.0	(1 0 10)	43.058
20	44.241	2.0456	59	6.7	HYDROCER...	2.0460	30.0	(2 0 5)	44.232
21	48.503	1.8753	94	10.7	LITHARGE, SYN	1.8720	37.0	(1 1 2)	48.595
22	49.201	1.8503	502	57.0	CERUSSITE, ...	1.8482	8.0	(0 2 3)	49.262
23	52.220	1.7503	113	12.8	CERUSSITE, ...	1.7517	1.0	(0 4 2)	52.175
24	52.338	1.7466	83	9.4	MASSICOT	1.7439	1.0	(3 1 0)	52.424
25	53.982	1.6972	89	10.1	HYDROCER...	1.6960	40.0	(1 2 2)	54.024
26	54.357	1.6864	92	10.4					
27	55.881	1.6439	28	3.2	CERUSSITE, ...	1.6424	1.0	(0 5 1)	55.938
28	57.061	1.6127	31	3.5	HYDROCER...	1.6130	30.0	(1 2 5)	57.050
29	58.923	1.5661	107	12.1	PLATTNERITE...	1.5670	9.0	(3 1 0)	58.887
30	59.079	1.5624	124	14.1	HYDROCER...	1.5620	10.0	(2 0 11)	59.094
31	60.460	1.5299	56	6.4	HYDROCER...	1.5300	30.0	(2 1 7)	60.457
32	60.858	1.5209	128	14.5	PLATTNERITE...	1.5253	12.0	(1 1 2)	60.663
33	61.079	1.5159	124	14.1	HYDROCER...	1.5130	20.0	(3 0 0)	61.209
34	62.501	1.4848	120	13.6	HYDROCER...	1.4850	20.0	(3 0 3)	62.491
35	62.659	1.4814	121	13.7	CERUSSITE, ...	1.4832	2.0	(3 1 2)	62.577
36	66.963	1.3963	86	9.8	PLATTNERITE...	1.3986	6.0	(2 0 2)	66.837
37	67.199	1.3919	69	7.8	HYDROCER...	1.3880	10.0	(2 1 10)	67.415
38	74.503	1.2725	90	10.2	PLATTNERITE...	1.2739	8.0	(3 2 1)	74.409
39	74.798	1.2682	62	7.0	CERUSSITE, ...	1.2702	1.0	(1 5 3)	74.665
40	78.462	1.2179	53	6.0	PLATTNERITE...	1.2179	5.0	(2 2 2)	78.465
41	78.660	1.2154	57	6.5	CERUSSITE, ...	1.2154	1.0	(4 2 1)	78.659
42	78.859	1.2128	46	5.2	CERUSSITE, ...	1.2130	1.0	(3 5 0)	78.845
43	84.143	1.1496	52	5.9	CERUSSITE, ...	1.1497	1.0	(4 2 2)	84.135

[MS30129A.RAW] OHCIJUN1 | PEAK ID REPORT

SCAN: 5.0/90.0/0.02/3(SEC), CU(35KV,40MA), I(MAX)=984, 01/29/03 18:09

PEAK: 15-PTS/PARABOLIC FILTER, THRESHOLD=3.0, CUTOFF=0.1%, BG=3/1.0, PEAK-TOP=SUMMIT

NOTE: INTENSITY = COUNTS, 2T(0)=0.0(°), WAVELENGTH TO COMPUTE D-SPACING = 1.54056A (CU/K-...

#	2-THETA	D(A)	HEIGHT	I%(H)	PHASE ID	D(A)	I%	(H K L)	2-THETA
44	84.440	1.1463	55	6.2	LITHARGE, SYN	1.1462	2.0	(1 1 4)	84.448
45	85.741	1.1322	60	6.8	PLATTNERITE...	1.1327	4.0	(4 1 1)	85.693
46	85.899	1.1305	69	7.8					
47	86.184	1.1275	29	3.3	CERUSSITE, ...	1.1279	1.0	(3 5 2)	86.144
48	89.094	1.0981	30	3.4					

LINE SHIFTS OF INDIVIDUAL PHASES:

PDF#41-1492 - PLATTNERITE, SYN <2T(0) = 0.0, D/D(0) = 1.0>

PDF#13-0131 - HYDROCERUSSITE, SYN <2T(0) = 0.0, D/D(0) = 1.0>

PDF#47-1734 - CERUSSITE, SYN <2T(0) = -0.06, D/D(0) = 1.0>

PDF#38-1477 - MASSICOT <2T(0) = 0.12, D/D(0) = 1.0>

PDF#05-0561 - LITHARGE, SYN <2T(0) = 0.0, D/D(0) = 1.0>

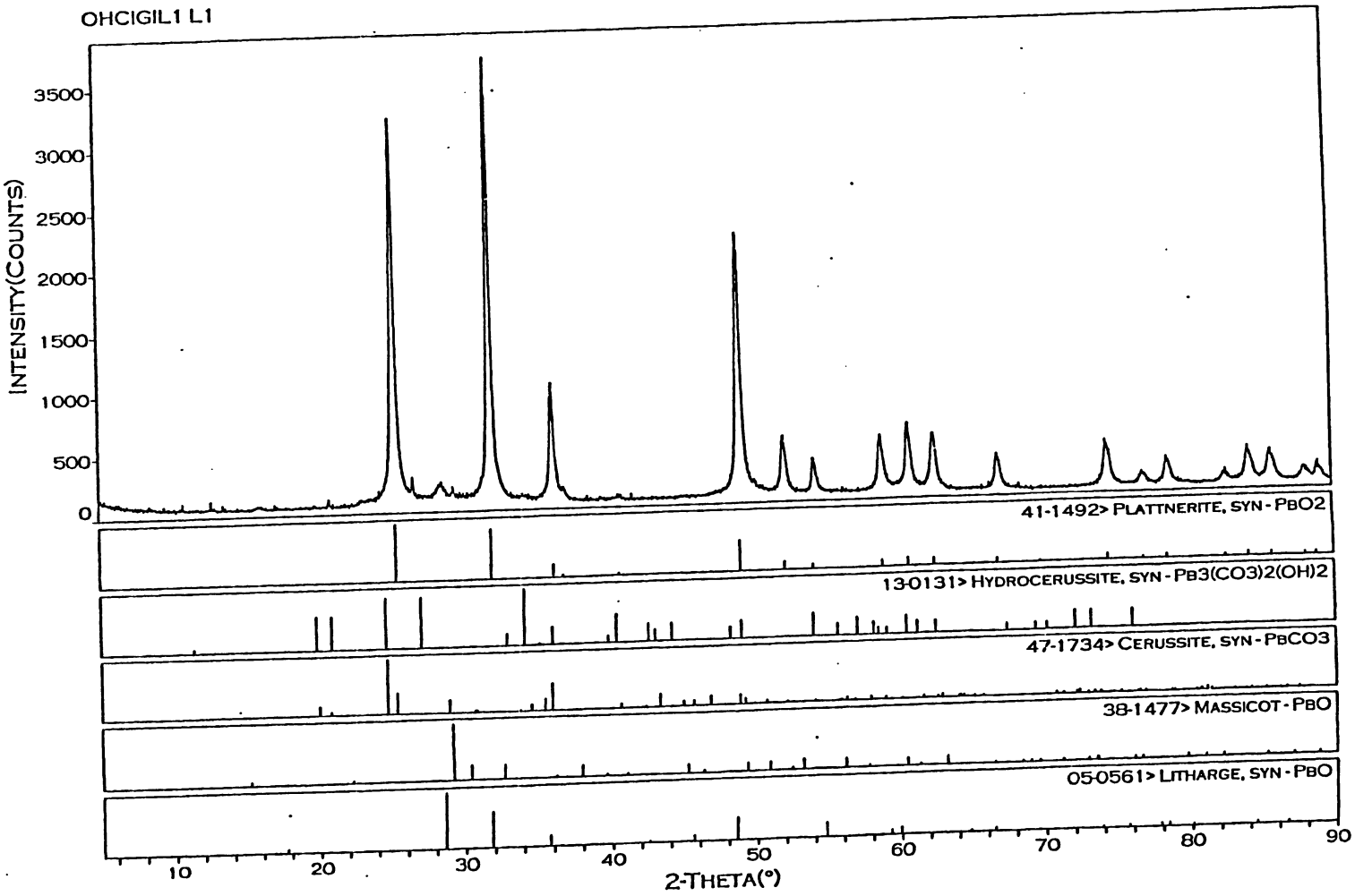
OHCIGIL1 L1
INTENSITY(COUNTS)
3500
3000
2500
2000
1500
1000
500
0
41-1492> PLATTNERITE, SYN - PBO2
13-0131> HYDROCERUSSITE, SYN - PB3(CO3)2(OH)2
47-1734> CERUSSITE, SYN - PBCO3
38-1477> MASSICOT - PBO
05-0561> LITHARGE, SYN - PBO
10
20
30
40
50
60
70
80
90
2-THETA(°)

[MS302048.RAW] OHCIGIL1 L1 | PEAK ID REPORT

SCAN: 5.0/90.0/0.01/5(SEC), CU(35KV,40MA), I(MAX)=3719, 02/05/03 04:16

PEAK: 15-PTS/PARABOLIC FILTER, THRESHOLD=3.0, CUTOFF=0.1%, BG=3/1.0, PEAK-TOP=SUMMIT

NOTE: INTENSITY = COUNTS, 2T(0)=0.0(°), WAVELENGTH TO COMPUTE D-SPACING = 1.54056A (CU/K-...

#	2-THETA	D(A)	HEIGHT	I%(H)	PHASE ID	D(A)	I%	(H K L)	2-THETA
1	8.474	10.4253	35	1.0					
2	8.474	10.4253	35	1.0					
3	9.480	9.3213	32	0.9					
4	12.688	6.9711	75	2.1					
5	13.529	6.5395	43	1.2					
6	15.882	5.5757	28	0.8					
7	16.098	5.5012	28	0.8					
8	16.178	5.4742	31	0.9					
9	17.127	5.1730	37	1.0					
10	17.283	5.1267	27	0.8					
11	19.931	4.4512	31	0.9	HYDROCER...	4.4700	60.0	(1 0 1)	19.846
12	20.900	4.2469	70	2.0	HYDROCER...	4.2500	60.0	(0 1 2)	20.884
13	25.440	3.4983	3070	85.9	PLATTNERITE...	3.5000	100.0	(1 1 0)	25.427
14	26.049	3.4178	208	5.8					
15	26.700	3.3360	128	3.6					
16	28.291	3.1519	66	1.8					
17	28.369	3.1434	75	2.1					
18	28.453	3.1343	99	2.8					
19	28.550	3.1239	105	2.9					
20	28.680	3.1101	117	3.3	LITHARGE, SYN	3.1150	100.0	(1 0 1)	28.633
21	28.851	3.0920	88	2.5	LITHARGE, SYN	3.1150	100.0	(1 0 1)	28.633
22	28.979	3.0786	67	1.9	CERUSSITE, ...	3.0792	21.0	(0 0 2)	28.973
23	29.441	3.0313	75	2.1	MASSICOT	3.0560	100.0	(1 1 1)	29.198
24	29.939	2.9821	43	1.2					
25	31.511	2.8368	169	4.7					
26	32.100	2.7861	3572	100.0	PLATTNERITE...	2.7970	88.0	(1 0 1)	31.971
27	32.678	2.7381	242	6.8	MASSICOT	2.7352	23.0	(2 0 0)	32.713
28	32.879	2.7218	118	3.3	HYDROCER...	2.7150	20.0	(1 0 7)	32.964
29	34.249	2.6160	38	1.1	HYDROCER...	2.6230	100.0	(1 1 0)	34.155
30	36.310	2.4721	950	26.6	PLATTNERITE...	2.4800	21.0	(2 0 0)	36.190
31	36.961	2.4300	112	3.1	PLATTNERITE...	2.4370	2.0	(1 1 1)	36.852
32	37.080	2.4225	91	2.5					
33	39.488	2.2802	29	0.8					
34	39.583	2.2749	27	0.8	MASSICOT	2.2721	1.0	(1 2 1)	39.634
35	40.709	2.2145	46	1.3	CERUSSITE, ...	2.2161	5.0	(2 2 0)	40.679
36	48.591	1.8721	141	3.9	LITHARGE, SYN	1.8720	37.0	(1 1 2)	48.595
37	49.180	1.8511	2091	58.5	CERUSSITE, ...	1.8482	8.0	(0 2 3)	49.262
38	49.689	1.8333	232	6.5					
39	49.848	1.8278	151	4.2					
40	52.160	1.7521	369	10.3	CERUSSITE, ...	1.7517	1.0	(0 4 2)	52.175
41	52.240	1.7496	454	12.7					
42	52.340	1.7465	375	10.5	MASSICOT	1.7439	1.0	(3 1 0)	52.424
43	54.320	1.6875	274	7.7	CERUSSITE, ...	1.6938	1.0	(3 1 0)	54.098

[MS30204B.RAW] OHCIGIL1 L1 | PEAK ID REPORT

SCAN: 5.0/90.0/0.01/5(SEC), CU(35KV,40MA), I(MAX)=3719, 02/05/03 04:16

PEAK: 15-PTS/PARABOLIC FILTER, THRESHOLD=3.0, CUTOFF=0.1%, BG=3/1.0, PEAK-TOP=SUMMIT

NOTE: INTENSITY = COUNTS, 2T(0)=0.0(°), WAVELENGTH TO COMPUTE D-SPACING = 1.54056A (CU/K-...

#	2-THETA	D(A)	HEIGHT	I%(H)	PHASE ID	D(A)	I%	(H K L)	2-THETA
44	54.390	1.6855	228	6.4					
45	54.782	1.6743	41	1.1	LITHARGE, SYN	1.6750	24.0	(2 1 1)	54.757
46	58.890	1.5669	384	10.8	PLATTNERITE...	1.5670	9.0	(3 1 0)	58.887
47	58.980	1.5647	431	12.1	CERUSSITE, ...	1.5647	3.0	(1 5 1)	58.980
48	59.069	1.5626	340	9.5	HYDROCER...	1.5620	10.0	(2 0 11)	59.094
49	59.390	1.5549	88	2.5	LITHARGE, SYN	1.5580	6.0	(2 0 2)	59.261
50	60.870	1.5206	500	14.0	PLATTNERITE...	1.5253	12.0	(1 1 2)	60.663
51	61.019	1.5173	360	10.1	HYDROCER...	1.5130	20.0	(3 0 0)	61.209
52	62.180	1.4917	56	1.6					
53	62.660	1.4814	435	12.2	CERUSSITE, ...	1.4832	2.0	(3 1 2)	62.577
54	62.759	1.4793	372	10.4	CERUSSITE, ...	1.4767	4.0	(3 3 0)	62.884
55	67.010	1.3954	278	7.8	PLATTNERITE...	1.3986	6.0	(2 0 2)	66.837
56	67.140	1.3930	254	7.1					
57	67.240	1.3912	191	5.3	HYDROCER...	1.3880	10.0	(2 1 10)	67.415
58	73.961	1.2805	49	1.4	LITHARGE, SYN	1.2820	2.0	(3 0 1)	73.861
59	74.480	1.2729	372	10.4	PLATTNERITE...	1.2739	8.0	(3 2 1)	74.409
60	74.580	1.2714	328	9.2	PLATTNERITE...	1.2739	8.0	(3 2 1)	74.409
61	74.740	1.2691	278	7.8	CERUSSITE, ...	1.2702	1.0	(1 5 3)	74.665
62	76.881	1.2390	99	2.8	PLATTNERITE...	1.2392	2.0	(4 0 0)	76.865
63	77.049	1.2367	90	2.5					
64	77.200	1.2347	62	1.7					
65	78.610	1.2160	218	6.1	CERUSSITE, ...	1.2154	1.0	(4 2 1)	78.659
66	78.741	1.2143	192	5.4					
67	78.769	1.2139	189	5.3	CERUSSITE, ...	1.2154	1.0	(4 2 1)	78.659
68	78.859	1.2128	156	4.4	CERUSSITE, ...	1.2130	1.0	(3 5 0)	78.845
69	79.159	1.2089	32	0.9					
70	82.402	1.1694	49	1.4					
71	82.472	1.1686	80	2.2	PLATTNERITE...	1.1683	2.0	(3 3 0)	82.496
72	82.591	1.1672	77	2.2					
73	82.729	1.1656	71	2.0	CERUSSITE, ...	1.1630	1.0	(1 7 1)	82.955
74	84.239	1.1485	260	7.3	CERUSSITE, ...	1.1497	1.0	(4 2 2)	84.135
75	84.360	1.1472	213	6.0	LITHARGE, SYN	1.1462	2.0	(1 1 4)	84.448
76	85.611	1.1336	162	4.5					
77	85.741	1.1322	209	5.9	PLATTNERITE...	1.1327	4.0	(4 1 1)	85.693
78	85.809	1.1315	241	6.7					
79	85.991	1.1295	180	5.0	CERUSSITE, ...	1.1279	1.0	(3 5 2)	86.144
80	88.090	1.1080	93	2.6	PLATTNERITE...	1.1084	2.0	(4 2 0)	88.046
81	88.170	1.1072	95	2.7	CERUSSITE, ...	1.1068	1.0	(4 4 0)	88.207
82	88.992	1.0991	103	2.9	PLATTNERITE...	1.1008	3.0	(1 0 3)	88.813
83	89.070	1.0983	116	3.2					
84	89.122	1.0978	130	3.6					
85	89.231	1.0967	85	2.4					

EDXA CWW Samples
Jun (red)
Gil (blu)

Red

Elmt	Line	Spectrum t	Apparent c	Stat. Sigm	k Ratio	k Ratio Sig	Fit Index	Inten. Corr	Std. Corrn	Element %	Sigma %	Atomic %
C	K	ED	1.770072	5.85E-02	0.147501	4.87E-03		0.47926	0.965367	7.529528	0.232288	32.66629
O	K	ED	2.52636	6.56E-02	4.74E-02	1.23E-03		0.485539	0.605231	10.60654	0.250109	34.54554
Al	K	ED	0.781231	1.66E-02	1.48E-02	3.14E-04		0.694429	0.95824	2.293844	4.90E-02	4.429973
Ca	K	ED	0.338988	1.88E-02	9.88E-03	5.48E-04		0.772909	1.161408	0.894279	4.94E-02	1.162671
Mn	K	ED	1.62335	0.039002	0.016234	3.90E-04		0.899729	1.301351	3.678887	8.70E-02	3.489434
Fe	K	ED	3.335435	5.12E-02	3.34E-02	5.12E-04		0.956875	1.336047	7.107446	0.106923	6.631702
Pb	M	ED	31.63953	0.130532	0.374418	1.54E-03		0.950446	0.960431	67.88948	0.288026	17.07438

* = <2 Sigma

Elmt	Line	Spectrum t	Apparent c	Stat. Sigm	k Ratio	k Ratio Sig	Fit Index	Inten. Corr	Std. Corrn	Element %	Sigma %	Atomic %
C	K	ED	2.936078	7.28E-02	0.244664	6.07E-03		0.469015	0.965367	8.211053	0.188985	32.27703
O	K	ED	4.704962	8.58E-02	8.84E-02	1.61E-03		0.484175	0.605231	12.74409	0.20696	37.60885
Al	K	ED	1.23494	2.06E-02	2.33E-02	3.89E-04		0.679648	0.95824	2.383664	4.00E-02	4.171043
Ca	K	ED	0.563003	2.30E-02	1.64E-02	6.72E-04		0.777022	1.161408	0.950531	0.038719	1.119728
Mn	K	ED	3.076456	5.08E-02	3.08E-02	5.08E-04		0.892583	1.301351	4.521576	7.34E-02	3.885893
Fe	K	ED	5.513782	6.56E-02	5.51E-02	6.56E-04		0.947388	1.336047	7.635	8.91E-02	6.454804
Pb	M	ED	45.40223	0.15785	0.537284	1.87E-03		0.93737	0.960431	63.55408	0.227711	14.48267

* = <2 Sigma

Elmt	Line	Spectrum t	Apparent c	Stat. Sigm	k Ratio	k Ratio Sig	Fit Index	Inten. Corr	Std. Corrn	Element %	Sigma %	Atomic %
C	K	ED	2.919108	6.73E-02	0.24325	5.61E-03		0.470911	0.965367	10.82354	0.226965	38.10761
O	K	ED	3.909135	7.91E-02	7.34E-02	1.48E-03		0.456468	0.605231	14.94847	0.263369	39.51168
Al	K	ED	0.66269	1.76E-02	1.25E-02	3.33E-04		0.68526	0.95824	1.688926	4.49E-02	2.647026
Ca	K	ED	0.252752	1.93E-02	7.37E-03	5.62E-04		0.767036	1.161408	0.575493	4.38E-02	0.607203
Mn	K	ED	0.788994	3.43E-02	7.89E-03	3.43E-04		0.884365	1.301351	1.558122	6.72E-02	1.199362
Fe	K	ED	3.456455	5.05E-02	3.46E-02	5.05E-04		0.938677	1.336047	6.430926	9.31E-02	4.869623
Pb	M	ED	34.53657	0.138263	0.408701	1.64E-03		0.943127	0.960431	63.97454	0.28017	13.0575

* = <2 Sigma

Blue

Elmt	Line	Spectrum t	Apparent c	Stat. Sigm	k Ratio	k Ratio Sig	Fit Index	Inten. Corr	Std. Corrn	Element %	Sigma %	Atomic %
C	K	ED	1.548259	6.16E-02	0.129017	5.13E-03		0.440699	0.965367	5.709804	0.215338	18.86967
O	K	ED	6.548759	9.19E-02	0.122981	1.73E-03		0.518775	0.605231	20.51496	0.240346	50.89793
Al	K	ED	1.618395	2.09E-02	3.06E-02	3.95E-04		0.643447	0.95824	4.08799	0.054022	6.013924
Ca	K	ED	1.200766	2.38E-02	3.50E-02	6.93E-04		0.801859	1.161408	2.433935	4.83E-02	2.41048
Mn	K	ED	5.460507	5.29E-02	5.46E-02	5.29E-04		0.876196	1.301351	10.12925	9.92E-02	7.318579
Fe	K	ED	3.884178	5.45E-02	3.88E-02	5.45E-04		0.924448	1.336047	6.829084	9.44E-02	4.853833
Pb	M	ED	27.71071	0.126187	0.327925	1.49E-03		0.895589	0.960431	50.29498	0.230278	9.635586

* = <2 Sigma

Elmt	Line	Spectrum t	Apparent c	Stat. Sigm	k Ratio	k Ratio Sig	Fit Index	Inten. Corr	Std. Corrn	Element %	Sigma %	Atomic %
C	K	ED	1.666804	6.29E-02	0.138895	5.24E-03		0.433147	0.965367	5.980157	0.213554	18.22693
O	K	ED	8.01927	9.83E-02	0.150597	1.85E-03		0.523527	0.605231	23.80418	0.237166	54.4679
Al	K	ED	1.861374	2.20E-02	3.52E-02	4.16E-04		0.638714	0.95824	4.529042	5.50E-02	6.144866
Ca	K	ED	1.226684	2.39E-02	3.58E-02	6.97E-04		0.805206	1.161408	2.367649	4.63E-02	2.162568
Mn	K	ED	5.271835	5.18E-02	5.27E-02	5.18E-04		0.870061	1.301351	9.416725	9.36E-02	6.274907
Fe	K	ED	3.93944	5.38E-02	0.039394	5.38E-04		0.916435	1.336047	6.680686	9.01E-02	4.379267
Pb	M	ED	26.94856	0.124838	0.318906	1.48E-03		0.886984	0.960431	47.22156	0.220332	8.343566

* = <2 Sigma

Elmt	Line	Spectrum t	Apparent c	Stat. Sigm	k Ratio	k Ratio Sig	Fit Index	Inten. Corr	Std. Corrn	Element %	Sigma %	Atomic %
C	K	ED	1.916873	6.44E-02	0.159734	5.37E-03		0.425788	0.965367	7.150407	0.224857	20.1883
O	K	ED	8.394033	0.100643	0.157634	1.89E-03		0.530516	0.605231	25.13307	0.242646	53.27224
Al	K	ED	2.063579	2.23E-02	3.90E-02	4.22E-04		0.629852	0.95824	5.203865	5.66E-02	6.540336
Ca	K	ED	1.292685	2.38E-02	3.77E-02	6.93E-04		0.820407	1.161408	2.502773	4.63E-02	2.11759
Mn	K	ED	5.840451	5.28E-02	5.84E-02	5.28E-04		0.8679	1.301351	10.68883	9.91E-02	6.597899
Fe	K	ED	4.155198	5.42E-02	4.16E-02	5.42E-04		0.911671	1.336047	7.239488	9.35E-02	4.395985
Pb	M	ED	23.19774	0.117031	0.274519	1.38E-03		0.875538	0.960431	42.08155	0.213514	6.887652

APPENDIX 2

MATERIAL TEST REPORT

DATE : 10/16/01
PAGE : 1
ORDER: 55677

Metal Samples Company
P.O. Box 8
152 Metal Samples Road
Munford, AL 36268
Ph. (256)358-4202 Fx. (256)358-4515

Customer: 11740 IT CORPORATION
Your PO#: VISA-JOHN BRANNON

Lot No. K287 Mill: HITACHI CABLE, LTD. Our Order Line No. 1
Description: CDA101 .125" X 12" X 7
Chemical Properties:

Bi:<I PPM	Cd:<1 PPM	Cu:99.990	Hg:<1 PPM
O:3 PPM	P:2 PPM	Pb:4 PPM	S:9 PPM
Se:<1 PPM	Te:<1 PPM	Zn:<1 PPM	

Physical Properties:
Hardness:HRF 29.1

Lot No. H621 Mill: VULCAN LEAD, INC. Our Order Line No. 2
Description: LEAD .125"X24"X25" Cert Only
Chemical Properties:
Not Available
Physical Properties:
Not Available

Lot No. C022 Mill: ARMCO INC. Our Order Line No. 3
Description: IRON 3/8PL 48 X 120
Chemical Properties:

C:0.030	Cu:0.020	Fe:BAL	Mn:0.060
P:0.008	S:0.008		

Physical Properties:
Not Available

Lot No. G866 Mill: BULLOCK Our Order Line No. 4
Description: CDA845 INGOT
Chemical Properties:

Cu:78.970	Fe:0.180	Ni:0.350	Pb:6.750
Sn:2.710	Zn:11.040		

Physical Properties:
Not Available

We certify that the Material Test Report is correct to the best of our knowledge and that the material supplied meets your required P.O. specifications.

THANK YOU, Quality Control Dept. Larry Barton (LEB)

Appendix 2 Manufactures' Coupon Metal Analysis

Schott Redox Electrodes from the Redox Study								
			Measured Values			Eh Values		
Date checked	Electrode ID	ZoBells	Methrom	Lights		ZoBells	Methrom	Lights
12/4/2001	MP2	238.4	247.4	439.4		445.4	454.4	646.4
	MP4	237.6	247.4	443.5		444.6	454.4	650.5
	MP6	236.8	271	442.7		443.8	478	649.7
	MP8	236.8	247.4	442.7		443.8	454.4	649.7
1/10/2002	MP4	239.2	244.1	423.9		446.2	451.1	630.9
1/23/2002	MP2	227.8	240.9	410.9		434.8	447.9	617.9
	MP4	227.8	239.2	410.9		434.8	446.2	617.9
	MP6	228.7	240	410.1		435.7	447	617.1
	MP8	228.7	240.9	410.1		435.7	447.9	617.1
2/11/2002	MP2	224.6	233.5	409.3		431.6	440.5	616.3
	MP4	225.4	231.9	402.8		432.4	438.9	609.8
	MP6	224.6	233.5	408.5		431.6	440.5	615.5
	MP8	227	235.2	410.1		434	442.2	617.1
3/4/2002	MP2	223	226.2	402		430	433.2	609
	MP4	225.4	224.6	395.5		432.4	431.6	602.5
	MP6	223.8	225.4	401.2		430.8	432.4	608.2
	MP8	227	226.2	398.7		434	433.2	605.7
3/19/2002	MP2	222.1	223	402.8		429.1	430	609.8
	MP4	226.2	220.5	393.8		433.2	427.5	600.8
	MP6	223	223	402		430	430	609
	MP8	227.8	224.6	400.4		434.8	431.6	607.4
4/2/2002	MP2	219.7	219.7	399.5		426.7	426.7	606.5
	MP4	224.6	217.3	397.9		431.6	424.3	604.9
	MP6	220.5	221.3	402.8		427.5	428.3	609.8
	MP8	225.4	223	399.5		432.4	430	606.5
4/23/2002	MP2	218.9	218.1	397.9		425.9	425.1	604.9
	MP4	224.6	217.3	389.8		431.6	424.3	596.8
	MP6	219.7	218.1	398.7		426.7	425.1	605.7
	MP8	225.4	220.5	395.5		432.4	427.5	602.5
5/22/2002	MP2	221.3	218.1	386.5		428.3	425.1	593.5
	MP4	227	218.1	380.8		434	425.1	587.8
	MP6	220.5	218.9	388.1		427.5	425.9	595.1
	MP8	227	222.1	389.8		434	429.1	596.8
8/15/2002	MP2	224.6	224.6	401.2		431.6	431.6	608.2
	MP4	228.7	226.2	402.1		435.7	433.2	609.1
	MP6	227	225.4	400.4		434	432.4	607.4
	MP8	223.5	230.3	406.2		430.5	437.3	613.2
10/17/2002	MP2	220.5	220.5	399.5		427.5	427.5	606.5
	MP4	214	207.5	393		421	414.5	600
	MP6	207.5	214.8	393.8		414.5	421.8	600.8
	MP8	224.6	224.6	402.8		431.6	431.6	609.8
10/30/2002	MP2	223	221.3	402		430	428.3	609
	MP4	206.7	206.7	391.4		413.7	413.7	598.4
	MP6	213.2	212.4	398.7		420.2	419.4	605.7
	MP8	222.1	223	405.2		429.1	430	612.2
11/14/2002	MP2	218.1	221.3	407.7		425.1	428.3	614.7
	MP4	213.2	215.6	400.4		420.2	422.6	607.4
	MP6	214	217.3	401.2		421	424.3	608.2
	MP8	221.3	226.2	414.2		428.3	433.2	621.2
12/3/2002	MP2	214	218.1	398.7		421	425.1	605.7
	MP4	216.4	218.9	398.7		423.4	425.9	605.7
	MP6	209.9	214	392.2		416.9	421	599.2
	MP8	215.6	222.1	402.8		422.6	429.1	609.8

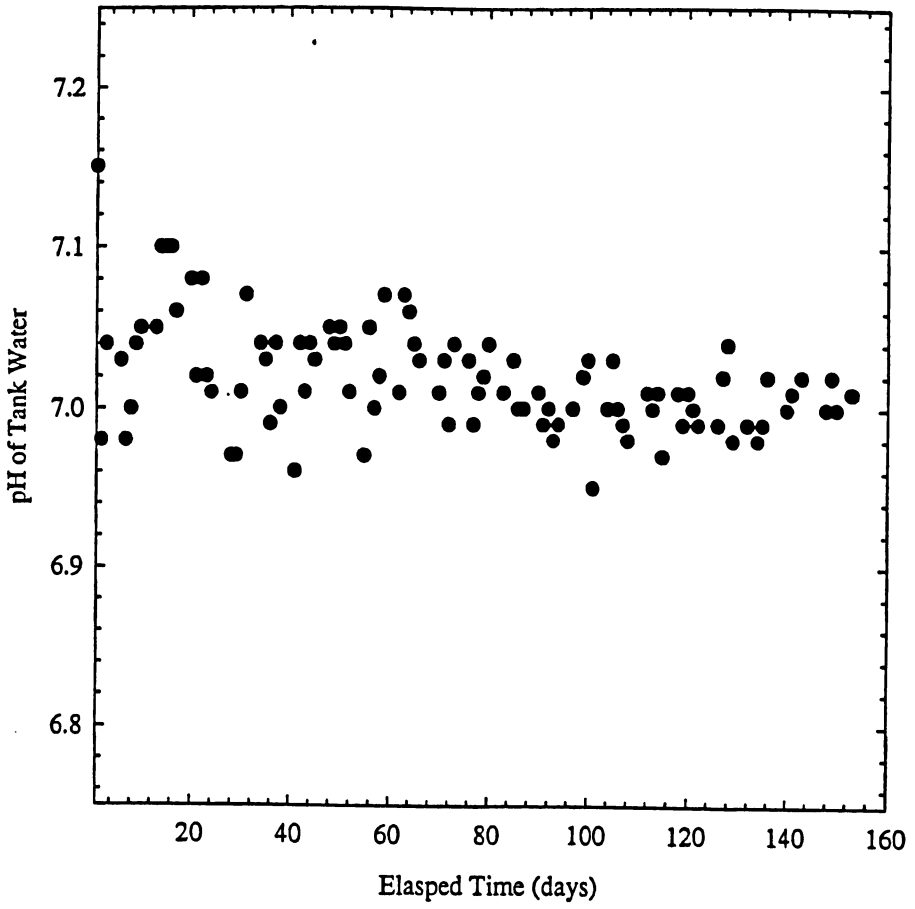

Appendix 2 Initial pH of new/or adjusted tank water prior to each flush and daily "run" in the loop apparatus system for the Chlorine Run.

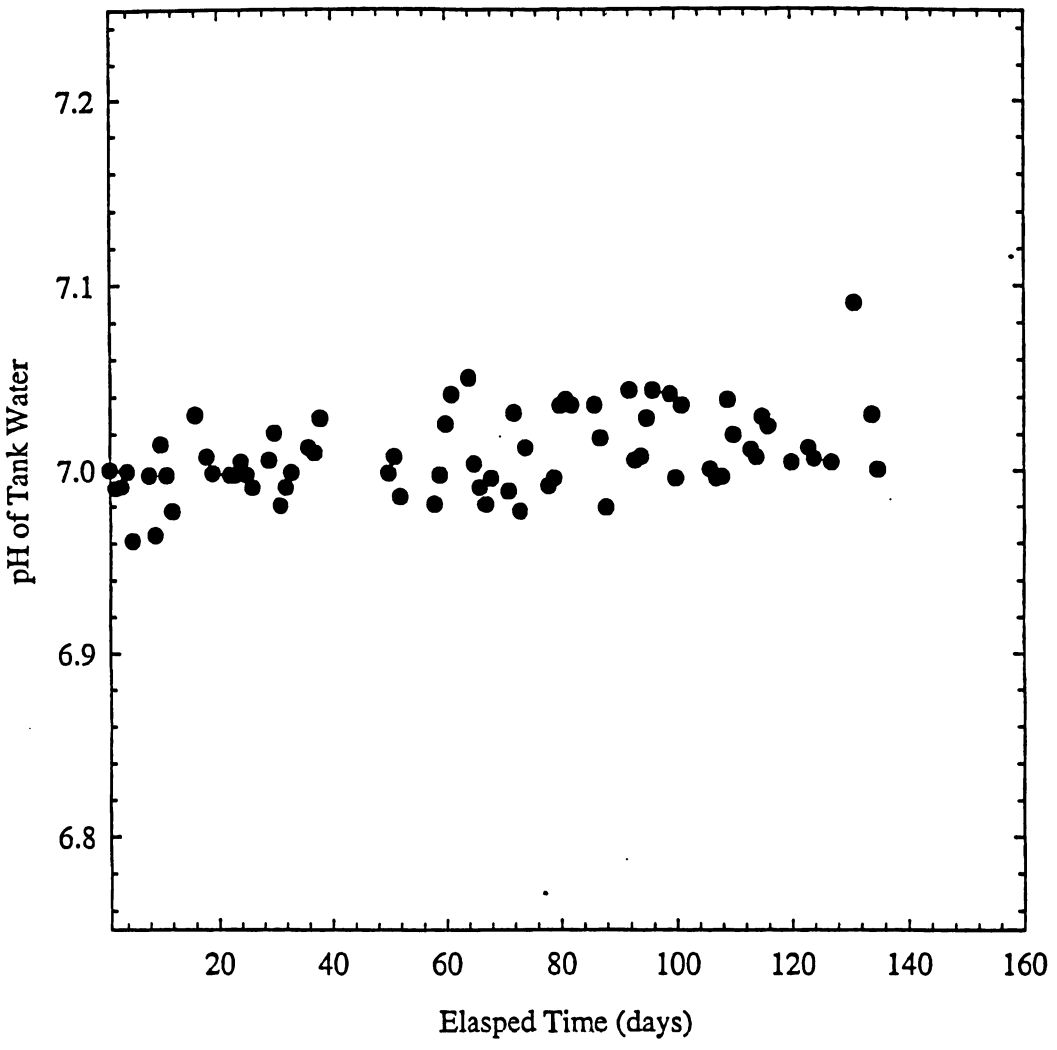

Appendix 2 pH of new/or adjusted Tank Water prior to each flush and daily "run" the loop apparatus system for the Dissolved Oxygen Run.

APPENDIX 3

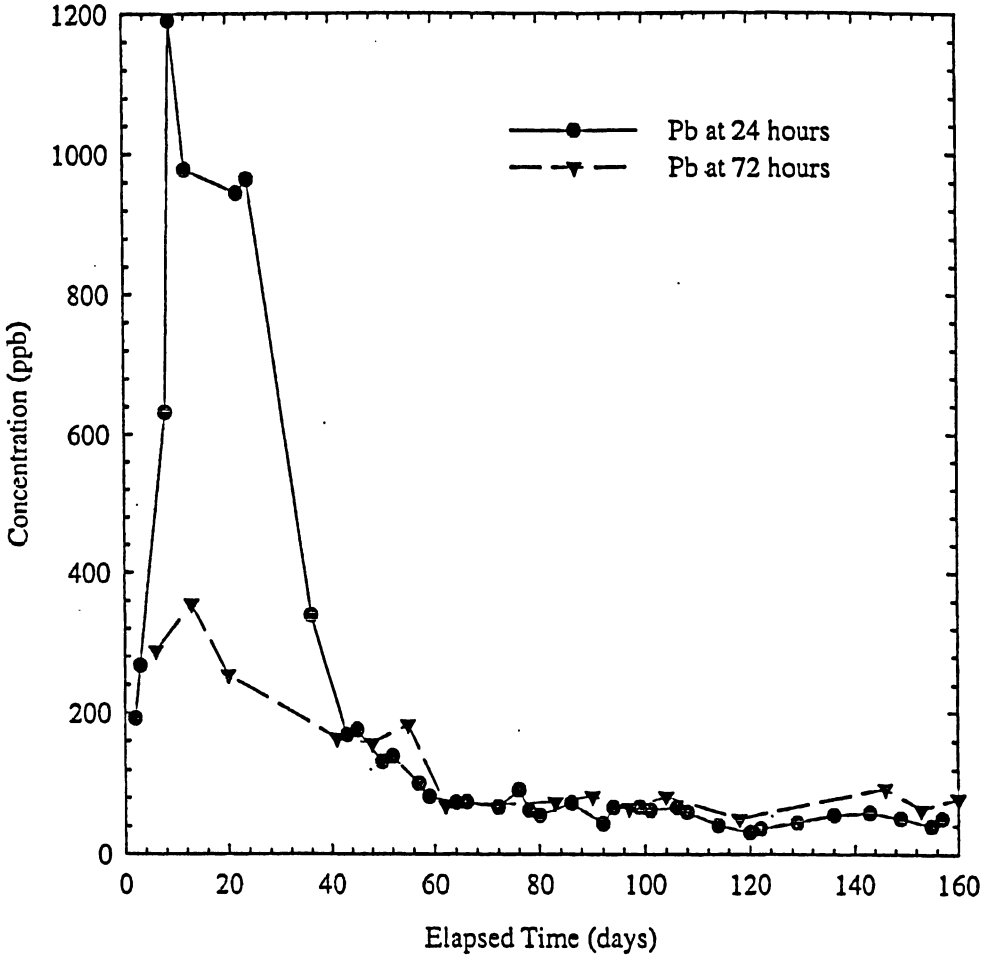

Appendix 3 Elapsed time versus lead metal release profile for 24 and 72 hour stagnation times for Cell #2.

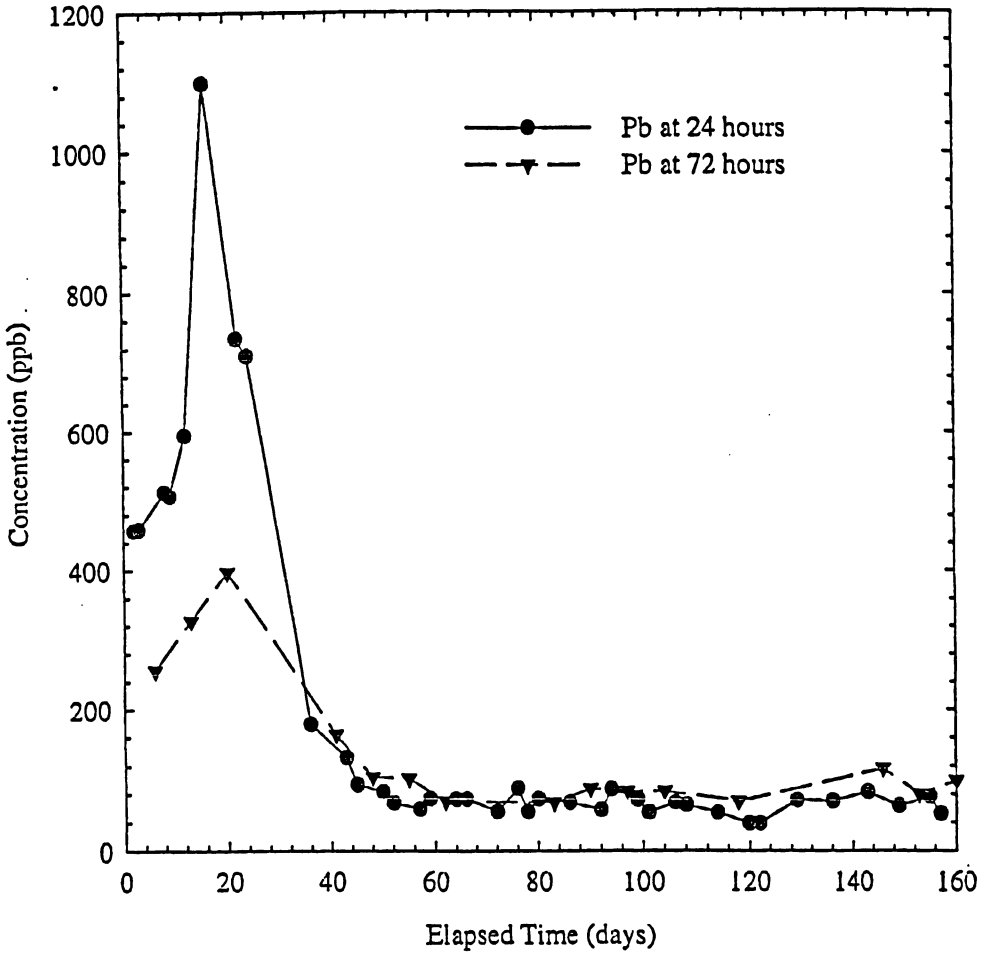

Appendix 3 Elapsed time versus lead metal release profile for 24 and 72 hour stagnation times for Cell #1.

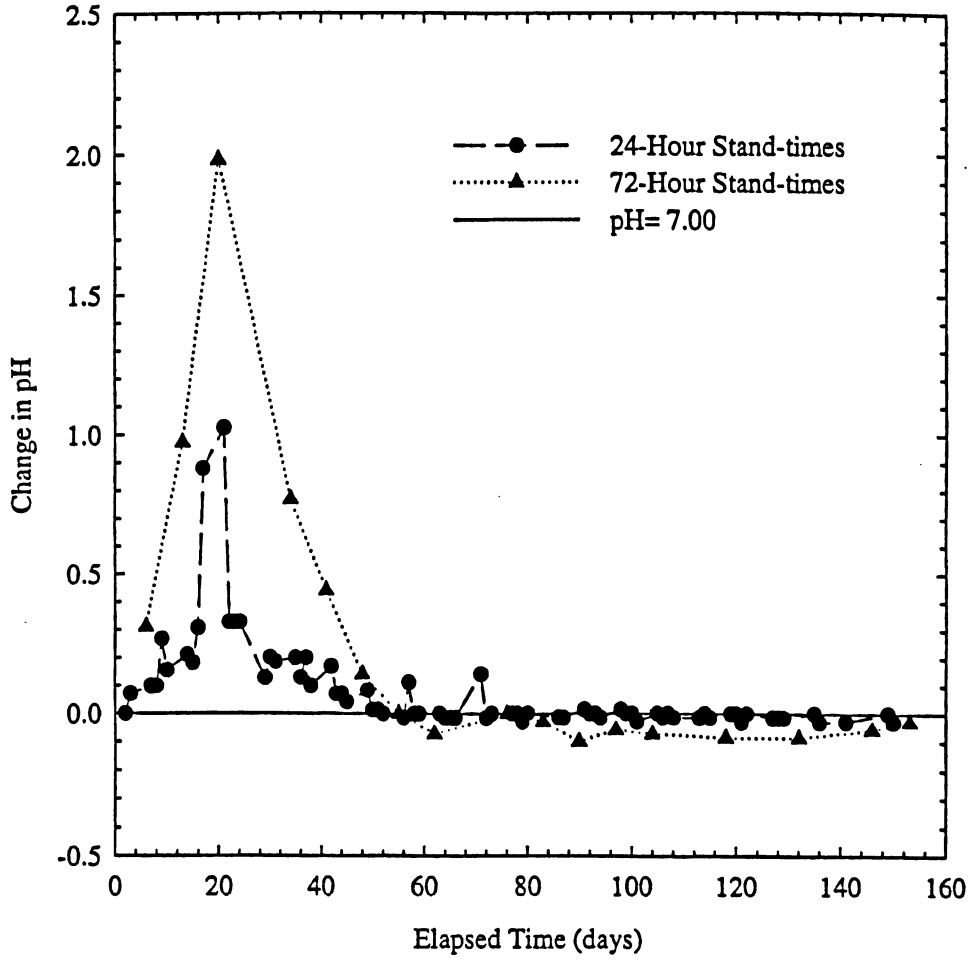

Appendix 3 Relative change in pH vs. elasped time for pure lead with free Cl concentra of 3.00mg/L, pH at 7.00, and an approximate DIC of 10 mg/L .

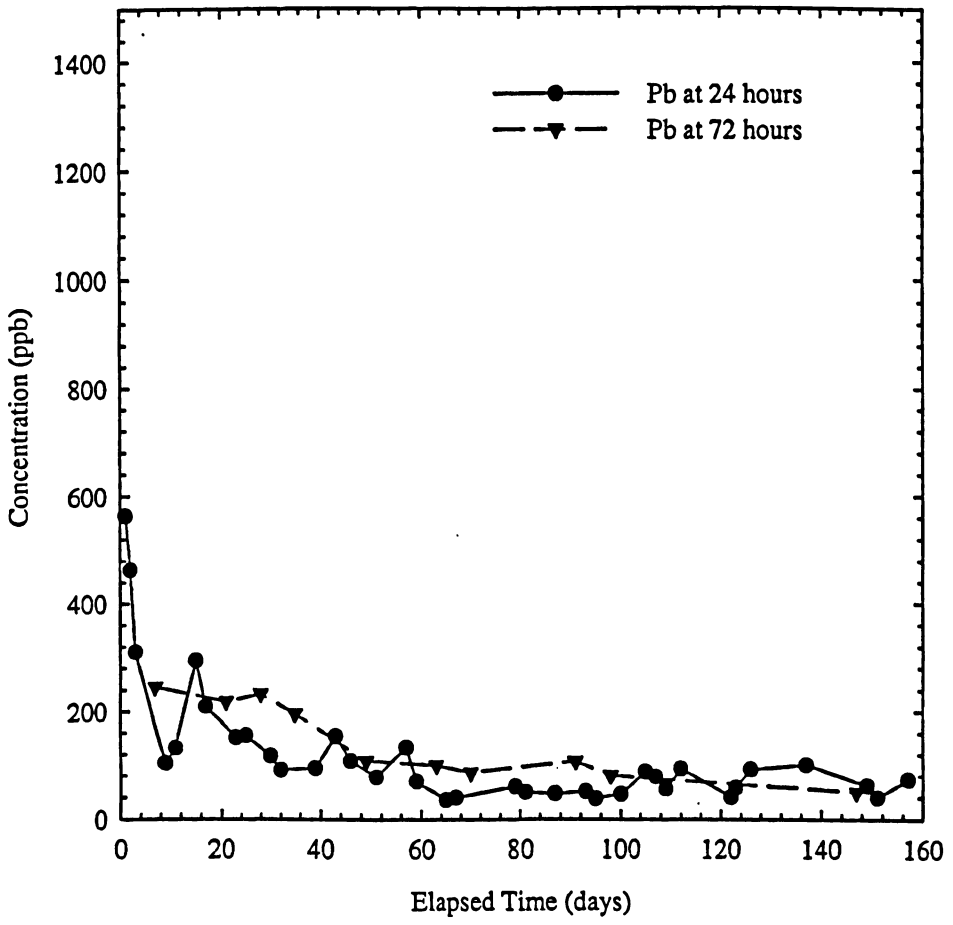

Appendix 3 DO RUN: Elapsed time versus lead metal release profile for 24 and 72 hour stagnation times for cell #1.

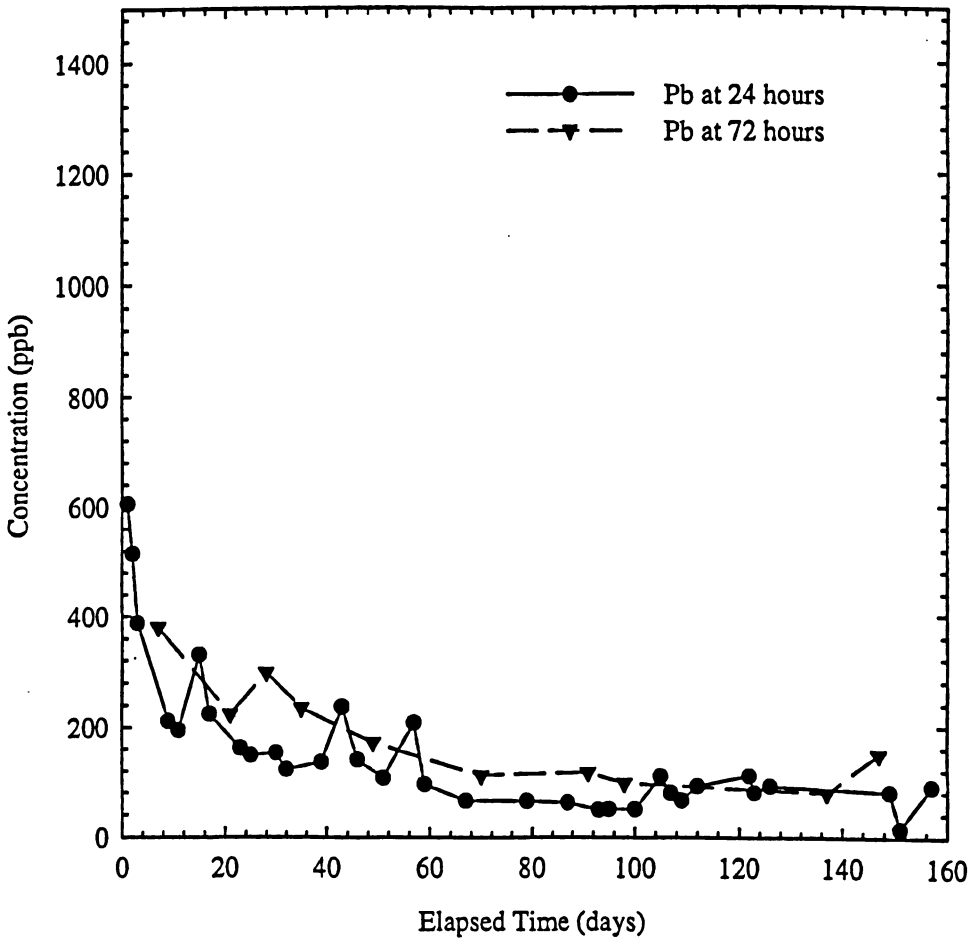

Appendix 3 DO RUN: Elapsed time versus lead metal release profile for 24 and 72 hour stagnation times for cell #9.

Appendix 3.9 Relative change in pH vs. Elapsed time: Dissolved Oxygen Run

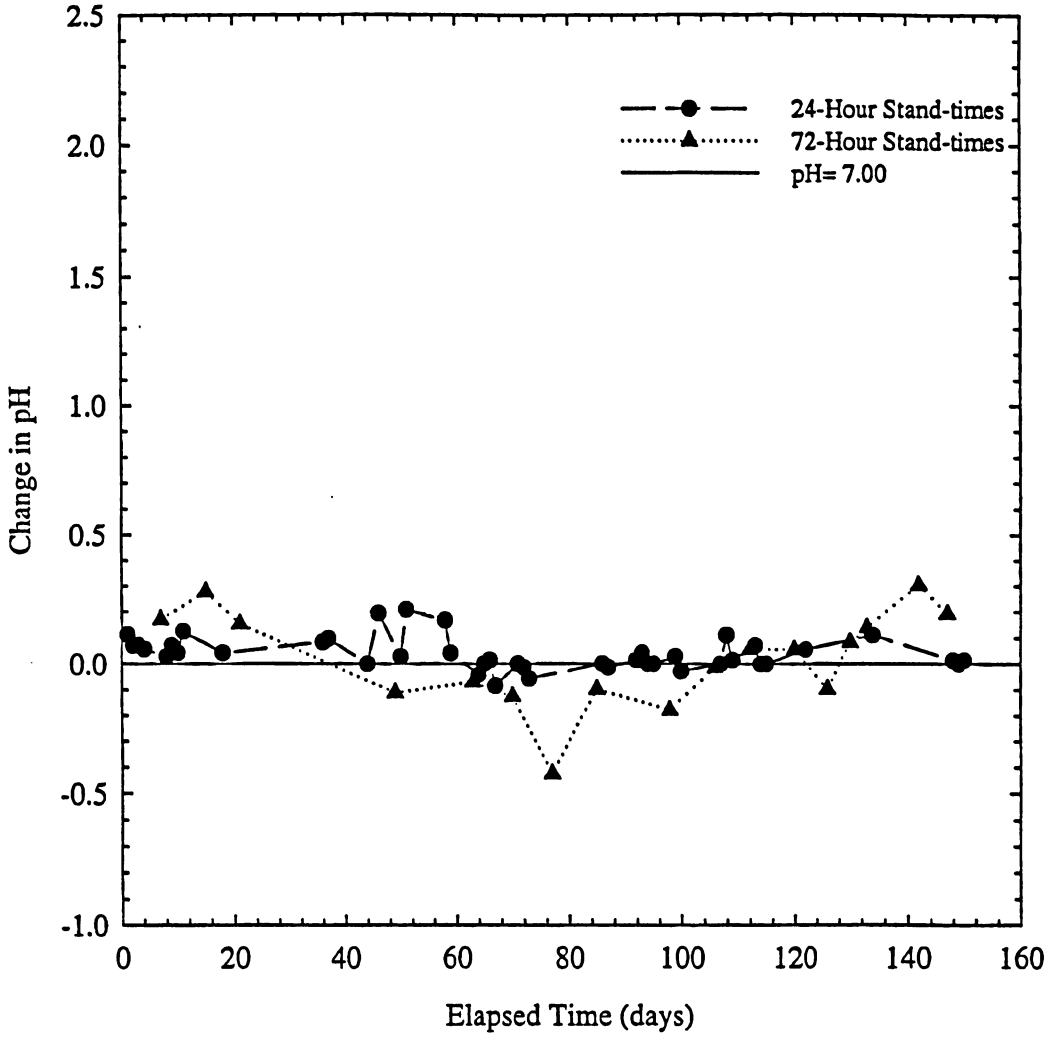

Appendix 3 Relative change in pH vs. elasped time for non-chlorinated pure lead with DO concentration at saturation, pH at 7.00, and an approximate DIC of 10 ppm.

APPENDIX 4

Red Brass

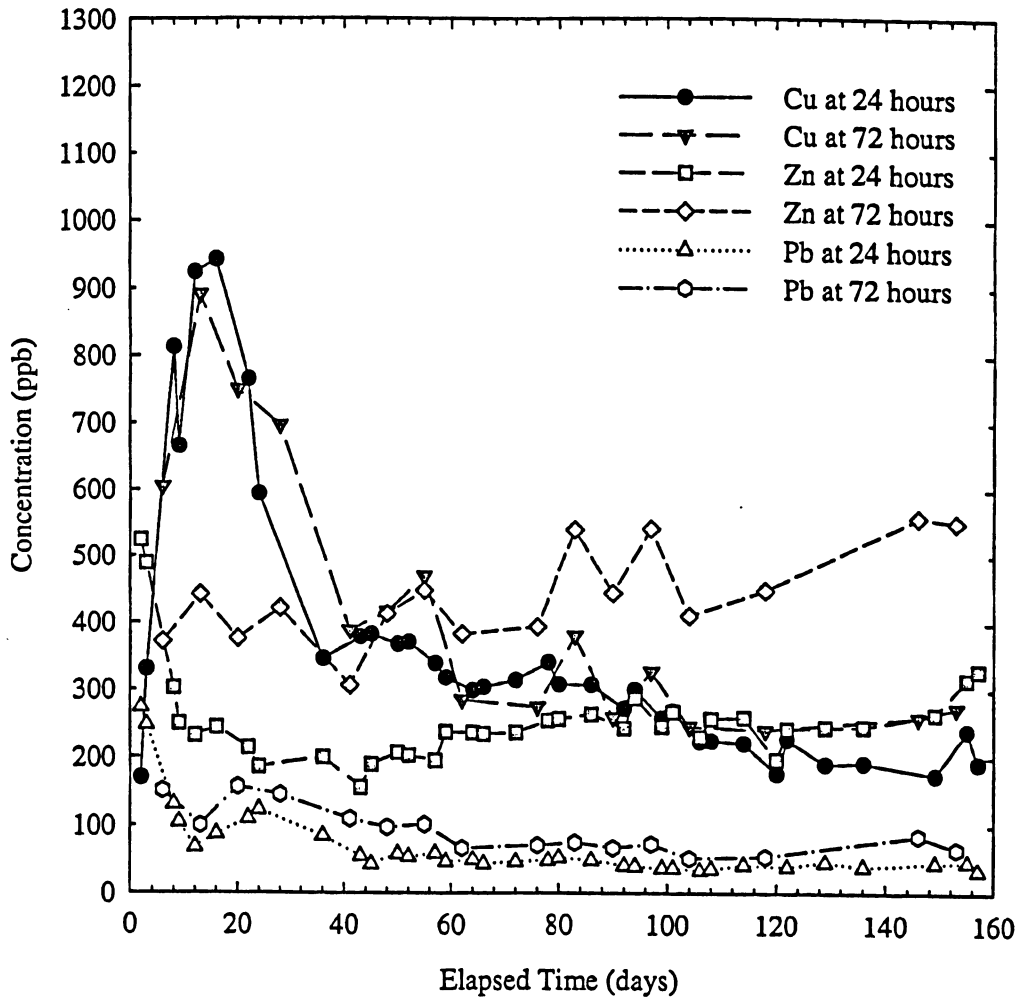

Appendix 4 Red Brass Free Chlorine Run: Elapsed time versus copper, zinc, and lead metal release profiles for 24 and 72 hour stagnation times for Cell #7.

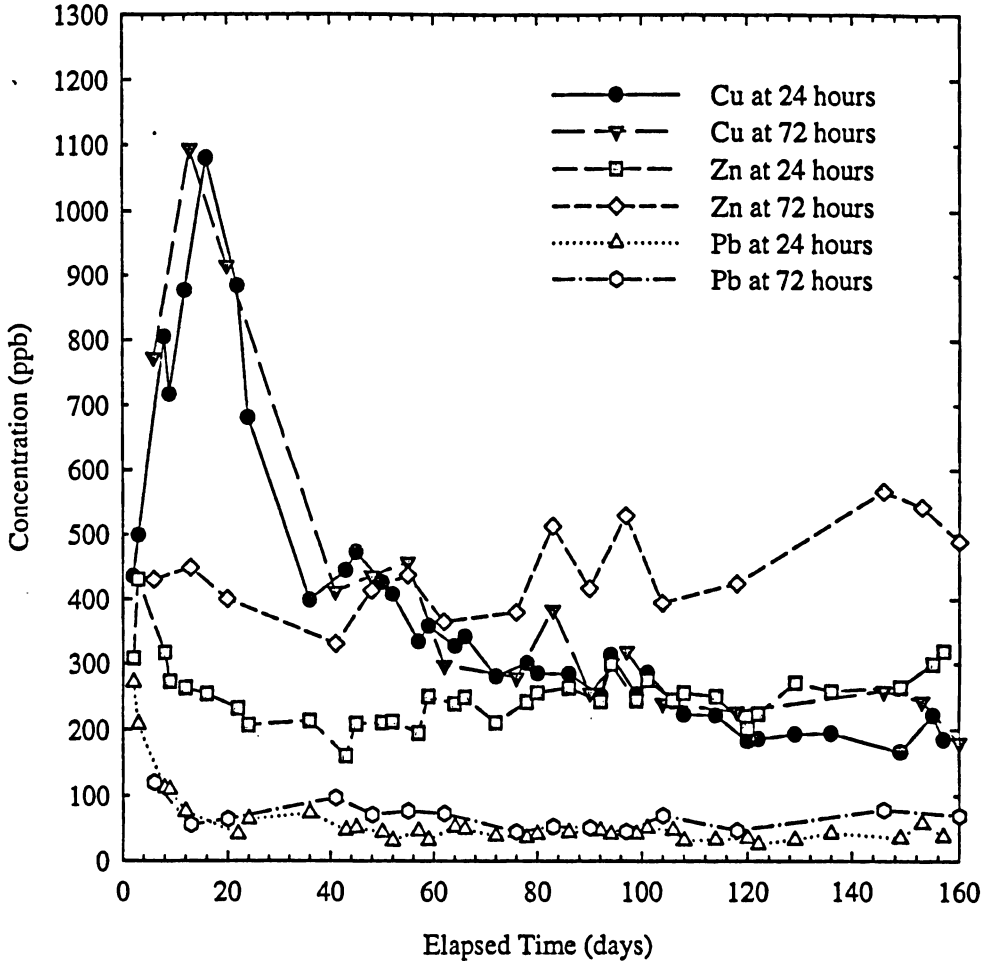

Appendix 4 Red Brass Free Chlorine Run: Elapsed time versus copper, zinc, and lead metal release profiles for 24 and 72 hour stagnation times for Cell #8.

Appendix 4.3 Selected Eh curves vs. 3-Day Stagnation Time: Free Chlorine Run

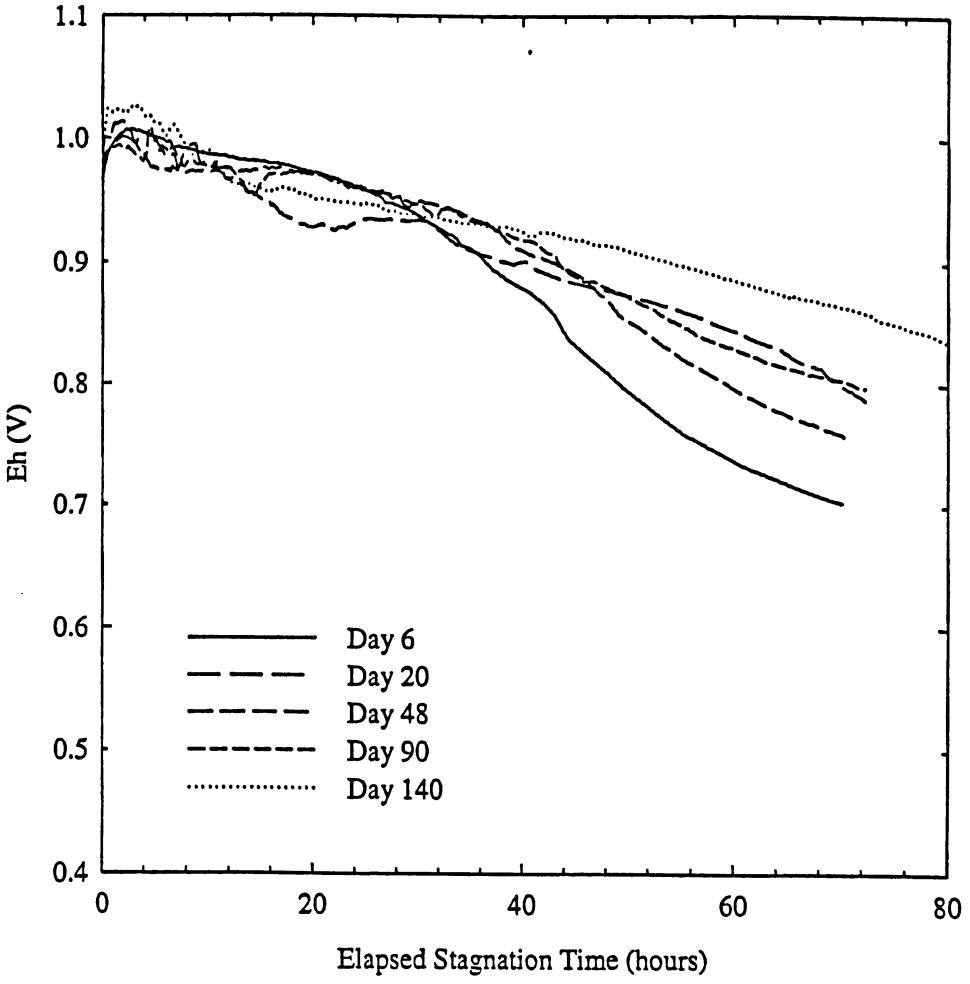

Appendix 4 Red brass 3-Day Stand-time Redox Profiles selected at various points throughout the160-Day study. The temperature is approximataly 23°C, pH is at 7.00, free chlorine begins at 3.00 mg/L, dissolved oxygen begins saturated, and dissolved inorganic carbon is 10.00 mg/L.

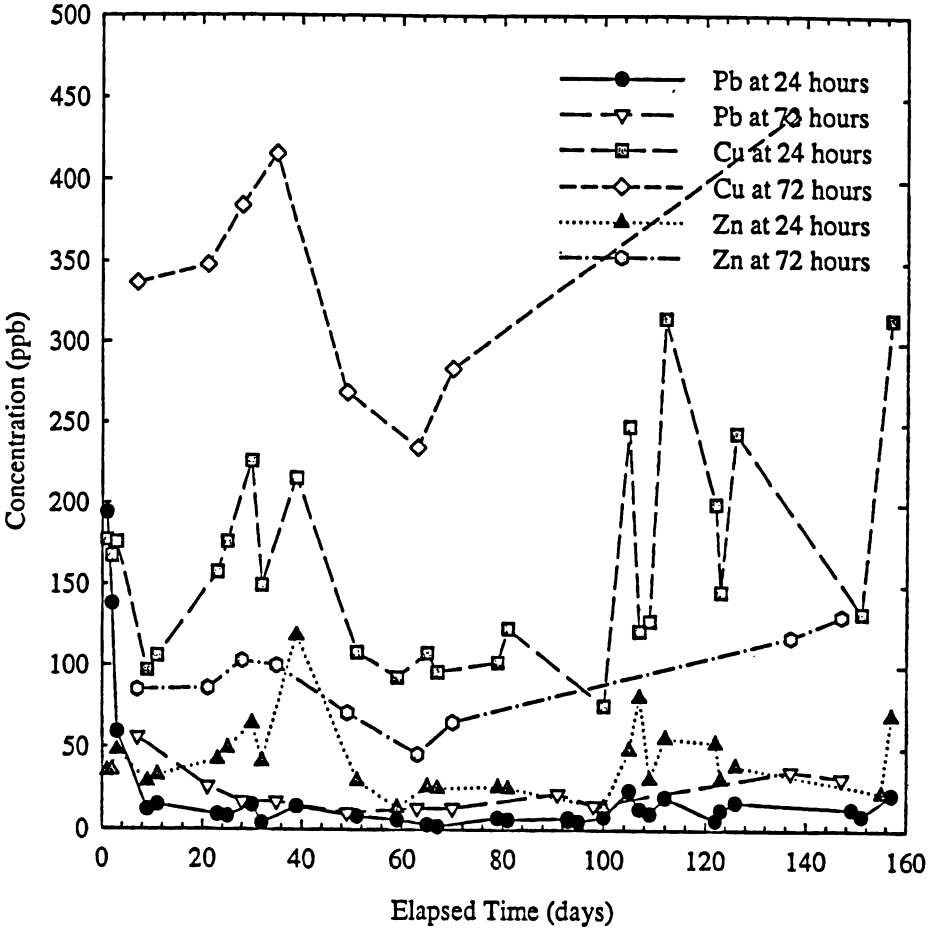

Appendix 4 Red Brass Dissolved Oxygen Run: Elapsed time versus copper, zinc, and lead metal release profiles for 24and 72 hour stagnation times for Cell #7.

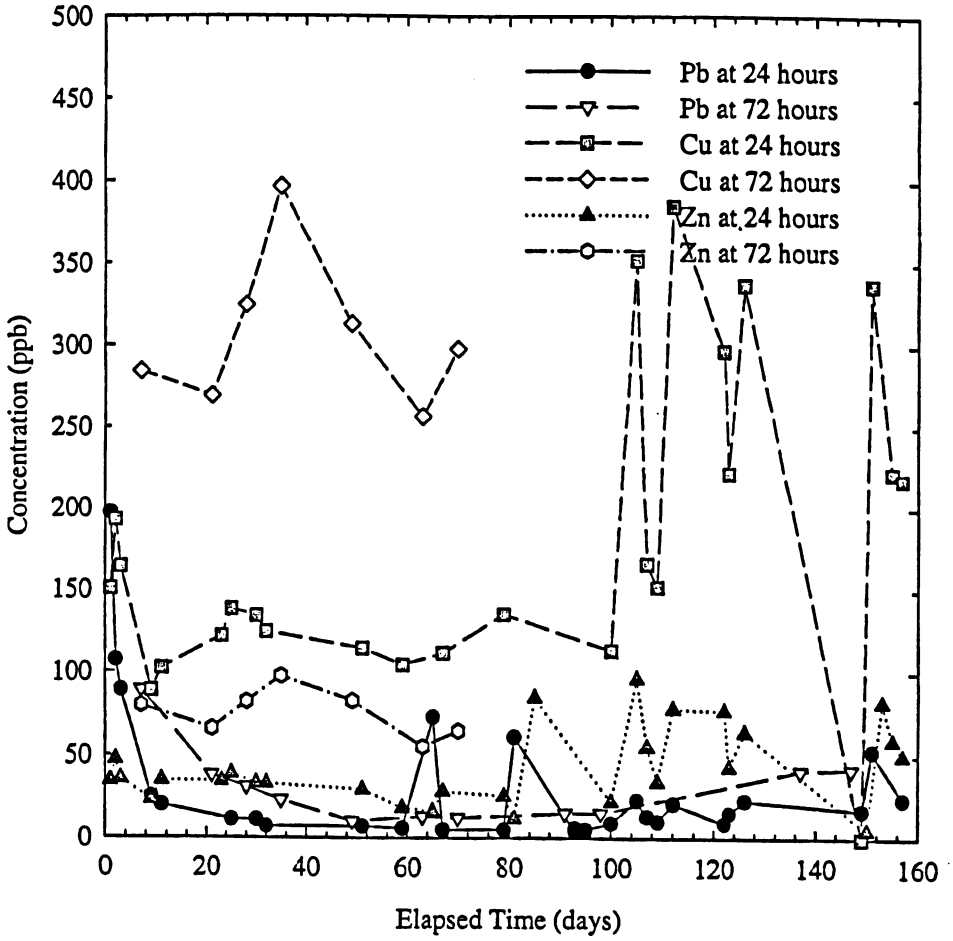

Appendix 4 Red Brass Dissolved Oxygen Run: Elapsed time versus copper, zinc, and lead metal release profilee for 24and 72 hour stagnation times for Cell #8.

APPENDIX 5

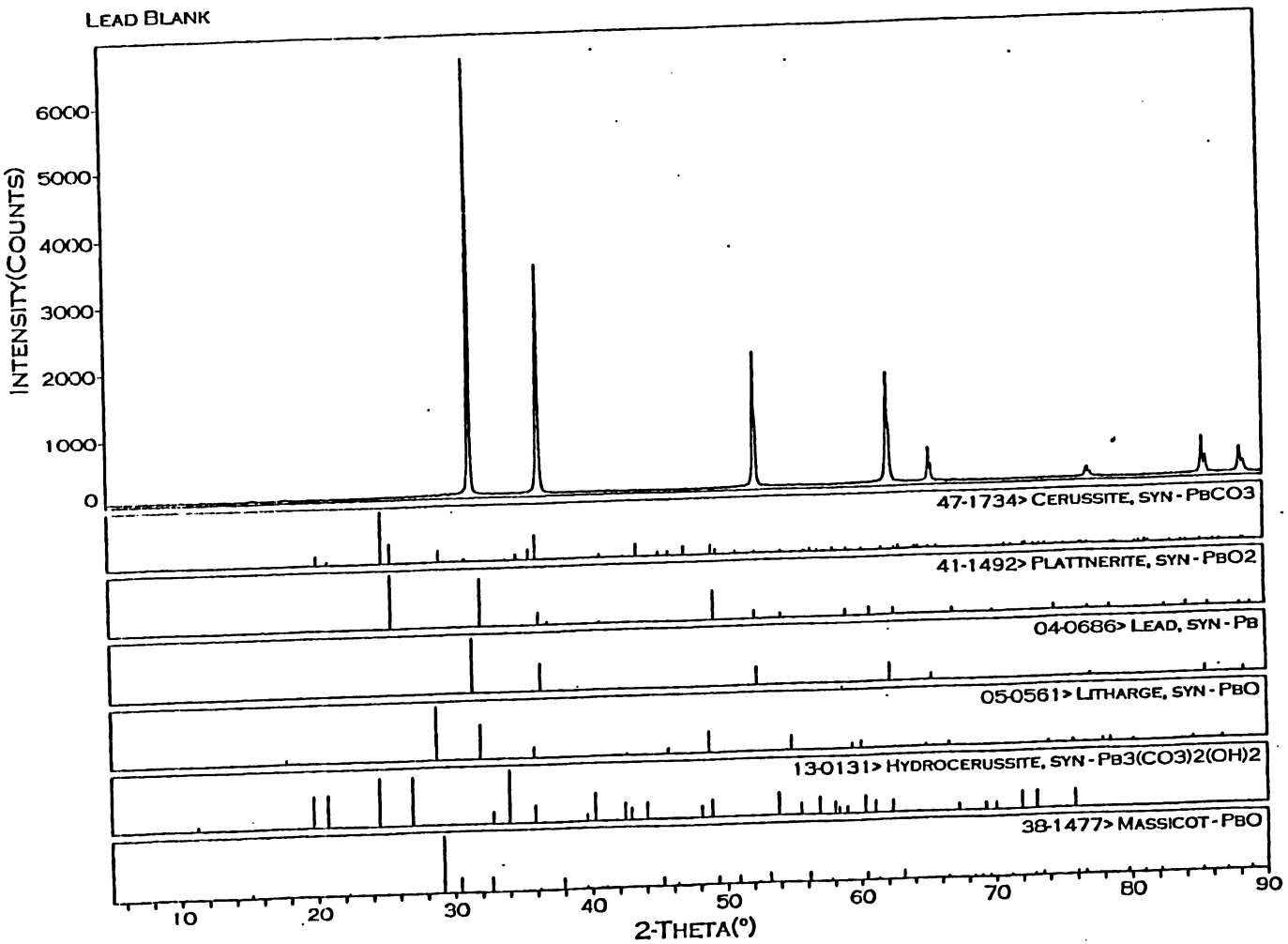
LEAD BLANK
INTENSITY(COUNTS)
6000
5000
4000
3000
2000
1000
0
47-1734> CERUSSITE, SYN - PBCO3
41-1492> PLATTNERITE, SYN - PBO2
04-0686> LEAD, SYN - PB
05-0561> LITHARGE, SYN - PBO
13-0131> HYDROCERUSSITE, SYN - PB3(CO3)2(OH)2
38-1477> MASSICOT - PBO
10
20
30
40
50
60
70
80
90
2-THETA(°)

[KS20710A.RAW] LEAD BLANK | PEAK ID REPORT

SCAN: 5.0/90.0/0.02/3(SEC), CU(35KV,40MA), I(MAX)=6641, 07/10/02 11:42

PEAK: 15-PTS/PARABOLIC FILTER, THRESHOLD=3.0, CUTOFF=0.1%, BG=3/1.0, PEAK-TOP=SUMMIT

NOTE: INTENSITY = COUNTS, 2T(0)=0.0(°), WAVELENGTH TO COMPUTE D-SPACING = 1.54056A (CU/K-...

#	2-THETA	D(A)	HEIGHT	I%(H)	PHASE ID	D(A)	I%	(H K L)	2-THETA
1	10.443	8.4639	25	0.4					
2	31.500	2.8377	6595	100.0	LEAD, SYN	2.8444	100.0	(1 1 1)	31.425
3	36.481	2.4609	3458	52.4	LEAD, SYN	2.4671	50.0	(2 0 0)	36.386
4	52.422	1.7440	2019	30.6	MASSICOT	1.7439	1.0	(3 1 0)	52.424
5	62.322	1.4886	1639	24.9	HYDROCER...	1.4876	20.0	(3 0 3)	62.371
6	65.423	1.4254	498	7.6	LEAD, SYN	1.4267	9.0	(2 2 2)	65.356
7	77.197	1.2347	148	2.2	LEAD, SYN	1.2364	2.0	(4 0 0)	77.074
8	85.582	1.1339	546	8.3	LEAD, SYN	1.1346	10.0	(3 3 1)	85.514
9	88.341	1.1055	372	5.6	LEAD, SYN	1.1057	7.0	(4 2 0)	88.316

LINE SHIFTS OF INDIVIDUAL PHASES:

PDF#04-0686 - LEAD, SYN <2T(0) = 0.12, D/D(0) = 1.0>

PDF#13-0131 - HYDROCERUSSITE, SYN <2T(0) = -0.12, D/D(0) = 1.0>

PDF#38-1477 - MASSICOT <2T(0) = 0.12, D/D(0) = 1.0>

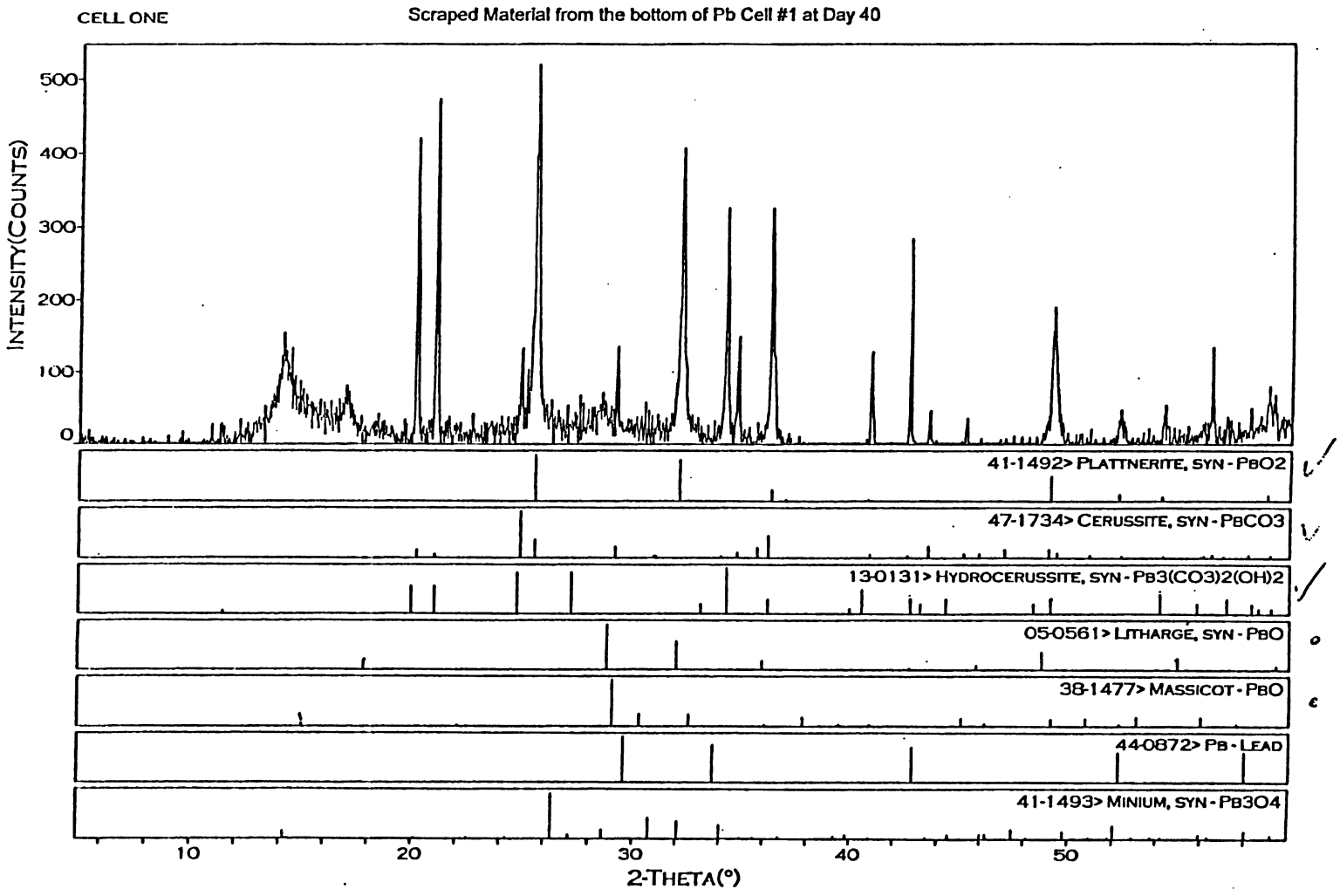
CELL ONE
Scraped Material from the bottom of Pb Cell #1 at Day 40
INTENSITY(COUNTS)
500
400
300
200
100
0
41-1492> PLATTNERITE, SYN - PBO2
47-1734> CERUSSITE, SYN - PBCO3
13-0131> HYDROCERUSSITE, SYN - PB3(CO3)2(OH)2
05-0561> LITHARGE, SYN - PBO
38-1477> MASSICOT - PBO
44-0872> PB - LEAD
41-1493> MINIUM, SYN - PB3O4
10
20
30
40
50
2-THETA(°)

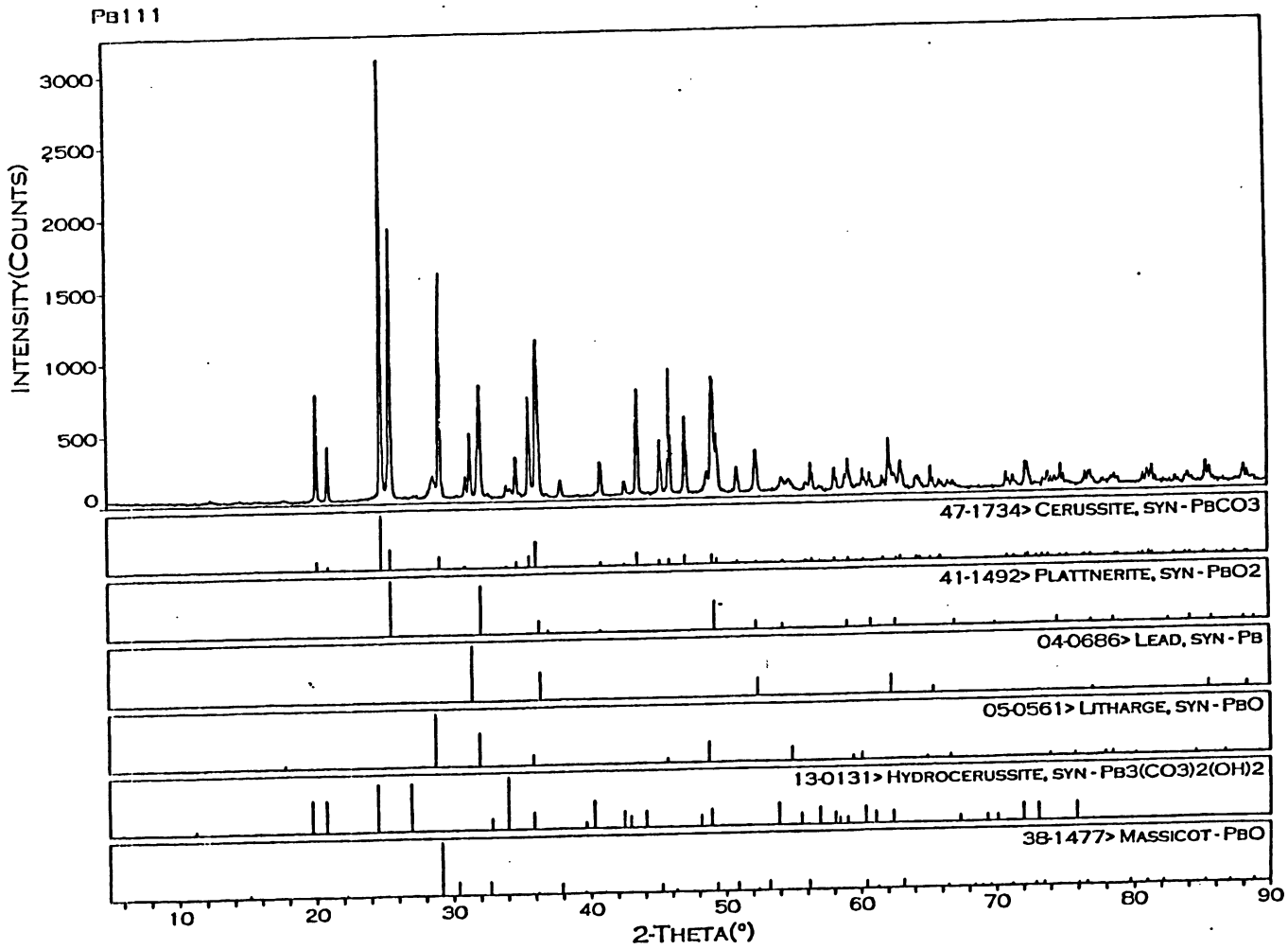
PB111
INTENSITY(COUNTS)
3000
2500
2000
1500
1000
500
0
47-1734> CERUSSITE, SYN - PBCO3
41-1492> PLATTNERITE, SYN - PBO2
04-0686> LEAD, SYN - PB
05-0561> LITHARGE, SYN - PBO
13-0131> HYDROCERUSSITE, SYN - PB3(CO3)2(OH)2
38-1477> MASSICOT - PBO
10
20
30
40
50
60
70
80
90
2-THETA(°)

[KS20711A.RAW] P8111 | PEAK ID REPORT

SCAN: 5.0/90.0/0.02/3(SEC), CU(35KV,40MA), I(MAX)=3105, 07/11/02 11:58

PEAK: 15-PTS/PARABOLIC FILTER, THRESHOLD=3.0, CUTOFF=0.1%, BG=3/1.0, PEAK-TOP=SUMMIT

NOTE: INTENSITY = COUNTS, 2T(0)=0.0(°), WAVELENGTH TO COMPUTE D-SPACING = 1.54056A (CU/K-...

#	2-THETA	D(A)	HEIGHT	I%(H)	PHASE ID	D(A)	I%	(H K L)	2-THETA
1	14.596	6.0636	21	0.7					
2	17.798	4.9795	22	0.7	LITHARGE, SYN	4.9844	5.0	(0 0 1)	17.780
3	20.200	4.3924	747	24.3	CERUSSITE, ...	4.3920	15.0	(1 1 0)	20.202
4	21.039	4.2190	380	12.3	CERUSSITE, ...	4.2280	5.0	(0 2 0)	20.994
5	24.939	3.5674	3079	100.0	CERUSSITE, ...	3.5730	100.0	(1 1 1)	24.900
6	25.601	3.4767	1877	61.0	PLATTNERITE...	3.4838	100.0	(1 1 0)	25.547
7	28.741	3.1036	154	5.0	LITHARGE, SYN	3.1023	100.0	(1 0 1)	28.753
8	29.217	3.0541	1576	51.2	MASSICOT	3.0560	100.0	(1 1 1)	29.198
9	31.100	2.8733	137	4.4	CERUSSITE, ...	2.8801	2.0	(0 1 2)	31.025
10	31.423	2.8445	439	14.3	LEAD, SYN	2.8444	100.0	(1 1 1)	31.425
11	32.140	2.7827	791	25.7	PLATTNERITE...	2.7868	88.0	(1 0 1)	32.091
12	32.727	2.7341	24	0.8	MASSICOT	2.7352	23.0	(2 0 0)	32.713
13	34.062	2.6299	83	2.7	HYDROCER...	2.6320	100.0	(1 1 0)	34.035
14	34.357	2.6080	58	1.9					
15	34.759	2.5788	270	8.8	CERUSSITE, ...	2.5793	9.0	(2 0 0)	34.751
16	35.686	2.5139	688	22.3	CERUSSITE, ...	2.5148	19.0	(1 1 2)	35.673
17	36.279	2.4741	1093	35.5	PLATTNERITE...	2.4721	21.0	(2 0 0)	36.310
18	38.018	2.3649	110	3.6	MASSICOT	2.3695	17.0	(2 0 1)	37.941
19	40.866	2.2064	234	7.6	CERUSSITE, ...	2.2068	5.0	(2 2 0)	40.859
20	42.678	2.1168	85	2.8	LITHARGE, SYN	2.1183	1.0	(1 0 2)	42.647
21	43.637	2.0725	727	23.6	CERUSSITE, ...	2.0765	21.0	(2 2 1)	43.548
22	45.298	2.0003	369	12.0	MASSICOT	2.0028	13.0	(2 2 0)	45.239
23	45.976	1.9723	865	28.1	CERUSSITE, ...	1.9754	7.0	(2 0 2)	45.901
24	47.140	1.9263	532	17.3	CERUSSITE, ...	1.9293	15.0	(1 3 2)	47.062
25	48.760	1.8660	135	4.4	LITHARGE, SYN	1.8677	37.0	(1 1 2)	48.715
26	49.122	1.8531	798	25.9	PLATTNERITE...	1.8517	52.0	(2 1 1)	49.164
27	49.481	1.8405	417	13.5	CERUSSITE, ...	1.8419	8.0	(0 2 3)	49.442
28	50.980	1.7899	168	5.5	CERUSSITE, ...	1.7917	3.0	(2 2 2)	50.926
29	52.378	1.7453	287	9.3	CERUSSITE, ...	1.7461	1.0	(0 4 2)	52.355
30	54.299	1.6880	82	2.7	CERUSSITE, ...	1.6886	1.0	(3 1 0)	54.278
31	54.821	1.6732	76	2.5	LITHARGE, SYN	1.6716	24.0	(2 1 1)	54.877
32	56.102	1.6380	53	1.7	CERUSSITE, ...	1.6376	1.0	(0 5 1)	56.118
33	56.445	1.6288	189	6.1	CERUSSITE, ...	1.6280	4.0	(3 1 1)	56.477
34	57.138	1.6107	26	0.8	CERUSSITE, ...	1.6141	1.0	(1 5 0)	57.009
35	58.216	1.5834	148	4.8	CERUSSITE, ...	1.5853	4.0	(2 4 1)	58.141
36	59.002	1.5642	91	3.0	PLATTNERITE...	1.5641	9.0	(3 1 0)	59.007
37	59.242	1.5584	201	6.5	CERUSSITE, ...	1.5604	3.0	(1 5 1)	59.160
38	60.336	1.5328	131	4.3	HYDROCER...	1.5328	30.0	(2 1 7)	60.337
39	60.855	1.5209	100	3.2	PLATTNERITE...	1.5226	12.0	(1 1 2)	60.783
40	61.804	1.4998	61	2.0	CERUSSITE, ...	1.5006	3.0	(2 2 3)	61.771
41	62.263	1.4899	340	11.0	LEAD, SYN	1.4904	32.0	(3 1 1)	62.239
42	62.776	1.4789	104	3.4	CERUSSITE, ...	1.4794	2.0	(3 1 2)	62.757
43	63.140	1.4713	191	6.2	MASSICOT	1.4705	12.0	(0 4 0)	63.180

[KS20711A.RAW] Pb111 | Peak ID Report

SCAN: 5.0/90.0/0.02/3(sec), Cu(35kV,40mA), I(max)=3105, 07/11/02 11:58

PEAK: 15-pts/Parabolic Filter, Threshold=3.0, Cutoff=0.1%, BG=3/1.0, Peak-Top=Summit

NOTE: Intensity = Counts, 2T(0)=0.0(°), Wavelength to Compute d-Spacing = 1.54056A (Cu/K-...

#	2-Theta	d(A)	Height	I%(H)	Phase ID	d(A)	I%	(H K L)	2-Theta
44	63.278	1.4684	127	4.1					
45	64.299	1.4475	77	2.5	Cerussite, ...	1.4472	3.0	(2 4 2)	64.317
46	64.575	1.4420	62	2.0	Cerussite, ...	1.4431	2.0	(0 2 4)	64.521
47	65.378	1.4262	147	4.8	Lead, syn	1.4267	9.0	(2 2 2)	65.356
48	65.557	1.4228	61	2.0					
49	66.004	1.4142	50	1.6	Cerussite, ...	1.4163	1.0	(0 6 0)	65.894
50	66.231	1.4099	35	1.1	Massicot	1.4054	1.0	(3 1 2)	66.470
51	66.644	1.4022	46	1.5	Litharge, syn	1.4028	5.0	(2 2 0)	66.613
52	67.035	1.3949	44	1.4	Plattnerite...	1.3964	6.0	(2 0 2)	66.957
53	70.958	1.3271	99	3.2	Cerussite, ...	1.3276	2.0	(3 3 2)	70.927
54	71.457	1.3191	76	2.5	Cerussite, ...	1.3195	1.0	(2 0 4)	71.433
55	71.674	1.3156	27	0.9					
56	72.382	1.3045	168	5.5	Cerussite, ...	1.3052	3.0	(1 3 4)	72.335
57	73.701	1.2844	34	1.1	Cerussite, ...	1.2867	2.0	(0 6 2)	73.547
58	74.033	1.2794	71	2.3	Litharge, syn	1.2802	2.0	(3 0 1)	73.981
59	74.524	1.2722	51	1.7	Plattnerite...	1.2721	8.0	(3 2 1)	74.529
60	74.978	1.2656	129	4.2	Cerussite, ...	1.2676	1.0	(1 5 3)	74.845
61	76.762	1.2406	88	2.9	Cerussite, ...	1.2423	1.0	(2 6 0)	76.642
62	77.100	1.2360	93	3.0	Lead, syn	1.2364	2.0	(4 0 0)	77.074
63	78.020	1.2237	30	1.0	Litharge, syn	1.2244	4.0	(2 2 2)	77.968
64	78.657	1.2154	51	1.7	Plattnerite...	1.2163	5.0	(2 2 2)	78.585
65	78.839	1.2130	58	1.9	Cerussite, ...	1.2131	1.0	(4 2 1)	78.839
66	80.972	1.1864	67	2.2	Massicot	1.1868	2.0	(0 0 4)	80.942
67	81.301	1.1824	97	3.2	Cerussite, ...	1.1827	4.0	(1 1 5)	81.282
68	81.598	1.1789	118	3.8	Cerussite, ...	1.1796	2.0	(0 2 5)	81.539
69	81.831	1.1761	37	1.2					
70	83.334	1.1587	40	1.3	Cerussite, ...	1.1609	1.0	(1 7 1)	83.135
71	83.530	1.1564	28	0.9					
72	84.059	1.1505	43	1.4	Cerussite, ...	1.1517	1.0	(2 6 2)	83.956
73	84.202	1.1489	64	2.1	Plattnerite...	1.1490	6.0	(3 1 2)	84.198
74	84.518	1.1454	35	1.1	Litharge, syn	1.1449	2.0	(1 1 4)	84.568
75	85.521	1.1345	138	4.5	Lead, syn	1.1346	10.0	(3 3 1)	85.514
76	85.782	1.1318	108	3.5	Plattnerite...	1.1314	4.0	(4 1 1)	85.813
77	88.320	1.1057	115	3.7	Lead, syn	1.1057	7.0	(4 2 0)	88.316
78	88.997	1.0990	26	0.8	Plattnerite...	1.0996	3.0	(1 0 3)	88.933

Line Shifts of Individual Phases:

PDF#47-1734 - Cerussite, syn <2T(0) = 0.12, d/d(0) = 1.0>

PDF#41-1492 - Plattnerite, syn <2T(0) = 0.12, d/d(0) = 1.0>

PDF#04-0686 - Lead, syn <2T(0) = 0.12, d/d(0) = 1.0>

PDF#05-0561 - Litharge, syn <2T(0) = 0.12, d/d(0) = 1.0>

PDF#13-0131 - Hydrocerussite, syn <2T(0) = -0.12, d/d(0) = 1.0>

PDF#38-1477 - Massicot <2T(0) = 0.12, d/d(0) = 1.0>

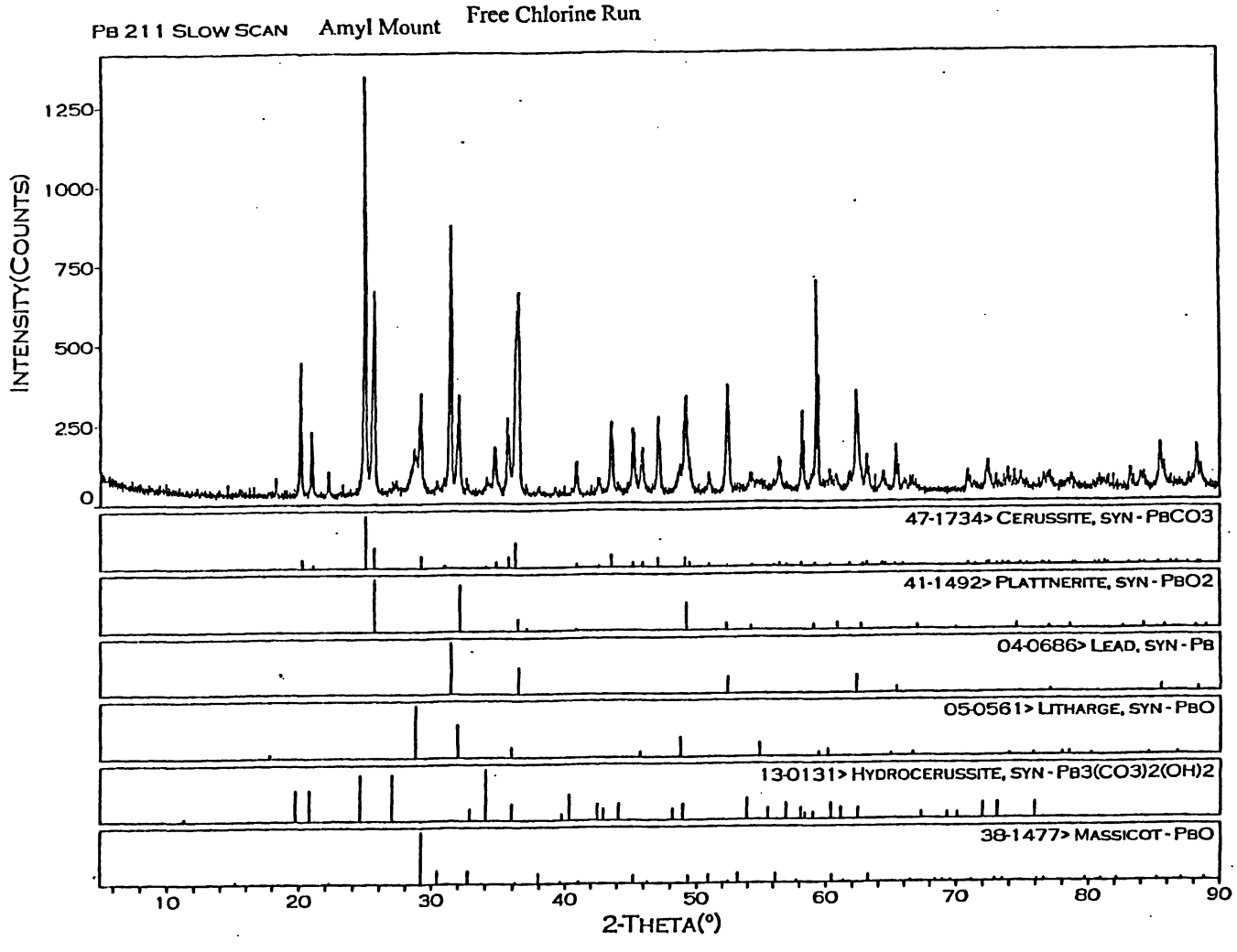
PB 211 SLOW SCAN Amyl Mount Free Chlorine Run
INTENSITY(COUNTS)
1250
1000
750
500
250
0
47-1734> CERUSSITE, SYN - PBCO3
41-1492> PLATTNERITE, SYN - PBO2
04-0686> LEAD, SYN - PB
05-0561> LITHARGE, SYN - PBO
13-0131> HYDROCERUSSITE, SYN - PB3(CO3)2(OH)2
38-1477> MASSICOT - PBO
10
20
30
40
50
60
70
80
90
2-THETA(°)

[KS20710B.RAW] Pb211 | PEAK ID REPORT

SCAN: 5.0/90.0/0.02/3(SEC), CU(35KV,40MA), I(MAX)=6852, 07/10/02 15:34

PEAK: 15-PTS/PARABOLIC FILTER, THRESHOLD=3.0, CUTOFF=0.1%, BG=3/1.0, PEAK-TOP=SUMMIT

NOTE: INTENSITY = COUNTS, 2T(0)=0.0(°), WAVELENGTH TO COMPUTE D-SPACING = 1.54056A (CU/K-...

#	2-THETA	D(A)	HEIGHT	I%(H)	PHASE ID	D(A)	I%	(H K L)	2-THETA
1	14.485	6.1102	34	0.5					
2	20.143	4.4047	838	12.3	CERUSSITE, ...	4.3920	15.0	(1 1 0)	20.202
3	20.984	4.2301	535	7.8	CERUSSITE, ...	4.2280	5.0	(0 2 0)	20.994
4	24.880	3.5758	3461	50.7	CERUSSITE, ...	3.5730	100.0	(1 1 1)	24.900
5	25.541	3.4847	2693	39.5	CERUSSITE, ...	3.4838	37.0	(0 2 1)	25.547
6	28.662	3.1120	113	1.7	LITHARGE, SYN	3.1023	100.0	(1 0 1)	28.753
7	29.145	3.0615	6820	100.0	CERUSSITE, ...	3.0606	21.0	(0 0 2)	29.153
8	31.024	2.8802	267	3.9	CERUSSITE, ...	2.8801	2.0	(0 1 2)	31.025
9	31.365	2.8497	284	4.2	LEAD, SYN	2.8444	100.0	(1 1 1)	31.425
10	32.081	2.7877	1423	20.9	PLATTNERITE...	2.7868	88.0	(1 0 1)	32.091
11	33.984	2.6358	104	1.5	CERUSSITE, ...	2.6339	1.0	(1 0 2)	34.009
12	34.275	2.6140	44	0.6	HYDROCER...	2.6320	100.0	(1 1 0)	34.035
13	34.696	2.5833	361	5.3	CERUSSITE, ...	2.5793	9.0	(2 0 0)	34.751
14	35.642	2.5169	917	13.4	CERUSSITE, ...	2.5148	19.0	(1 1 2)	35.673
15	36.217	2.4782	1359	19.9	MASSICOT	2.4803	1.0	(2 1 0)	36.186
16	36.983	2.4287	36	0.5	PLATTNERITE...	2.4294	2.0	(1 1 1)	36.972
17	37.940	2.3695	104	1.5	MASSICOT	2.3695	17.0	(2 0 1)	37.941
18	40.842	2.2076	501	7.3	CERUSSITE, ...	2.2068	5.0	(2 2 0)	40.859
19	42.606	2.1203	147	2.2	CERUSSITE, ...	2.1213	1.0	(0 4 0)	42.584
20	43.538	2.0770	773	11.3	CERUSSITE, ...	2.0765	21.0	(2 2 1)	43.548
21	45.219	2.0036	421	6.2	MASSICOT	2.0028	13.0	(2 2 0)	45.239
22	45.861	1.9770	244	3.6	CERUSSITE, ...	1.9754	7.0	(2 0 2)	45.901
23	47.080	1.9286	700	10.3	CERUSSITE, ...	1.9293	15.0	(1 3 2)	47.062
24	48.720	1.8675	108	1.6	LITHARGE, SYN	1.8677	37.0	(1 1 2)	48.715
25	49.181	1.8511	1402	20.6	PLATTNERITE...	1.8517	52.0	(2 1 1)	49.164
26	49.456	1.8414	516	7.6	CERUSSITE, ...	1.8419	8.0	(0 2 3)	49.442
27	50.900	1.7925	143	2.1	MASSICOT	1.7924	13.0	(2 0 2)	50.902
28	52.317	1.7472	364	5.3	LEAD, SYN	1.7463	31.0	(2 2 0)	52.348
29	54.235	1.6899	170	2.5	PLATTNERITE...	1.6906	6.0	(0 0 2)	54.209
30	54.725	1.6759	61	0.9					
31	54.959	1.6693	37	0.5	LITHARGE, SYN	1.6716	24.0	(2 1 1)	54.877
32	56.019	1.6402	71	1.0	CERUSSITE, ...	1.6410	1.0	(2 4 0)	55.992
33	56.417	1.6296	164	2.4	CERUSSITE, ...	1.6280	4.0	(3 1 1)	56.477
34	57.065	1.6126	39	0.6	CERUSSITE, ...	1.6141	1.0	(1 5 0)	57.009
35	58.147	1.5852	177	2.6	CERUSSITE, ...	1.5853	4.0	(2 4 1)	58.141
36	58.979	1.5648	154	2.3	HYDROCER...	1.5649	10.0	(2 0 1 1)	58.974
37	59.198	1.5595	232	3.4	CERUSSITE, ...	1.5604	3.0	(1 5 1)	59.160
38	60.298	1.5337	368	5.4	CERUSSITE, ...	1.5338	1.0	(0 0 4)	60.291
39	60.798	1.5222	185	2.7	PLATTNERITE...	1.5226	12.0	(1 1 2)	60.783
40	60.976	1.5182	78	1.1	HYDROCER...	1.5157	20.0	(3 0 0)	61.089
41	61.761	1.5008	145	2.1	CERUSSITE, ...	1.5006	3.0	(2 2 3)	61.771
42	62.236	1.4905	238	3.5	LEAD, SYN	1.4904	32.0	(3 1 1)	62.239
43	62.583	1.4830	168	2.5	PLATTNERITE...	1.4830	10.0	(3 0 1)	62.583

[KS30205A.RAW] Pb 211 Slow Scan									Peak ID Report
SCAN: 5.0/90.0/0.01/5(sec), Cu(35kV,40mA), I(max)=1349, 02/06/03 05:53									
PEAK: 15-pts/Parabolic Filter, Threshold=3.0, Cutoff=0.1%, BG=3/1.0, Peak-Top=Summit									
NOTE: Intensity = Counts, 2T(0)=0.0(°), Wavelength to Compute d-Spacing = 1.54056A (Cu/K-...									
#	2-Theta	d(A)	Height	I%(H)	Phase ID	d(A)	I%	(H K L)	2-Theta
44	54.313	1.6877	46	3.5	Cerussite, ...	1.6886	1.0	(3 1 0)	54.278
45	54.850	1.6724	28	2.1	Litharge, syn	1.6716	24.0	(2 1 1)	54.877
46	56.011	1.6404	27	2.1	Cerussite, ...	1.6410	1.0	(2 4 0)	55.992
47	56.411	1.6297	99	7.6					
48	56.541	1.6263	90	6.9	Cerussite, ...	1.6280	4.0	(3 1 1)	56.477
49	58.158	1.5849	243	18.5	Cerussite, ...	1.5853	4.0	(2 4 1)	58.141
50	58.889	1.5669	35	2.7	Hydrocer...	1.5649	10.0	(2 0 11)	58.974
51	59.239	1.5585	645	49.2	Cerussite, ...	1.5604	3.0	(1 5 1)	59.160
52	60.282	1.5340	44	3.4	Cerussite, ...	1.5338	1.0	(0 0 4)	60.291
53	60.441	1.5304	29	2.2	Massicot	1.5309	11.0	(2 2 2)	60.419
54	60.739	1.5236	37	2.8	Plattnerite...	1.5226	12.0	(1 1 2)	60.783
55	61.833	1.4992	44	3.4	Cerussite, ...	1.5006	3.0	(2 2 3)	61.771
56	62.240	1.4904	293	22.3	Lead, syn	1.4904	32.0	(3 1 1)	62.239
57	62.410	1.4867	229	17.5	Hydrocer...	1.4876	20.0	(3 0 3)	62.371
58	63.040	1.4734	90	6.9	Cerussite, ...	1.4729	4.0	(3 3 0)	63.064
59	64.380	1.4459	55	4.2	Cerussite, ...	1.4472	3.0	(2 4 2)	64.317
60	65.321	1.4274	138	10.5	Lead, syn	1.4267	9.0	(2 2 2)	65.356
61	65.558	1.4228	76	5.8					
62	66.002	1.4143	30	2.3	Cerussite, ...	1.4163	1.0	(0 6 0)	65.894
63	66.189	1.4107	27	2.1					
64	66.520	1.4045	34	2.6	Massicot	1.4054	1.0	(3 1 2)	66.470
65	66.681	1.4015	42	3.2	Litharge, syn	1.4028	5.0	(2 2 0)	66.613
66	66.906	1.3973	30	2.3	Plattnerite...	1.3964	6.0	(2 0 2)	66.957
67	70.890	1.3283	65	5.0	Cerussite, ...	1.3276	2.0	(3 3 2)	70.927
68	71.401	1.3200	27	2.1	Cerussite, ...	1.3195	1.0	(2 0 4)	71.433
69	72.319	1.3055	64	4.9	Cerussite, ...	1.3052	3.0	(1 3 4)	72.335
70	72.420	1.3039	87	6.6					
71	73.069	1.2939	37	2.8	Hydrocer...	1.2938	30.0	(2 2 3)	73.075
72	73.670	1.2848	31	2.4	Cerussite, ...	1.2867	2.0	(0 6 2)	73.547
73	73.949	1.2807	51	3.9	Cerussite, ...	1.2805	2.0	(2 4 3)	73.960
74	74.431	1.2736	51	3.9	Plattnerite...	1.2721	8.0	(3 2 1)	74.529
75	74.911	1.2666	41	3.1	Cerussite, ...	1.2676	1.0	(1 5 3)	74.845
76	76.640	1.2423	43	3.3	Cerussite, ...	1.2423	1.0	(2 6 0)	76.642
77	76.910	1.2386	43	3.3	Plattnerite...	1.2376	2.0	(4 0 0)	76.985
78	77.110	1.2359	50	3.8	Lead, syn	1.2364	2.0	(4 0 0)	77.074
79	78.398	1.2188	25	1.9	Litharge, syn	1.2174	5.0	(3 1 1)	78.500
80	78.551	1.2168	28	2.1	Plattnerite...	1.2163	5.0	(2 2 2)	78.585
81	78.820	1.2133	33	2.5	Cerussite, ...	1.2131	1.0	(4 2 1)	78.839
82	80.899	1.1873	40	3.1	Cerussite, ...	1.1876	2.0	(3 5 1)	80.869
83	81.613	1.1787	38	2.9	Cerussite, ...	1.1796	2.0	(0 2 5)	81.539
84	81.987	1.1743	39	3.0	Massicot	1.1723	3.0	(3 1 3)	82.151
85	83.252	1.1596	64	4.9	Cerussite, ...	1.1609	1.0	(1 7 1)	83.135
86	84.090	1.1502	44	3.4	Plattnerite...	1.1490	6.0	(3 1 2)	84.198

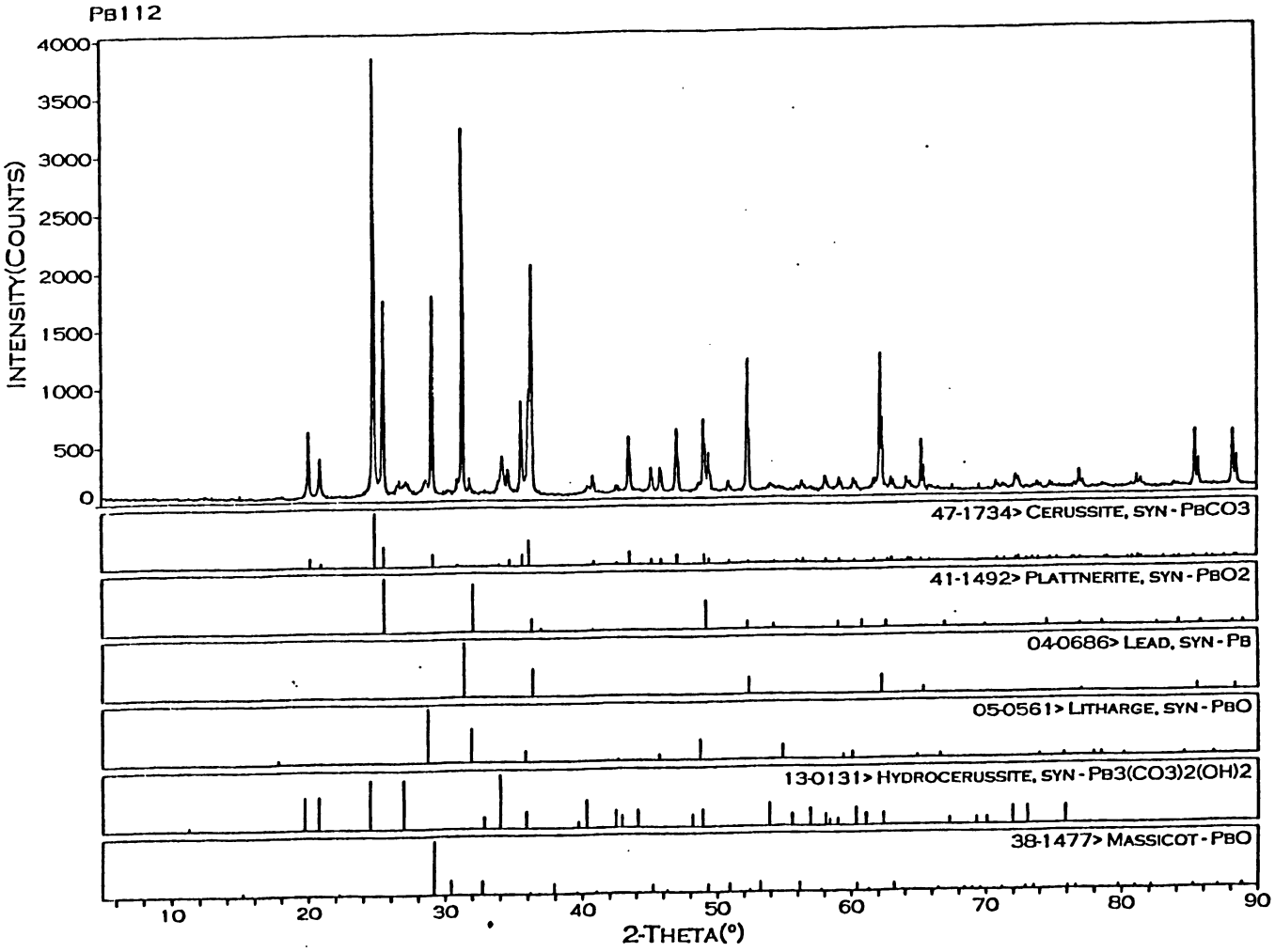
PB112
INTENSITY(COUNTS)
4000
3500
3000
2500
2000
1500
1000
500
0
47-1734> CERUSSITE, SYN - PBCO3
41-1492> PLATTNERITE, SYN - PBO2
04-0686> LEAD, SYN - PB
05-0561> LITHARGE, SYN - PBO
13-0131> HYDROCERUSSITE, SYN - PB3(CO3)2(OH)2
38-1477> MASSICOT - PBO
10
20
30
40
50
60
70
80
90
2-THETA(°)

[KS30203A.RAW] PB112 | PEAK ID REPORT

SCAN: 5.0/90.0/0.02/3(SEC), CU(35KV,40MA), I(MAX)=3839, 02/03/03 13:49

PEAK: 15-PTS/PARABOLIC FILTER, THRESHOLD=3.0, CUTOFF=0.1%, BG=3/1.0, PEAK-TOP=SUMMIT

NOTE: INTENSITY = COUNTS, 2T(0)=0.0(°), WAVELENGTH TO COMPUTE D-SPACING = 1.54056A (CU/K-...

#	2-THETA	D(A)	HEIGHT	I%(H)	PHASE ID	D(A)	I%	(H K L)	2-THETA
1	20.101	4.4139	584	15.5	CERUSSITE, ...	4.3920	15.0	(1 1 0)	20.202
2	20.939	4.2390	329	8.7	CERUSSITE, ...	4.2280	5.0	(0 2 0)	20.994
3	24.824	3.5838	3774	100.0	CERUSSITE, ...	3.5730	100.0	(1 1 1)	24.900
4	25.520	3.4876	1651	43.7	CERUSSITE, ...	3.4838	37.0	(0 2 1)	25.547
5	26.602	3.3481	73	1.9					
6	27.337	3.2597	82	2.2					
7	28.640	3.1143	126	3.3	LITHARGE, SYN	3.1023	100.0	(1 0 1)	28.753
8	29.087	3.0675	1718	45.5	CERUSSITE, ...	3.0606	21.0	(0 0 2)	29.153
9	30.319	2.9456	30	0.8	MASSICOT	2.9346	24.0	(0 2 0)	30.435
10	30.963	2.8857	125	3.3	CERUSSITE, ...	2.8890	2.0	(1 2 1)	30.927
11	31.323	2.8533	3164	83.8	LEAD, SYN	2.8444	100.0	(1 1 1)	31.425
12	31.881	2.8047	120	3.2	LITHARGE, SYN	2.7987	62.0	(1 1 0)	31.951
13	33.962	2.6375	102	2.7	CERUSSITE, ...	2.6339	1.0	(1 0 2)	34.009
14	34.241	2.6166	315	8.3	HYDROCER...	2.6320	100.0	(1 1 0)	34.035
15	34.641	2.5873	206	5.5	CERUSSITE, ...	2.5793	9.0	(2 0 0)	34.751
16	35.601	2.5197	774	20.5	CERUSSITE, ...	2.5148	19.0	(1 1 2)	35.673
17	36.160	2.4820	891	23.6	CERUSSITE, ...	2.4820	46.0	(0 2 2)	36.160
18	36.319	2.4715	1986	52.6	PLATTNERITE...	2.4721	21.0	(2 0 0)	36.310
19	40.442	2.2285	71	1.9	HYDROCER...	2.2374	50.0	(2 0 2)	40.276
20	40.804	2.2096	154	4.1	PLATTNERITE...	2.2108	1.0	(2 1 0)	40.782
21	42.662	2.1176	46	1.2	LITHARGE, SYN	2.1183	1.0	(1 0 2)	42.647
22	43.501	2.0787	475	12.6	CERUSSITE, ...	2.0765	21.0	(2 2 1)	43.548
23	45.179	2.0053	196	5.2	CERUSSITE, ...	2.0049	6.0	(0 4 1)	45.187
24	45.858	1.9772	201	5.3	CERUSSITE, ...	1.9754	7.0	(2 0 2)	45.901
25	47.040	1.9302	549	14.5	CERUSSITE, ...	1.9293	15.0	(1 3 2)	47.062
26	48.644	1.8702	67	1.8	LITHARGE, SYN	1.8677	37.0	(1 1 2)	48.715
27	49.023	1.8567	624	16.5	CERUSSITE, ...	1.8547	15.0	(1 1 3)	49.077
28	49.417	1.8428	332	8.8	CERUSSITE, ...	1.8419	8.0	(0 2 3)	49.442
29	50.895	1.7927	85	2.3	MASSICOT	1.7924	13.0	(2 0 2)	50.902
30	52.278	1.7484	1139	30.2	PLATTNERITE...	1.7497	12.0	(2 2 0)	52.239
31	53.881	1.7002	38	1.0	HYDROCER...	1.6995	40.0	(1 2 2)	53.904
32	54.039	1.6956	51	1.4					
33	54.643	1.6782	34	0.9	LITHARGE, SYN	1.6716	24.0	(2 1 1)	54.877
34	56.022	1.6401	38	1.0	CERUSSITE, ...	1.6410	1.0	(2 4 0)	55.992
35	56.417	1.6296	81	2.1	CERUSSITE, ...	1.6280	4.0	(3 1 1)	56.477
36	58.123	1.5858	117	3.1	CERUSSITE, ...	1.5853	4.0	(2 4 1)	58.141
37	59.178	1.5600	95	2.5	CERUSSITE, ...	1.5604	3.0	(1 5 1)	59.160
38	59.283	1.5575	65	1.7	LITHARGE, SYN	1.5551	6.0	(2 0 2)	59.381
39	60.257	1.5346	93	2.5	CERUSSITE, ...	1.5338	1.0	(0 0 4)	60.291
40	60.417	1.5309	65	1.7	MASSICOT	1.5309	11.0	(2 2 2)	60.419
41	61.722	1.5017	85	2.3	CERUSSITE, ...	1.5006	3.0	(2 2 3)	61.771
42	62.198	1.4913	1159	30.7	LEAD, SYN	1.4904	32.0	(3 1 1)	62.239
43	63.038	1.4734	89	2.4	CERUSSITE, ...	1.4729	4.0	(3 3 0)	63.064

[KS30203A.RAW] PB112 | PEAK ID REPORT

SCAN: 5.0/90.0/0.02/3(SEC), CU(35KV,40MA), I(MAX)=3839, 02/03/03 13:49

PEAK: 15-PTS/PARABOLIC FILTER, THRESHOLD=3.0, CUTOFF=0.1%, BG=3/1.0, PEAK-TOP=SUMMIT

NOTE: INTENSITY = COUNTS, 2T(0)=0.0(°), WAVELENGTH TO COMPUTE D-SPACING = 1.54056A (CU/K-...

#	2-THETA	D(A)	HEIGHT	I%(H)	PHASE ID	D(A)	I%	(H K L)	2-THETA
44	63.210	1.4698	64	1.7	MASSICOT	1.4705	12.0	(0 4 0)	63.180
45	64.182	1.4499	102	2.7	CERUSSITE, ...	1.4491	2.0	(1 1 4)	64.223
46	64.484	1.4438	67	1.8	CERUSSITE, ...	1.4431	2.0	(0 2 4)	64.521
47	65.283	1.4281	420	11.1	CERUSSITE, ...	1.4284	1.0	(1 5 2)	65.269
48	65.867	1.4168	31	0.8	CERUSSITE, ...	1.4163	1.0	(0 6 0)	65.894
49	70.861	1.3287	67	1.8	CERUSSITE, ...	1.3276	2.0	(3 3 2)	70.927
50	71.379	1.3203	46	1.2	CERUSSITE, ...	1.3195	1.0	(2 0 4)	71.433
51	72.302	1.3057	115	3.0	CERUSSITE, ...	1.3052	3.0	(1 3 4)	72.335
52	72.497	1.3027	99	2.6	CERUSSITE, ...	1.3025	4.0	(3 1 3)	72.508
53	73.642	1.2853	29	0.8	CERUSSITE, ...	1.2867	2.0	(0 6 2)	73.547
54	73.961	1.2805	53	1.4	CERUSSITE, ...	1.2805	2.0	(2 4 3)	73.960
55	74.125	1.2781	37	1.0	LITHARGE, SYN	1.2802	2.0	(3 0 1)	73.981
56	74.858	1.2674	53	1.4	CERUSSITE, ...	1.2676	1.0	(1 5 3)	74.845
57	76.643	1.2422	40	1.1	CERUSSITE, ...	1.2423	1.0	(2 6 0)	76.642
58	77.008	1.2373	151	4.0	PLATTNERITE...	1.2376	2.0	(4 0 0)	76.985
59	77.260	1.2338	67	1.8	LEAD, SYN	1.2364	2.0	(4 0 0)	77.074
60	80.839	1.1880	33	0.9	CERUSSITE, ...	1.1876	2.0	(3 5 1)	80.869
61	81.237	1.1832	97	2.6	CERUSSITE, ...	1.1827	4.0	(1 1 5)	81.282
62	81.502	1.1800	75	2.0	CERUSSITE, ...	1.1796	2.0	(0 2 5)	81.539
63	83.982	1.1514	34	0.9	CERUSSITE, ...	1.1517	1.0	(2 6 2)	83.956
64	85.478	1.1350	488	12.9	LEAD, SYN	1.1346	10.0	(3 3 1)	85.514
65	88.257	1.1063	475	12.6	LEAD, SYN	1.1057	7.0	(4 2 0)	88.316

LINE SHIFTS OF INDIVIDUAL PHASES:

PDF#47-1734 - CERUSSITE, SYN <2T(0) = 0.12, D/D(0) = 1.0>

PDF#41-1492 - PLATTNERITE, SYN <2T(0) = 0.12, D/D(0) = 1.0>

PDF#04-0686 - LEAD, SYN <2T(0) = 0.12, D/D(0) = 1.0>

PDF#05-0561 - LITHARGE, SYN <2T(0) = 0.12, D/D(0) = 1.0>

PDF#13-0131 - HYDROCERUSSITE, SYN <2T(0) = -0.12, D/D(0) = 1.0>

PDF#38-1477 - MASSICOT <2T(0) = 0.12, D/D(0) = 1.0>

APPENDIX 6

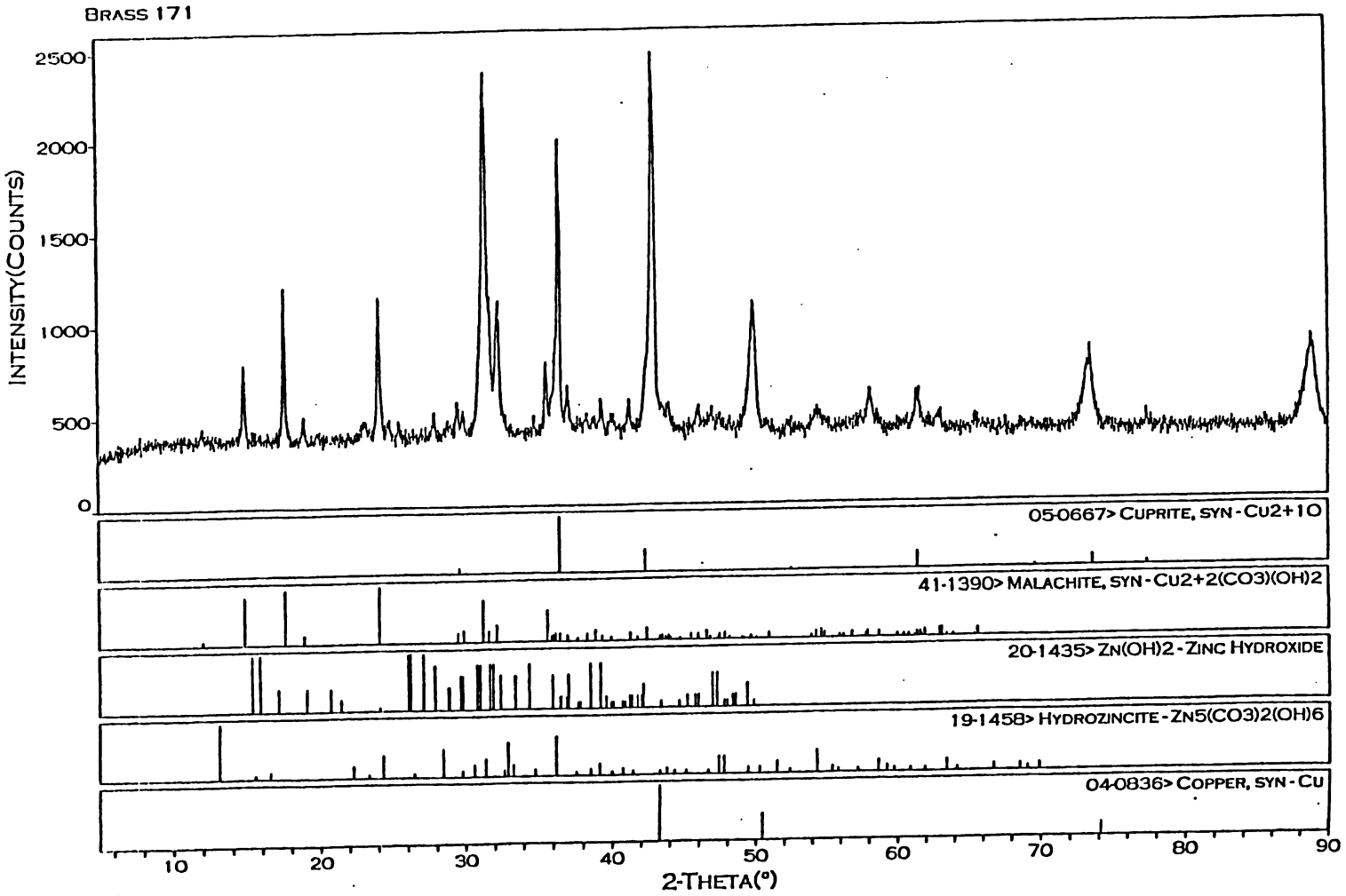
BRASS 171
INTENSITY(COUNTS)
2500
2000
1500
1000
500
0
05-0667> CUPRITE, SYN - CU2+1O
41-1390> MALACHITE, SYN - CU2+2(CO3)(OH)2
20-1435> ZN(OH)2 - ZINC HYDROXIDE
19-1458> HYDROZINCITE - ZN5(CO3)2(OH)6
04-0836> COPPER, SYN - CU
10
20
30
40
50
60
70
80
90
2-THETA(°)

[KS20725A.RAW] Brass 171 | Peak ID Report

SCAN: 5.0/90.0/0.02/3(sec), Cu(35kV,40mA), I(max)=2476, 07/25/02 13:12

PEAK: 15-pts/Parabolic Filter, Threshold=3.0, Cutoff=0.1%, BG=3/1.0, Peak-Top=Summit

NOTE: Intensity = Counts, 2T(0)=0.0(°), Wavelength to Compute d-Spacing = 1.54056A (Cu/K-...

#	2-Theta	d(A)	Height	I%(H)	Phase ID	d(A)	I%	(H K L)	2-Theta
1	12.042	7.3435	83	4.1	Malachite, ...	7.3700	6.0	(1 1 0)	11.999
2	14.859	5.9572	411	20.5	Malachite, ...	5.9700	84.0	(0 2 0)	14.827
3	17.600	5.0350	843	42.0	Malachite, ...	5.0400	96.0	(1 2 0)	17.582
4	18.932	4.6836	135	6.7	Malachite, ...	4.6960	15.0	(2 0 0)	18.882
5	23.215	3.8284	76	3.8	Hydrozincite	3.8100	5.0	(1 1 1)	23.328
6	24.120	3.6867	745	37.1	Malachite, ...	3.6900	100.0	(2 2 0)	24.098
7	24.847	3.5804	79	3.9					
8	25.487	3.4919	89	4.4					
9	27.915	3.1935	130	6.5	Zn(OH)2	3.2000	80.0	(0 2 0)	27.857
10	29.522	3.0232	145	7.2	Malachite, ...	3.0280	15.0	(2 3 0)	29.474
11	29.953	2.9807	108	5.4	Malachite, ...	2.9850	20.0	(0 4 0)	29.909
12	31.420	2.8448	1822	90.7	Hydrozincite	2.8500	30.0	(-2 2 0)	31.361
13	31.739	2.8169	670	33.4	Zn(OH)2	2.8240	80.0	(0 2 4)	31.657
14	32.338	2.7661	533	26.5	Zn(OH)2	2.7620	60.0	(2 1 7)	32.387
15	36.040	2.4900	155	7.7	Malachite, ...	2.4890	11.0	(1 3-1)	36.055
16	36.460	2.4623	1545	76.9	Zn(OH)2	2.4630	20.0	(1 2 6)	36.449
17	37.081	2.4225	174	8.7	Zn(OH)2	2.4270	60.0	(1 1 9)	37.009
18	38.398	2.3423	68	3.4	Malachite, ...	2.3470	11.0	(4 0 0)	38.319
19	38.932	2.3114	69	3.4	Malachite, ...	2.3150	17.0	(1 5 0)	38.870
20	39.395	2.2853	143	7.1	Malachite, ...	2.2890	8.0	(2 2 1)	39.329
21	40.043	2.2498	93	4.6	Zn(OH)2	2.2490	10.0		40.058
22	40.202	2.2413	94	4.7					
23	41.320	2.1832	155	7.7	Malachite, ...	2.1850	12.0	(0 4 1)	41.284
24	42.440	2.1281	270	13.4	Malachite, ...	2.1280	20.0	(2 5 0)	42.443
25	42.940	2.1045	2008	100.0					
26	46.153	1.9652	103	5.1	Malachite, ...	1.9700	8.0	(3 2 1)	46.034
27	47.055	1.9296	88	4.4	Zn(OH)2	1.9320	60.0	(1 3 5)	46.993
28	49.880	1.8267	677	33.7	Zn(OH)2	1.8280	10.0	(4 2 8)	49.843
29	53.988	1.6970	73	3.6	Malachite, ...	1.6980	4.0	(5 3 0)	53.955
30	54.280	1.6886	101	5.0	Malachite, ...	1.6890	11.0	(0 6 1)	54.266
31	54.501	1.6823	117	5.8	Malachite, ...	1.6780	13.0	(3 6 0)	54.651
32	57.538	1.6005	69	3.4					
33	58.123	1.5858	201	10.0	Malachite, ...	1.5910	9.0	(0 1 2)	57.913
34	61.398	1.5088	187	9.3	Cuprite, syn	1.5087	27.0	(2 2 0)	61.404
35	62.959	1.4751	88	4.4	Malachite, ...	1.4750	12.0	(5 5 0)	62.963
36	63.105	1.4720	99	4.9	Malachite, ...	1.4720	13.0	(1 7 1)	63.106
37	67.622	1.3843	73	3.6					
38	73.280	1.2907	333	16.6					
39	73.440	1.2883	423	21.1	Cuprite, syn	1.2861	17.0	(3 1 1)	73.586
40	77.407	1.2319	105	5.2	Cuprite, syn	1.2322	4.0	(2 2 2)	77.383
41	77.747	1.2273	69	3.4					
42	85.571	1.1340	73	3.6					
43	88.601	1.1029	351	17.5					

[KS20725A.RAW] BRASS 171 | PEAK ID REPORT

SCAN: 5.0/90.0/0.02/3(SEC), CU(35KV,40MA), I(MAX)=2476, 07/25/02 13:12

PEAK: 15-PTS/PARABOLIC FILTER, THRESHOLD=3.0, CUTOFF=0.1%, BG=3/1.0, PEAK-TOP=SUMMIT

NOTE: INTENSITY = COUNTS, 2T(0)=0.0(°), WAVELENGTH TO COMPUTE D-SPACING = 1.54056A (CU/K-...

#	2-THETA	D(A)	HEIGHT	I%(H)	PHASE ID	D(A)	I%	(H K L)	2-THETA
44	88.960	1.0994	402	20.0					

LINE SHIFTS OF INDIVIDUAL PHASES:

PDF#05-0667 - CUPRITE, SYN <2T(0) = 0.06, D/D(0) = 1.0>

PDF#41-1390 - MALACHITE, SYN <2T(0) = 0.0, D/D(0) = 1.0>

PDF#20-1435 - ZINC HYDROXIDE <2T(0) = 0.0, D/D(0) = 1.0>

PDF#19-1458 - HYDROZINCITE <2T(0) = 0.0, D/D(0) = 1.0>

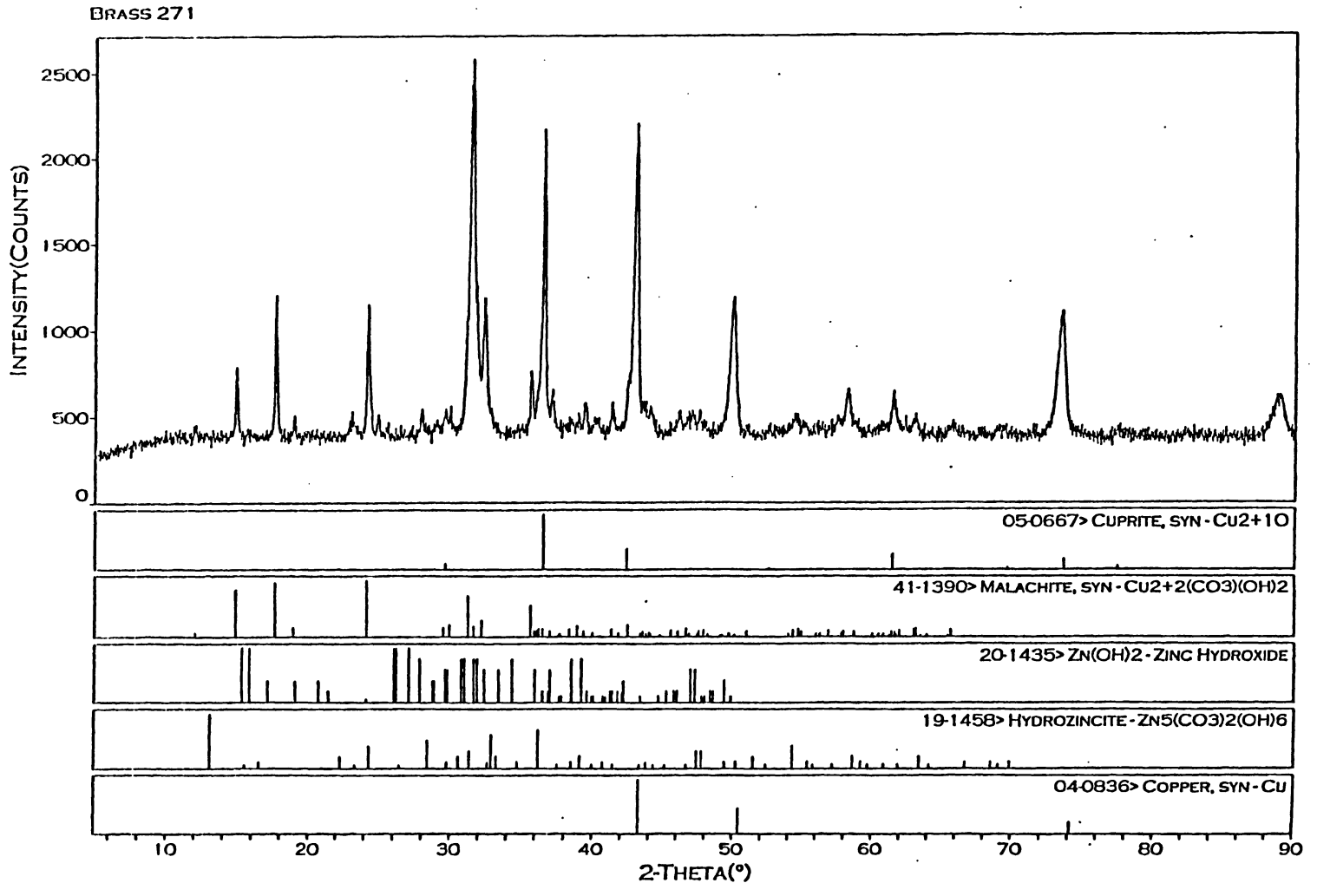
BRASS 271
INTENSITY(COUNTS)
2500
2000
1500
1000
500
0
05-0667> CUPRITE, SYN - Cu2+1O
41-1390> MALACHITE, SYN - Cu2+2(CO3)(OH)2
20-1435> Zn(OH)2 - ZINC HYDROXIDE
19-1458> HYDROZINCITE - Zn5(CO3)2(OH)6
04-0836> COPPER, SYN - Cu
10
20
30
40
50
60
70
80
90
2-THETA(°)

[KS207258.RAW] Brass 271 | Peak ID Report

SCAN: 5.0/90.0/0.02/3(sec), Cu(35kV,40mA), I(max)=1522, 07/25/02 19:15

PEAK: 15-pts/Parabolic Filter, Threshold=3.0, Cutoff=0.1%, BG=3/1.0, Peak-Top=Summit

NOTE: Intensity = Counts, 2T(0)=0.0(°), Wavelength to Compute d-Spacing = 1.54056A (Cu/K-...

#	2-Theta	d(A)	Height	I%(H)	Phase ID	d(A)	I%	(H K L)	2-Theta
1	11.977	7.3832	60	4.0	Malachite, ...	7.3700	6.0	(1 1 0)	11.999
2	14.821	5.9722	259	17.4	Malachite, ...	5.9700	84.0	(0 2 0)	14.827
3	17.597	5.0358	558	37.5	Malachite, ...	5.0400	96.0	(1 2 0)	17.582
4	22.808	3.8957	39	2.6					
5	23.104	3.8464	67	4.5	Hydrozincite	3.8100	5.0	(1 1 1)	23.328
6	24.100	3.6897	560	37.6	Malachite, ...	3.6900	100.0	(2 2 0)	24.098
7	24.817	3.5847	99	6.6					
8	27.839	3.2021	106	7.1	Zn(OH)2	3.2000	80.0	(0 2 0)	27.857
9	28.996	3.0769	32	2.1	Zn(OH)2	3.0900	40.0	(1 2 1)	28.870
10	29.541	3.0213	109	7.3	Malachite, ...	3.0280	15.0	(2 3 0)	29.474
11	31.321	2.8536	1484	99.7	Hydrozincite	2.8500	30.0	(-2 2 0)	31.361
12	31.719	2.8186	567	38.1	Zn(OH)2	2.8240	80.0	(0 2 4)	31.657
13	32.281	2.7708	550	36.9	Zn(OH)2	2.7620	60.0	(2 1 7)	32.387
14	32.757	2.7317	111	7.5	Hydrozincite	2.7400	10.0	(4 0 1)	32.655
15	32.979	2.7138	43	2.9	Hydrozincite	2.7200	60.0	(0 2 1)	32.902
16	35.579	2.5212	293	19.7	Malachite, ...	2.5180	55.0	(2 4 0)	35.626
17	35.902	2.4993	141	9.5	Malachite, ...	2.4990	9.0	(0 3 1)	35.906
18	36.441	2.4635	1489	100.0	Zn(OH)2	2.4630	20.0	(1 2 6)	36.449
19	37.077	2.4227	168	11.3	Zn(OH)2	2.4270	60.0	(1 1 9)	37.009
20	38.231	2.3522	42	2.8	Malachite, ...	2.3470	11.0	(4 0 0)	38.319
21	38.884	2.3142	73	4.9	Malachite, ...	2.3150	17.0	(1 5 0)	38.870
22	39.343	2.2882	144	9.7	Malachite, ...	2.2890	8.0	(2 2 1)	39.329
23	40.023	2.2509	66	4.4	Zn(OH)2	2.2490	10.0		40.058
24	41.281	2.1852	141	9.5	Malachite, ...	2.1850	12.0	(0 4 1)	41.284
25	41.690	2.1647	33	2.2	Zn(OH)2	2.1600	20.0	(6 0 2)	41.784
26	42.381	2.1310	180	12.1	Cuprite, syn	2.1321	37.0	(2 0 0)	42.357
27	42.939	2.1046	1258	84.5					
28	43.439	2.0815	83	5.6	Zn(OH)2	2.0830	10.0	(5 1 6)	43.406
29	43.678	2.0707	116	7.8	Malachite, ...	2.0660	4.0	(2 4 1)	43.781
30	43.977	2.0573	127	8.5	Malachite, ...	2.0570	6.0	(3 1 1)	43.983
31	46.098	1.9674	90	6.0	Malachite, ...	1.9700	8.0	(3 2 1)	46.034
32	46.659	1.9451	59	4.0	Hydrozincite	1.9440	5.0	(-1 3 1)	46.686
33	46.988	1.9322	85	5.7	Zn(OH)2	1.9320	60.0	(1 3 5)	46.993
34	47.781	1.9020	63	4.2	Hydrozincite	1.9020	30.0	(3 3 0)	47.780
35	49.262	1.8482	87	5.8	Malachite, ...	1.8510	1.0	(3 3 1)	49.183
36	49.820	1.8288	568	38.1	Zn(OH)2	1.8280	10.0	(4 2 8)	49.843
37	50.259	1.8138	138	9.3	Hydrozincite	1.8140	10.0	(-3 3 1)	50.255
38	50.854	1.7940	42	2.8					
39	50.863	1.7937	37	2.5	Malachite, ...	1.7920	8.0	(5 2 0)	50.915
40	52.557	1.7398	41	2.8	Cuprite, syn	1.7411	1.0	(2 1 1)	52.514
41	54.303	1.6879	84	5.6	Hydrozincite	1.6880	40.0	(8 0 0)	54.301
42	54.623	1.6788	43	2.9	Malachite, ...	1.6780	13.0	(3 6 0)	54.651
43	54.910	1.6707	60	4.0	Malachite, ...	1.6720	8.0	(4 5 0)	54.864

[KS20725B.RAW] Brass 271 : Peak ID Report

SCAN: 5.0/90.0/0.02/3(sec), Cu(35kV,40mA), I(max)=1522, 07/25/02 19:15

PEAK: 15-pts/Parabolic Filter, Threshold=3.0, Cutoff=0.1%, BG=3/1.0, Peak-Top=Summit

NOTE: Intensity = Counts, 2T(0)=0.0(°), Wavelength to Compute d-Spacing = 1.54056A (Cu/K-...

#	2-Theta	d(A)	Height	I%(H)	Phase ID	d(A)	I%	(H K L)	2-Theta
44	55.169	1.6635	32	2.1	Hydrozincite	1.6570	10.0	(-8 0 1)	55.403
45	57.403	1.6039	64	4.3	Hydrozincite	1.6090	5.0	(-5 3 1)	57.205
46	58.099	1.5864	171	11.5	Malachite, ...	1.5910	9.0	(0 1 2)	57.913
47	58.505	1.5763	101	6.8	Hydrozincite	1.5730	20.0	(-6 2 2)	58.640
48	58.754	1.5702	50	3.4	Malachite, ...	1.5720	8.0	(3 5 1)	58.681
49	60.555	1.5278	71	4.8	Malachite, ...	1.5310	3.0	(1 1 2)	60.414
50	61.432	1.5080	182	12.2	Cuprite, syn	1.5087	27.0	(2 2 0)	61.404
51	61.869	1.4984	42	2.8	Hydrozincite	1.4980	5.0	(-8 0 2)	61.889
52	62.856	1.4772	63	4.2					
53	63.014	1.4739	66	4.4	Malachite, ...	1.4750	12.0	(5 5 0)	62.963
54	65.423	1.4254	60	4.0	Malachite, ...	1.4260	1.0	(3 3-2)	65.390
55	69.359	1.3538	45	3.0					
56	73.062	1.2940	315	21.2					
57	73.400	1.2889	494	33.2	Cuprite, syn	1.2861	17.0	(3 1 1)	73.586
58	73.913	1.2812	62	4.2	Copper, syn	1.2780	20.0	(2 2 0)	74.130
59	82.116	1.1727	56	3.8					
60	84.295	1.1479	23	1.5					
61	87.995	1.1089	76	5.1					
62	88.349	1.1054	122	8.2					
63	88.716	1.1018	179	12.0					
64	88.919	1.0998	183	12.3					
65	89.021	1.0988	170	11.4					
66	89.692	1.0923	48	3.2	Copper, syn	1.0900	17.0	(3 1 1)	89.931
67	89.692	1.0923	48	3.2					

Line Shifts of Individual Phases:

PDF#05-0667 - Cuprite, syn <2T(0) = 0.06, d/d(0) = 1.0>

PDF#41-1390 - Malachite, syn <2T(0) = 0.0, d/d(0) = 1.0>

PDF#20-1435 - Zinc Hydroxide <2T(0) = 0.0, d/d(0) = 1.0>

PDF#19-1458 - Hydrozincite <2T(0) = 0.0, d/d(0) = 1.0>

PDF#04-0836 - Copper, syn <2T(0) = 0.0, d/d(0) = 1.0>

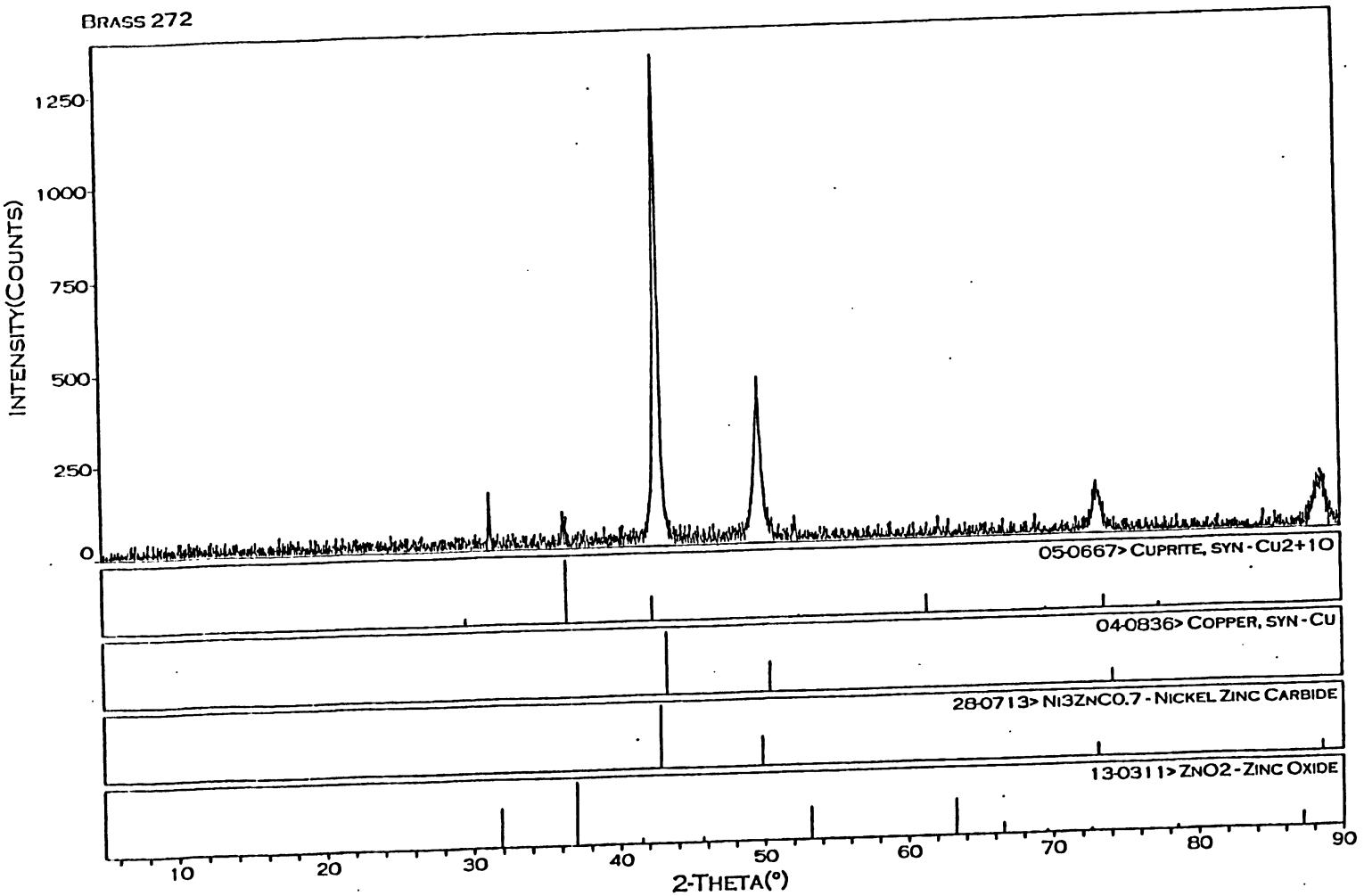
BRASS 272
INTENSITY(COUNTS)
1250
1000
750
500
250
0
05-0667> CUPRITE, SYN - CU2+1O
04-0836> COPPER, SYN - CU
28-0713> NI3ZNC0.7 - NICKEL ZINC CARBIDE
13-0311> ZNO2 - ZINC OXIDE
10
20
30
40
50
60
70
80
90
2-THETA(°)

[KS302111A.RAW] Brass 272 | Peak ID Report

SCAN: 5.0/90.0/0.02/1 (sec), Cu(35kV,40mA), I(max)=1329, 02/11/03 12:28

PEAK: 15-pts/Parabolic Filter, Threshold=3.0, Cutoff=0.1%, BG=3/1.0, Peak-Top=Summit

NOTE: Intensity = Counts, 2T(0)=0.0(°), Wavelength to Compute d-Spacing = 1.54056A (Cu/K-...

#	2-Theta	d(A)	Height	I%(H)	Phase ID	d(A)	I%	(H K L)	2-Theta
1	31.326	2.8531	136	10.4					
2	36.324	2.4712	74	5.7					
3	36.542	2.4570	69	5.3	Cuprite, syn	2.4611	100.0	(1 1 1)	36.478
4	42.880	2.1073	1303	100.0	Ni3ZnC0.7	2.1102	100.0	(1 1 1)	42.819
5	43.708	2.0693	44	3.4					
6	49.067	1.8551	40	3.1					
7	49.841	1.8281	422	32.4	Ni3ZnC0.7	1.8279	45.0	(2 0 0)	49.845
8	50.479	1.8065	76	5.8	Copper, syn	1.8080	46.0	(2 0 0)	50.433
9	52.305	1.7476	51	3.9	Cuprite, syn	1.7411	1.0	(2 1 1)	52.514
10	57.973	1.5895	19	1.5					
11	62.303	1.4890	43	3.3					
12	73.104	1.2934	101	7.8	Ni3ZnC0.7	1.2931	18.0	(2 2 0)	73.124
13	73.223	1.2916	118	9.1					
14	73.481	1.2877	86	6.6	Cuprite, syn	1.2861	17.0	(3 1 1)	73.586
15	87.140	1.1176	16	1.2	ZnO2	1.1170	20.0	(3 3 1)	87.196
16	88.295	1.1059	105	8.1					
17	88.443	1.1045	100	7.7	Ni3ZnC0.7	1.1029	12.0	(3 1 1)	88.599
18	88.763	1.1013	129	9.9					
19	88.976	1.0992	122	9.4					
20	89.350	1.0956	49	3.8					

Line Shifts of Individual Phases:

PDF#05-0667 - Cuprite, syn <2T(0) = 0.06, d/d(0) = 1.0>

PDF#04-0836 - Copper, syn <2T(0) = 0.0, d/d(0) = 1.0>

PDF#28-0713 - Nickel Zinc Carbide <2T(0) = 0.06, d/d(0) = 1.0>

PDF#13-0311 - Zinc Oxide <2T(0) = 0.0, d/d(0) = 1.0>